

UNIVERSIDAD CARLOS III DE MADRID

ESCUELA POLITÉCNICA SUPERIOR

**INGENIERÍA TÉCNICA DE TELECOMUNICACIÓN
SISTEMAS DE TELECOMUNICACIÓN**



PROYECTO FINAL DE CARRERA

**DISEÑO DE ANTENA INTEGRADA
EN BANDA DE MILIMÉTRICAS**

**AUTOR: YUCHEN DU
TUTOR: DANIEL SEGOVIA VARGAS
DIRECTOR: JAVIER MONTERO DE PAZ**

7 de Septiembre de 2012

TÍTULO: *DISEÑO DE ANTENA INTEGRADA EN BANDA DE MILIMÉTRICAS.*

AUTOR: *YUCHEN DU*

TUTOR: *DANIEL SEGOVIA VARGAS*

DIRECTOR: *JAVIER MONTERO DE PAZ*

La defensa del presente Proyecto Fin de Carrera se realizó el día 7 de Septiembre de 2012; siendo calificada por el siguiente tribunal:

PRESIDENTE:

SECRETARIO

VOCAL

Habiendo obtenido la siguiente calificación:

CALIFICACIÓN:

Presidente

Secretario

Vocal

Agradecimientos

Me gustaría empezar agradeciendo a Doctor Daniel Segovia Vargas por haberme ofrecido la oportunidad de realizar el Proyecto Fin de Carrera en el grupo de Radiofrecuencia. También me gustaría agradecer a doctorando Javier Montero de Paz, por sus consejos y su guía durante toda la realización del proyecto. Gracias a ambos por haber solucionado los problemas con los que me he encontrado a lo largo del año. Sin vuestra ayuda este proyecto no hubiera sido posible.

Gracias a mis padres por haberme dado la posibilidad de estudiar esta carrera. Su apoyo constante durante toda mi vida me ha permitido ser lo que soy. Gracias por haber confiado siempre en mí.

A mis compañeros de la universidad, Virginia, Felipe, Juan Antonio y David, por todo estos años que hemos pasado juntos en la carrera. Especialmente a Virginia, por tanto tiempo que hemos tenido que aguantarnos en la universidad.

A mis padres,

Resumen

En este proyecto se ha desarrollado un receptor heterodino que incluye transiciones de microondas de milimétricas, filtros y un circuito mezclador. En este trabajo discutimos el diseño de un sistema de un pixel como estudio previo a la implementación de un array de pixeles. Para ello, se ha tomado como referencia [1].

Se ha diseñado un mezclador subarmónico utilizando líneas de microstrip. Se incluyen diversos elementos tales como circuitos de adaptación de impedancias, así como filtros, para mejorar la adaptación y aislamiento entre los puertos del mezclador. Las dimensiones de todos los elementos fueron optimizados para conseguir una mejor eficiencia de conversión.

Se propuso utilizar una guía onda rectangular para excitar el puerto LO del mezclador subarmónico. Se han estudiado varias topologías de transiciones para conseguir una transición de guía onda rectangular a CPS, eligiendo finalmente la opción de guía onda rectangular - CPS - microstrip. Se utilizó una antena Yagi Uda para implementar la transición guía onda rectangular a CPS.

Se lanzaron simulaciones paramétricas para optimizar las propiedades de la transmisión. Se construyó una transición de microstrip a CPS bajo la topología back to back para medir el rendimiento real. La transición guía onda rectangular a microstrip fue diseñado con éxito obteniendo una pérdida de inserción de 2 dB.

Abstract

In this project a heterodyne receiver has been developed. The needed elements are millimeter wave microwave transition circuits, filters and a mixer circuit. Here, the design of a one pixel system is discussed as previous work for a pixel array. For this end, [1] was taken as reference.

A subharmonic mixer has been designed in microstrip technology. Several elements such as matching networks and filtering stages were included to improve matching and isolation between mixer ports. The physical dimension of all the elements were optimized to achieve a better mixer efficiency.

Rectangular waveguide excitation for the LO input of the subharmonic mixer was proposed. Several types of transition have been analyzed to obtain a rectangular waveguide to microstrip transition. The option rectangular waveguide - CPS - microstrip was chosen. A Yagi Uda antenna has been used to achieve rectangular waveguide to CPS transition.

Parametric simulations have been launched to optimize the transition performance. A back to back microstrip to CPS transition was constructed to verify its actual behavior. The rectangular waveguide to microstrip transition was successfully obtained with an insertion loss of 2 dB.

Contents

1	Introduction and Motivation	25
1.1	Objectives	26
1.2	Outline of the project	28
2	Active Element Design and Characterization	29
2.1	Introduction	29
2.2	Mixer Diode	29
2.2.1	Diodes	29
2.2.2	Diode characterization	34
2.3	Mixers	36
2.3.1	Mixer basics	36
2.3.2	Diode mixer topologies	37
2.4	Mixer circuitry overview	42
2.4.1	Mixer topology	42
2.4.2	Transmission Line Technology	44
2.4.3	Matching and filtering	46
2.5	Mixer Circuit Design	47
2.6	Layout	51
2.7	Conclusion	52
3	Microwave transitions	55
3.1	Introduction	55
3.2	CPW to CPS Transition	55
3.2.1	Wideband CPW to CPS balun	56
3.2.2	Lumped-element Transition	57
3.2.3	Very compact CPW to CPS balun	58
3.2.4	Coplanar Waveguide to Coplanar Stripline Transition	61
3.3	Microstrip to CPS Transition	62

3.3.1	Coplanar Stripline to Microstrip Transition	63
3.3.2	A Wideband Microstrip to CPS Transition	64
3.3.3	A Broadband Transition Between Microstrip and Coplanar Stripline	65
3.3.4	Wideband Microstrip to CPS/Slotline Transitions	67
3.3.5	Compact Microstrip to CPS Transition	68
3.4	Waveguide Transitions	70
3.4.1	Microstrip to Waveguide Transition Using Quasi-Yagi Antenna	71
3.4.2	CPW to Rectangular Waveguide using Fin-Line Taper	73
3.4.3	Wideband CPW to Rectangular Waveguide Transition	75
3.5	Conclusion	77
4	Microstrip to coplanar stripline transition	79
4.1	Introduction	79
4.2	Coplanar stripline theory	80
4.3	CST set up	81
4.3.1	CST mesh specification	81
4.3.2	CST waveguide port definition	83
4.4	CPS parametrization	84
4.5	Microstrip to CPS transition	86
4.6	Back to back transition	90
4.7	Dipole prototype	93
4.8	Conclusion	96
5	Rectangular waveguide to microstrip transition	99
5.1	Introduction	99
5.2	Rectangular waveguide	99
5.3	Yagi Uda antenna	101
5.4	Rectangular waveguide to CPS transition	102
5.4.1	Early prototype	103
5.5	Rectangular waveguide to microstrip transition	105
5.6	Conclusion	107
6	Conclusions and future research lines	109
6.1	Conclusions	109
6.2	Future research lines	110
	Appendices	113
A	Layout	113
A.1	Mixer circuit	113
A.2	Back to back microstrip to CPS transition	117

B Budget	119
References	121

List of Figures

1.1	Frequency spectrum [2]	26
1.2	General overview	27
2.1	Generic diode representation	30
2.2	Large signal microwave diode model [3]	31
2.3	I-V curves for several diodes [3]	31
2.4	Schottky diode cross section [3]	32
2.5	Linear diode model [3]	33
2.6	Subharmonic diode mixer block diagram [4]	34
2.7	I - V curve of a single MACOM mixer diode [4]	35
2.8	Simulated I - V curve at 25 ^o	36
2.9	Mixer multiplier model [3]	37
2.10	Switching approach mixer [3]	38
2.11	Single ended mixer diode [3]	38
2.12	Single balanced mixer using 180 ^o hybrid [3]	39
2.13	Single balanced mixer using 90 ^o hybrid [3]	40
2.14	Double balanced mixer using transformer hybrids [3]	41
2.15	Subharmonic diode mixer block diagram	42
2.16	Block diagram of the subharmonic mixer to be implemented	43
2.17	Microstrip line (a) Physical view (b) Field lines [5]	44
2.18	Single stub block diagram	46
2.19	Generated LPF a) Frequency response b) Circuit schematic c) Layout	48
2.20	Frequency response of microstrip stepped impedance low pass filter	49
2.21	Generated frequency components at IF port	50
2.22	Conversion efficiency vs RF frequency	51
2.23	LO - IF isolation vs LO frequency	52
2.24	RF - IF isolation vs RF frequency	52
2.25	Layout and block diagram	53

3.1	Wideband balun, layout and transmission line model [6]	56
3.2	Electrical field pattern for the CPW-to-CPS balun [6]	57
3.3	Measured (solid) and simulated (dashed) S-parameters for the back-to-back balun	57
3.4	Lumped-element balun, layout and equivalent circuit model [7]	58
3.5	Measured and simulated results for back-to-back lumped-element transition [7]	59
3.6	Layout of Lumped element transition implement with a MIM capacitor, along with measured and simulated results [7]	60
3.7	Back-to-back balun configuration: a)uniplanar b)double layer [8]	60
3.8	S-parameter for double layer design in back to back configuration [8]	61
3.9	(a) Physical configuration (b) equivalent circuit model [9]	62
3.10	S-parameters of back to back CPW to CPS transition with $\theta=60^\circ$ [9]	63
3.11	Layout of back to back configuration of the proposed CPS to microstrip transition [10]	64
3.12	FDTD simulation and measurement of back to back configuration of the CPS to microstrip transition [10]	64
3.13	Microstrip to CPS back to back transition structure [11]	65
3.14	Measured return and insertion loss of the proposed transition [11]	65
3.15	Layout of the proposed transition, including a highlighted area [12]	66
3.16	Simulated and measured (a) insertion loss and (b) return loss of back to back configuration [12]	66
3.17	Microstrip to CPS transition using (a) rectangular stub (b) radial stub [13]	67
3.18	Cross section view of electric distributions [13]	67
3.19	Measured S parameters for back to back transition using (A1) rectangular stub and (B1) radial stub [13]	68
3.20	Simulated and measured S parameters of the optimal design [13]	69
3.21	Microstrip to slotline transition [13]	69
3.22	Simulated and measured S parameters for microstrip to slotline back to back transition [13]	69
3.23	Top and bottom view of constructed back to back microstrip to CPS transition [14]	70
3.24	Measured S parameters of the transition shown in Figure 3.23 [14]	70
3.25	Proposed microstrip to waveguide transition [15]	71
3.26	Schematic of the quasi Yagi antenna [15]	72
3.27	Simulated S parameters of waveguide to CPS transition [15]	72
3.28	Measured S parameters of waveguide to microstrip transition [15]	73
3.29	Overall picture of the proposed transition [16]	74
3.30	Circuit layout of the proposed transition [16]	74
3.31	Simulated and measured S parameters of CPW to waveguide transition [16]	75
3.32	Overall view of the proposed CPW to waveguide transition [17]	75
3.33	Top view of the proposed transition [17]	76

3.34 S parameters of the proposed transition. Solid: simulated results; Dashed: measured results [17]	76
4.1 Cross section of a standard CPS line [18]	80
4.2 Characteristic impedance of CPS as a function of S and W [18]	82
4.3 Return loss varying mesh configuration	82
4.4 Calculated port impedance varying its size	84
4.5 Variation of W , fixing S to 0.06 mm	85
4.6 Variation of S , fixing W to 0.20 mm	86
4.7 Microstrip to CPS transition using a rectangular stub [13]	87
4.8 One section quarter wavelength Chebyshev impedance transformer [19]	87
4.9 Microstrip to CPS transition	89
4.10 Simulated S parameters of Microstrip to CPS transition	89
4.11 Back to back topology of Microstrip to CPS transition	90
4.12 Simulated S parameters of back to back Microstrip to CPS transition	91
4.13 Back to back topology of Microstrip to CPS transition with ports	91
4.14 Back to back topology of Microstrip to CPS transition	92
4.15 Simulated and measured S parameters	92
4.16 Physical overview of a dipole antenna attached to the proposed microstrip to CPS transition	93
4.17 Radiation pattern for the circuit in Figure 4.16	94
4.18 E plane cut radiation pattern	95
4.19 H plane cut radiation pattern	95
4.20 Insertion loss	96
4.21 3D radiation pattern	96
5.1 Cross section of a standard CPS line [5]	100
5.2 Generic configuration of Yagi Uda antenna [20]	102
5.3 Early prototype	104
5.4 Simulated S_{11} of the early prototype	104
5.5 Radiation pattern of the early prototype	105
5.6 Layout of the rectangular waveguide to microstrip transition	106
5.7 Simulated S parameters of the rectangular waveguide to microstrip transition	107
A.1 RF matching circuit and mixer diode	113
A.2 OL matching network with IF matching network on top	114
A.3 IF filtering stage with microstrip definition	115
A.4 Complete layout of the mixer circuit	116
A.5 Top view	117
A.6 Detailed top view	118

A.7 Bottom view 118

List of Tables

2.1	MA4E1318 Electrical Specifications at 25°C [4]	35
2.2	Dimensions of the stepped impedance low pass filter	49
2.3	Insertion loss for each one of the mixer ports	50
4.1	Component physical properties	79
4.2	Mesh properties used in CST microwave studio	83
4.3	Selected waveguide port size	84
4.4	Selected CPS parameters	86
4.5	Theoretical Microstrip to CPS transition parameters	88
4.6	Optimized Microstrip to CPS transition parameters	88
4.7	Microstrip to CPS transition	90
5.1	Usable rectangular waveguides for 46 GHz	101
5.2	Rectangular waveguides used in an early prototype	103
5.3	Parameters of the rectangular waveguide to microstrip transition	106
B.1	Personnel budget	119
B.2	Equipment cost	119
B.3	Other cost	120
B.4	Summary of costs	120

Acronyms

CPS Coplanar Stripline

CPW Coplanar Waveguide

IF Intermediate Frequency

LO Local Oscillator

RF Radiofrequency

LTSA Linear Tapered Slot Antenna

Introduction and Motivation

Microwave technologies have become extremely popular over the past decades. They managed to be present in a lot of aspects in current life. In fact, a big portion of electronic devices requires some kind of microwave technology to achieve its functionality.

Microwave techniques can be found in a very wide range of applications. Starting off with radio communications, they are the backbone of nowadays mobile communications. Practically all generations of personal mobile phone protocols, from GSM to LTE, use frequencies that are considered “microwaves”. Other wireless devices also use microwave frequencies as carrier frequencies, that can be the case of bluetooth equipment. But this does not end there. Aside from communication, microwaves can also be used for many other applications such as radio astronomy, navigation and biomedical uses.

In Figure 1.1 we can find a graphical representation of the frequency spectrum, emphasizing on the microwave band. Some well known microwave applications are also shown next to their working frequency band.

So many uses contributes to the occupation of the available bandwidth. The reality is that the lower frequencies of the band, considered as microwaves, are already somehow saturated. This is what led to the research and development of millimeter wave microwave technologies, that is, frequencies at which the wavelength is in the range of millimeters. Millimeter waves occupy the upper frequencies of the microwave band, as we can see in Figure 1.1, and present a very broad bandwidth that has not been extensively used yet.

The poor use, of course, is due to the fact that at higher frequencies it is harder to design and develop equipments than at lower frequencies. The main reason is that the size of the circuits get smaller (as a consequence of a reduction of wavelength) and thus undesired effects appears unavoidably, both due to an increase in the manufacturing difficulty, as well as the elements approaches to stages where advanced physics should be applied.

In any case, it is important to develop this millimeter band as it presents several advantages. First of all, the higher the frequency is the more the available bandwidth can be got. Secondly, smaller wavelength means smaller antennas and, hence, higher resolution in the imaging sector,

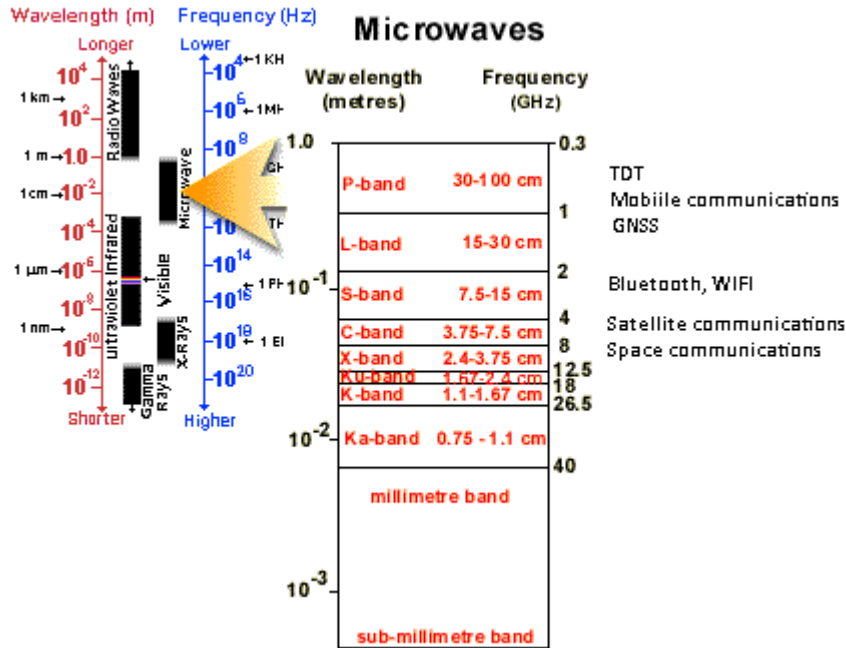


Figure 1.1: Frequency spectrum [2]

that would benefit both security imaging as well as health control imaging.

Some applications in the millimeter band are:

- High speed data links at 40 GHz and 60 GHz
- Millimeter Wave Therapy from 40 GHz to 70 GHz
- Atmospheric monitoring from 57 GHz to 59 GHz
- Multi-gigabit wireless communications at 70 GHz, 80 GHz and 90 GHz
- Automotive cruise control radar at 77 GHz
- Concealed weapons detection at 94 GHz

1.1 Objectives

In this project, we aim to design a heterodyne receiver with a mixer circuit. First let us see the concept in Figure 1.2.

The main idea is actually pretty simple: upon the reception of a 100 GHz RF signal, it will be down converted to a 8 GHz IF signal for easier post processing. In Figure 1.2 the radiating element is represented by a simple half wavelength dipole, at the rightmost part of the figure. The received signal is then driven to a mixer circuit, represented as a gray box. It is possible

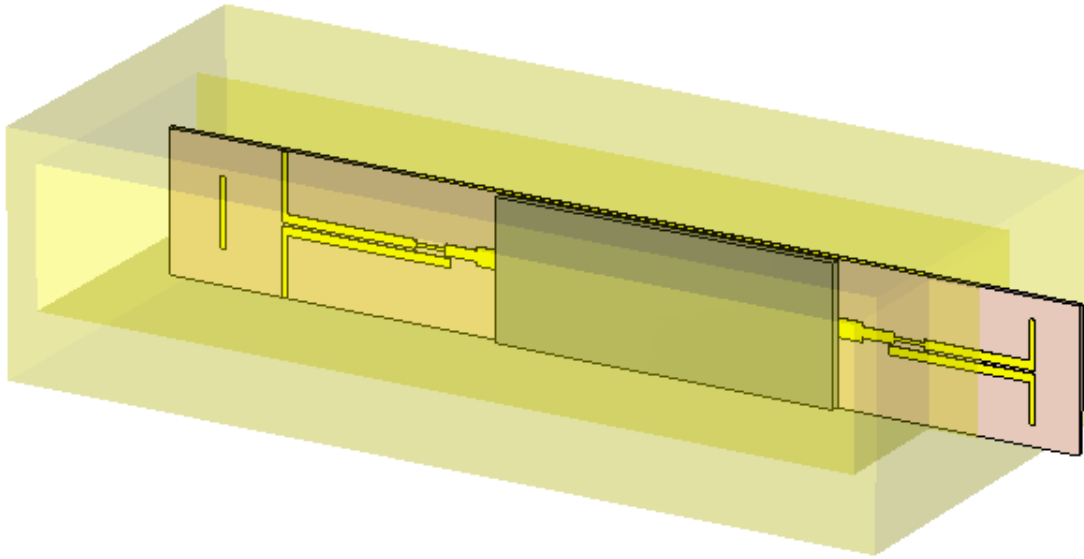


Figure 1.2: General overview

that a transition stage will be necessary between the antenna and the mixer, given the condition that the mixer and the antenna are not connected to transmission lines of the same technology.

In this project, the mixer circuitry will be developed using microstrip technology. This allows easier design and simple connection to the mixer diode. As the dipole has to be connected to a CPS line, a microstrip to CPS transition would be required.

Another concern about the mixer circuitry is that the sub harmonic mixer topology is chosen. The benefit of this kind of mixers is that, when a very low IF frequency is desired, the LO frequency does not have to be very close to the RF frequency. Conversion efficiency might be affected negatively, but a better isolation between ports yields to a higher quality output IF signal. Thus, a LO excitation of 46 GHz is chosen to achieve the aforementioned 8 GHz IF signal from the 100 GHz input RF signal. Additional reason for choosing 46 GHz excitation is the possibility to measure microwave circuits at that frequency using the equipment available in the laboratory.

On the other hand, for excitation purposes, rectangular waveguides are still very much used in contrast with planar technologies. The reason is very simple: a rectangular waveguide presents power losses much lower than the ones in planar technologies. For this reason, we will also aim to excite the 46 GHz LO signal through a rectangular waveguide. Again, as the mixer would be constructed using microstrip technology, some transition stage will be necessary.

Before going for microstrip, the waves inside the rectangular waveguide has to be transformed and passed to a planar technology. One of the easiest means to do so is by using a Yagi Uda antenna, that can be seen at the left part in Figure 1.2. However the output of this transition is a CPS line, thus again a CPS to microstrip would be required.

Considering now the IF output, it will be in the side of the LO excitation. The reasons will

be discussed in Section 2. To allow that, a small hole should be performed in the wall of the rectangular waveguide. This may lead to an undesired behavior but it is most likely unarmful.

The proposed receiver can serve multiple purposes. One possible scenario is to use receivers of such kind for imaging systems. Thanks to the reduced size of the structure, several receivers can be joined together to form a millimeter wave imaging array.

1.2 Outline of the project

The present project will be divided into six chapters. The first chapter, which is the current one, introduces a brief idea of what we should expect from the project.

The second chapter focuses on the active part of the circuit, mainly the mixer circuitry. Several mixer topologies were analyzed and a subharmonic mixer design were developed. Relevant results regarding the mixer performance are presented.

The third chapter belongs to a previous study of the project. Several microwave transitions have been studied, including both the ones that have been used in later chapters, as well as others that have not been used for the goals of this work.

The fourth chapter deals with the CPS to microstrip transition. Both CPS and microstrip technologies are studied and the topology of the transition is reviewed. A back to back transition was also designed, constructed and measured. At the end of that chapter, a prototype including a dipole antenna is presented.

The fifth chapter combines chapter 4 with the rectangular waveguide to CPS transition. It also shows an early prototype of a receiver scheme where the goals of the project were still not properly defined. The rectangular waveguide to microstrip transition will be shown at the end with successful results.

The final chapter summarizes the obtained results, analyzes the outcomes and dissects possible future research lines.

Active Element Design and Characterization

2.1 Introduction

Active elements have always been an important part of microwave components. Ranging from amplifiers to diodes, they are essential in a wide range of microwave applications. In this project, we are interested in using diodes to construct a mixer circuit aiming to down convert a signal from radio frequency to a more manageable intermediate frequency.

In this section, we will focus on the the design of simulation of the mixer circuitry. First, a brief introduction regarding diodes, and specifically, Schottky diodes will be given. Later on we will explain the topologies available for the construction of a mixer. Next, some theoretical background of the technologies used in the mixer circuitry will be presented. Finally, the mixer is designed and the performance is tested by simulations.

2.2 Mixer Diode

2.2.1 Diodes

As we know, a diode is an active device that has an asymmetric behavior. It can be used for multiple applications, ranging from signal rectifiers to microwave mixers. There exist different types of diodes, such as the pn junction, the Schottky diode, the pin diode or the varactor diode. [3] The choice of a specific type of the diode depends on the application.

A diode is usually represented as in Figure 2.1. The positive terminal is called anode while the negative one is called cathode. Ideally, there is only current flow from the anode to the cathode. This behavior can be obtained by using doped materials. For instance, a conventional p - n diode is constructed by joining a p type material, that is, a material where there are excessive holes for electrons to occupy, and n type material, where free electrons are available.

The basic diode model follow the Shockley equation: [3]

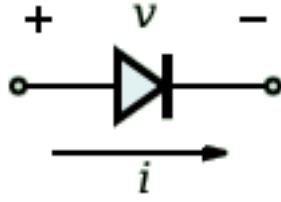


Figure 2.1: Generic diode representation

$$\text{Current} = I_s \left(e^{V_j/NV_t} - 1 \right) \quad (2.1)$$

Where V_j is the voltage across the junction and V_t the thermal voltage defined as kT/q , k is the Boltzmann constant, T the absolute temperature and q the charge of an electron. N is the ideality factor (also known as quality factor) and varies between 1.04 and 1.08 in a typical scenario. This factor along with I_s , the reverse bias saturation current can be used to simulate the specific diode model as they are responsible to adjust the current-voltage relation of the device. In fact, by modifying I_s one can obtain the characteristics of silicon diffused junction diode or Schottky barrier diodes. In any case, the equation at 2.1 does not take into account the non ideal behavior of the diodes.

When V_j in equation 2.1 is much bigger than the thermal voltage, the exponential is very big, thus the -1 factor can be omitted:

$$I_{forward} = I_s \left(e^{V_j/NV_t} \right) \quad (2.2)$$

However, when higher currents are applied, its effects should be modeled by including a series resistance that acts for both the bulk resistance effect as well as the high level injection. In this high current scenario, and similarly in the low current case in which recombination effects take place, the currents do not longer follow equation 2.2 but, instead, they approach as indicated by equation 2.3. [3]

$$I_{forward} = I_s \left(e^{V_j/2NV_t} \right) \quad (2.3)$$

It is also possible to construct a large signal microwave diode model, that results handy when trying to obtain some of the diode parameters. The model is shown in Figure 2.2 and can be used to simulate junction diodes, varactor diodes and Schottky diodes.

In Figure 2.2, the diode capacitance is modeled with a voltage dependent capacitor in parallel with a nonlinear current source that behaves similarly to equation 2.2. C_b is the beam lead parasitic capacitance, R_d is the series resistance, C_p is the package parasitic capacitance and L_p the package parasitic inductance.

The capacitance of a step junction or linearly graded junction can be approximated to [3]:

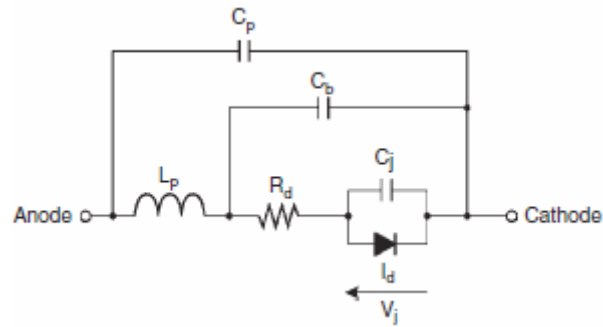


Figure 2.2: Large signal microwave diode model [3]

$$Capacitance = \frac{C_{J_0}}{(1 - V_j/\phi)^M} \quad (2.4)$$

Where C_{J_0} is the zero bias value, ϕ is the junction barrier potential and M is the grading coefficient. The junction barrier potential is around 0.7 V for silicon junction diodes and between 0.58 to 0.85 V for Schottky barrier diodes. The grading coefficient can go from 0.5 to 6, depending on the junction used in the diode. [3]

In Figure 2.3 we can see the I - V curves for several diodes belonging to different technologies.

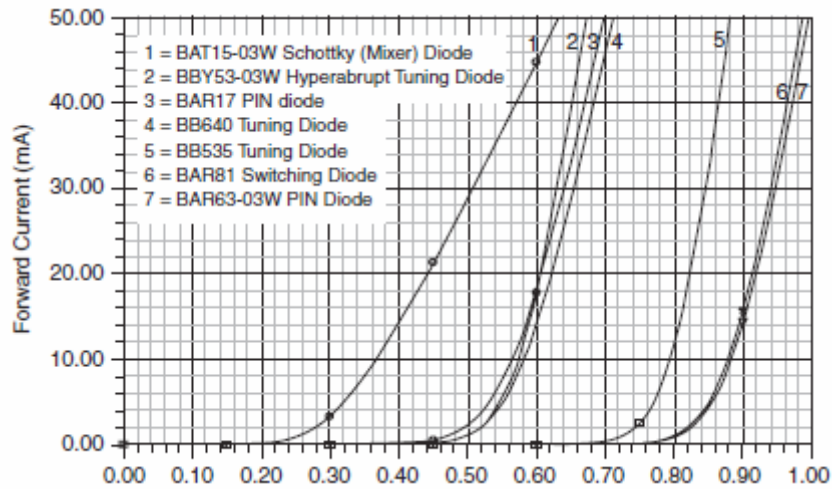


Figure 2.3: I-V curves for several diodes [3]

Schottky Diodes

The main attraction of Schottky barrier diodes is that the current flows only in one type of doping material, that is, in the case of a n-type Schottky diode, the current flows from the metal to the n-type material. As in a Schottky diode the flow of holes can be considered negligible, it

is said to be a majority carrier device (electrons only) and the transit time goes to 0. Thus, the diffusion capacitance is also 0, allowing to work at higher speeds.

In Figure 2.4 we can see the cross section of a Schottky diode. The diode works when a potential is applied between the metal and the semiconductor. At the fabrication stage, when the metal makes contact with the n-type semiconductor, the electrons comes out from the semiconductor and goes into the metal, creating the depletion layer where the atoms are positively charged due to the lack of electrons. This diffusion process continues until no more electrons can flow from the semiconductor to the metal. The created internal voltage difference is called contact potential and varies from 0.3 to 0.8 V in Schottky diodes.

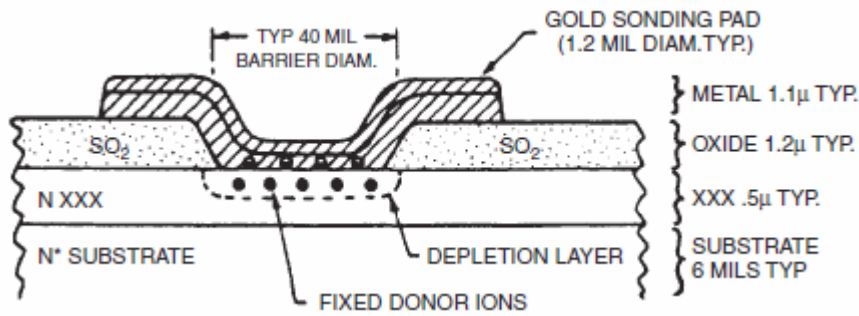


Figure 2.4: Schottky diode cross section [3]

If a positive voltage is produced at the metal layer, the internal voltage difference becomes lower thus the flow of electrons from the semiconductor to the metal is possible. As there is no flow of holes (as a result of being a majority carrier device), if the applied voltage goes from positive to negative, the forward current stops almost instantaneously, taking, at most, some picoseconds. Thus, there is non delay effect related to charge storage. For all these reasons, Schottky barrier diodes are ideal for microwave applications as they are capable of working at very high frequencies.

The I - V behavior of a Schottky barrier diode is defined by the Richardson equation: [3]

$$I_{forward} = AA_{RC}T^2 \exp\left(-\frac{q\phi_B}{kT}\right) \left[\exp\left(-\frac{qV_J}{kT}\right) - M \right] \quad (2.5)$$

Where A is the area (expressed in cm^2), A_{RC} the modified Richardson constant, T the absolute temperature, ϕ_B the barrier height, V_J the voltage across the depletion layer, and M the avalanche multiplication factor. q is the electron charge and k the Boltzmann constant. The barrier height is slightly larger than the contact potential.

Executed experiments have demonstrated that the accuracy of the Richard equation is quite good. However, the fact that the area, the barrier height and the avalanche multiplication factor depend on the applied voltage has made it not very practical in circuit design. A simplification of the equation 2.5 is obtained, achieving reasonable results: [3]

$$I_{forward} = I_S \left[\exp\left(\frac{V_J}{0.028}\right) - 1 + \frac{K}{1 - V_B/V} \right] \quad (2.6)$$

Where I_S is the saturation current, 0.028 is the thermal voltage at room temperature times the forward slope factor, K is the reverse slope factor and V_B the breakdown voltage. Once again, equation 2.6 does not fit perfectly with equation 2.5, but it is much easier to use for circuit design purposes and thus a better choice. Note that all the previous equations are not temperature independent.

Schottky barrier diodes are much used in mixer applications, primarily due to its speed advantages. Similarly to Figure 2.2, a linear diode model can be obtained for mixer diodes and it is shown in Figure 2.5.

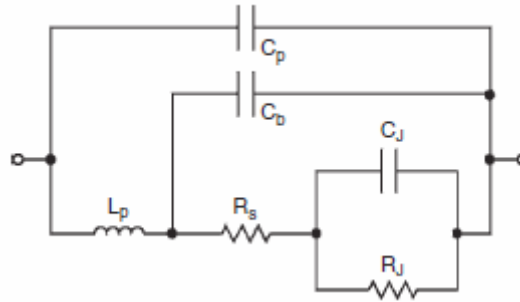


Figure 2.5: Linear diode model [3]

As we can see, the nonlinear current source has been replaced with the junction resistance R_J . Ideally, the contact resistance (or the serial resistance), the beam lead capacitance, the package inductance and the package capacitance are all 0. However, depending on the design and fabrication of Schottky barrier diodes, usually they are nonzero introducing some undesired behavior in the real diode devices.

There are some concerns when designing a Schottky barrier diode for mixer purposes. The barrier height has a direct implication upon the forward voltage. The higher it is, the higher is the forward voltage, and the higher is the required Local Oscillator (from now on LO) driving voltage, which introduces some limitations regarding the LO sources to be used. However, if a good dynamic range is desired, then these limitations can be ignored as a high LO signal should be used anyway.

Extreme values for LO signals are not recommended. For low LO levels, the noise figure is bad mainly due to conversion losses. As for very high power LO levels, typical problems such as heating and excess noise appears, as well as reverse conduction. High breakdown voltages are advised for very high LO excitation.

2.2.2 Diode characterization

The very first step of the mixer circuitry design is to determine and obtain a software model of the mixer diode to be able to perform simulations in a later stage. The mixer diode that we are going to use is the MA4E1318 chip, from M/A-COM Technology Solutions. This device consists on an anti parallel pair of GaAs Flip Chip Schottky Barrier Diodes, as we can see in Figure 2.6.

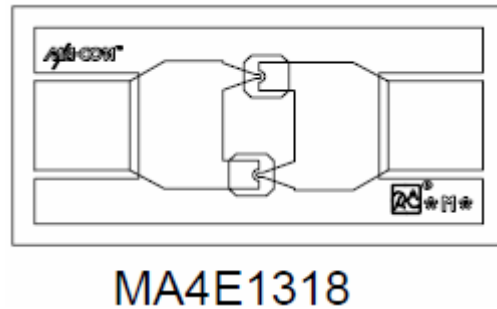


Figure 2.6: Subharmonic diode mixer block diagram [4]

The main features of this MACOM chip are:

- Low series resistance
- Low capacitance
- High Cutoff frequency
- Silicon Nitride passivation
- Polymide scratch protection
- Designed for easy circuit insertion

This device can be employed for applications ranging up to 80 GHz. The working frequency of our project will go up to 100GHz, thus some undesired effects might be encountered. This device was chosen as it is the one available in the laboratory. The anti parallel pair that is the MA4E1318 is specifically meant to be used for subharmonic mixers. The principal electrical specifications of the device are summarized in the Table 2.1.

As we have already said, what we want to achieve is a diode model that behaves just like the selected MACOM commercial device so that we can perform simulations and design a mixer. In particular, we want to adjust a diode model to have the same I - V curve than the one of the MACOM device, that is shown in Figure 2.7.

The software that is going to be used for the mixer simulation is the AWR Microwave Studio 2009, [21]. The SPICE diode element used to model the MACOM mixer diode is the SDIODE. The equivalent circuit of this part is a current source in parallel with a capacitance and, both of

Parameter	Unit	Typical value
Junction Capacitance at 0V	pF	0.02
Total Capacitance at 0V	pF	0.045
Junction Capacitance Difference	pF	0.005
Series Resistance at +10mA	Ohms	4
Forward voltage at +1mA	V	0.7
Forward voltage difference at 1ma	V	0.005

Table 2.1: MA4E1318 Electrical Specifications at 25°C [4]

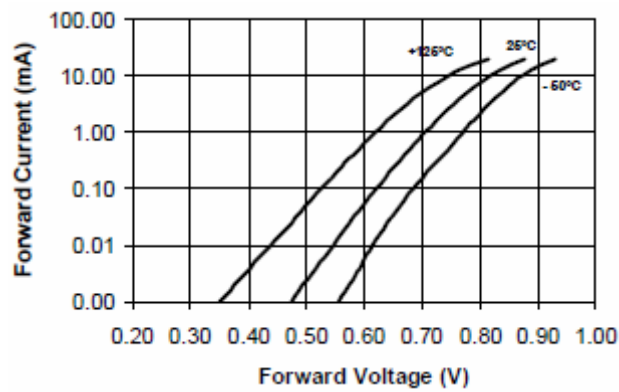


Figure 2.7: I - V curve of a single MACOM mixer diode [4]

them, in series with a resistance. Even though the equivalent circuit is quite simple, the SPICE model is indeed capable of handling some undesired behavior as a wide range of parameters can be modified.

The parameters that can be found in Table 2.1 are used to model the diode, as well as other variables:

- Zero-voltage junction capacitance: 0.02 pF
- Zero-voltage periphery junction capacitance: 0.025 pF (that makes a total zero-voltage capacitance of 0.045 pF)
- The series resistance is set to 6 ohm instead of 4 so as to adapt better the slope of the I-V curve
- Ideality factor: 1.07
- Bottom built in voltage / forward voltage: 0.7 V
- Reverse bias saturation current: 0.04 pA

The rest of the parameters are left as default of the SDIODE SPICE model of AWR Microwave studio. The result is shown in Figure 2.8.

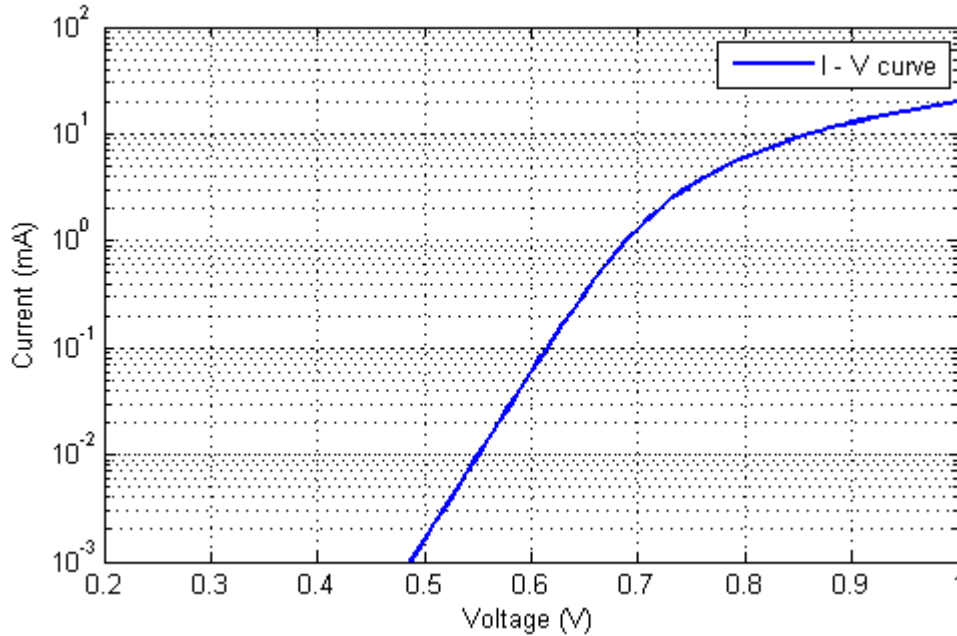


Figure 2.8: Simulated I - V curve at 25^o

As we can see, the curve obtained from simulations in Figure 2.8 is pretty alike to the aimed one at Figure 2.7, while it is true that at voltages higher than 0.7 V the obtained curve does not follow the ideal one very precisely. This is due to the fact that the mixer Diode manufacturer does not provide enough information to model the element correctly and, under such situation, it is complicated to match it in a better way. Note that we are focusing on the mixer diode working at room temperature, that is, around +25^oC. The curves that corresponds to +125^oC and -50^oC in Figure 2.7 is not meant to be matched in simulation.

2.3 Mixers

2.3.1 Mixer basics

Over the years, multiple mixer implementations have been designed to construct frequency converters that have applications in RF scenarios. In the receiver side, the superheterodyne receiver became the dominating one, where the received RF signal is shifted down with the LO drive and converted to IF, where the manipulation of signals comes much more handy.

The mixer acts ideally as a multiplier, and the result can be seen in Figure 2.9.

When two signals are present at the input of the mixer, they are multiplied with each other, thus the output signal has frequency components at the sum and difference of the frequencies of the input signals.

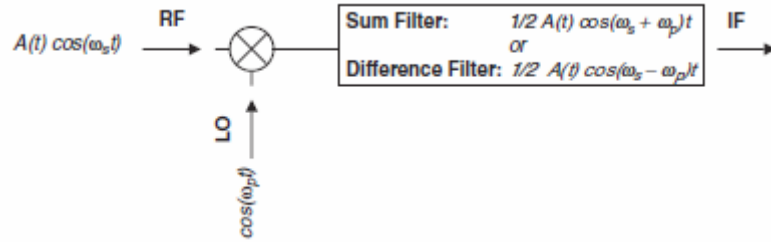


Figure 2.9: Mixer multiplier model [3]

More precisely, the current flow in a diode can be expressed as:

$$I = a_0 + a_1 V + a_2 V^2 + a_3 V^3 + \dots \quad (2.7)$$

Where V is the addition of the input signals. Assuming that the LO excitation is much larger than the RF signal, the frequency components that will appear in the resulting signal can be summed up to:

$$\omega_d = n\omega_p \pm \omega_s \quad (2.8)$$

Where ω_p is the frequency of the LO excitation, ω_s the frequency of the RF signal, and n can take any integer value, creating a series of harmonic signals. That is, the resulting mixer signal creates frequency components that are linear combinations of the frequencies of the input signals LO and RF.

A first approach of a mixer can be obtained using a switch that turns on and off at a frequency of ω_p , that is, acting as the LO. It is a first order approximation of a mixer diode. A graphical representation of this behavior can be seen in Figure 2.10. In fact, its behavior is the same one of a single-ended mixer, that we will go through in the next section. The RF signal that is applied to the IF port is cut down periodically by the switch, and from the modulation theorem, a modulated signal will appear at the IF port along with some other harmonics. Note that DC component is also present at the IF port.

2.3.2 Diode mixer topologies

Now we will briefly review the main diode mixer topologies, which are the single ended diode mixers, the single balanced diode mixers, and the double balanced diode mixers.

Single ended diode mixer

The single ended diode mixer is the most simple topology among mixer diode implementations. It has several advantages, such as simplicity, low cost (as only one microwave diode is required) and good conversion characteristics, that is, a good transmission coefficient.

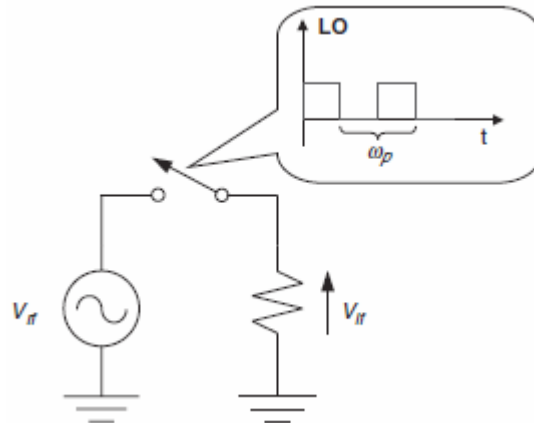


Figure 2.10: Switching approach mixer [3]

In this configuration, the three ports (LO, RF and IF) are connected to the anode of the diode, while the cathode of the mixer diode is connected to ground, as we can see in Figure 2.11. The functionality of this mixer is similar to the switch approach. The LO signal determines when the forward current flow is produced at the diode and thus when the signal at the RF port is propagated to the IF port, producing the multiplier effect.

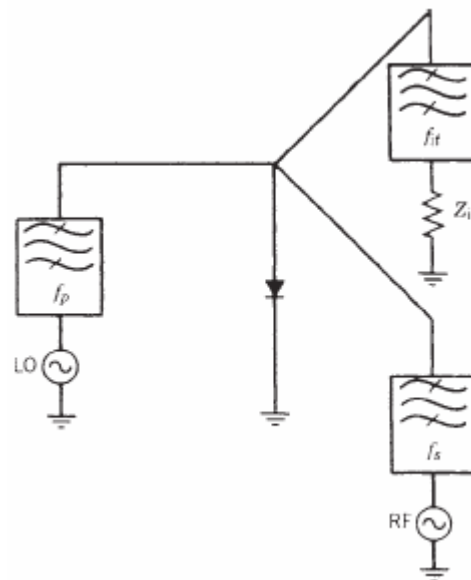


Figure 2.11: Single ended mixer diode [3]

Figure 2.11 shows that as all the ports are connected together to the same pin of the mixer diode, it is obvious that some circuitry has to be implemented for matching and isolation purposes among the three ports. In the scheme, band pass filters are recommended to avoid the presence of undesired signals at each one of the ports.

The first step is to determine the impedance of the diode at LO frequency, that depends on the LO power, LO frequency, DC bias and the characteristics of the diode itself. Large signal S parameter S_{11} is measured at a certain frequency range for this purpose. As for the impedance at RF and IF frequencies, it is important to point out that their measurement must be done under the presence of LO excitation.

When the large signal LO impedance and small signal are obtained, impedance matching circuits are constructed. One approach is to consider each of the ports independently and perform the impedance matching operation on a two port network. That means that for each one of the ports, a separate matching network is obtained considering the impedance of the diode at the corresponding frequency.

Finally, one should ensure signal isolation from one port to another. This can be done with the matching network, by having a very high return loss at the undesired frequencies. If this is not enough to guarantee a correct isolation, some filtering processes, such like a low pass filter in the IF port can be considered.

Single balanced mixer

The advantages of the single ended diode mixer, as we have already mentioned, are mainly regarding cost and conversion loss. However, it does not behave so well when high dynamic range is required. Having all the ports connected together at the same point, using huge LO excitation can result problematic as it would be very complicated to separate it from the RF and IF signals. Something similar happens when higher bandwidth is desired.

The balanced mixers offers features such as a much better LO noise suppression than the single ended mixer while rejecting some of the undesired spurious signals. A bigger dynamic range can be achieved, as now the RF signal is divided between several diodes. Nevertheless, balanced mixers have greater conversion loss, a more difficult design process and a higher power drain.

Single balanced mixers are usually based on designs using 90° hybrids and designs using 180° hybrids, depending on the specific application. An example of the single balanced mixer using a 180° hybrid can be found at Figure 2.12.

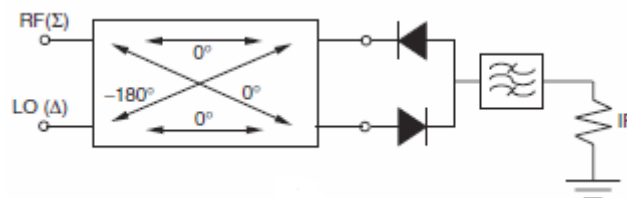


Figure 2.12: Single balanced mixer using 180° hybrid [3]

When the RF signal is applied, the signals at the two diode ports will be in phase for the 180° hybrid. By the contrary, the signals corresponding to the presence of the LO excitation

will be out of phase at the diode ports. This prevents the presence of the LO signal at the RF port. Since the two diodes are placed in the opposite direction, the fact that the LO signals are 180° out of phase makes the diode conductance waveforms to be in phase.

Regarding the noise factors, the AM noise is canceled at the IF side, even though this cancellation is not perfect due to non ideal diode matching and hybrid design. As for the spurious signals, considering that reversing a diode is the same as reversing the voltage and thus the sign of the odd terms of equation 2.7, spurious signals of the form $m f_{rf} + n f_{lo}$ where m and n are even integers are removed, as well as the components of $\pm 2 f_{rf} \pm f_{lo}$.

When a 90° hybrid is used, the behavior of the system is slightly different. The corresponding scheme is shown in Figure 2.13. Now the RF and LO signals at the diode ports are 90° out of phase at both diode ports. This implies that at one diode port the LO voltage leads the RF signal, being the other way around at the second diode port. As the diodes are not placed in the same direction, the resulting IF currents are added in phase. A better LO to RF isolation can be achieved with the 90° hybrid, but $\pm 2 f_{rf} \pm f_{lo}$ spurious are maintained.

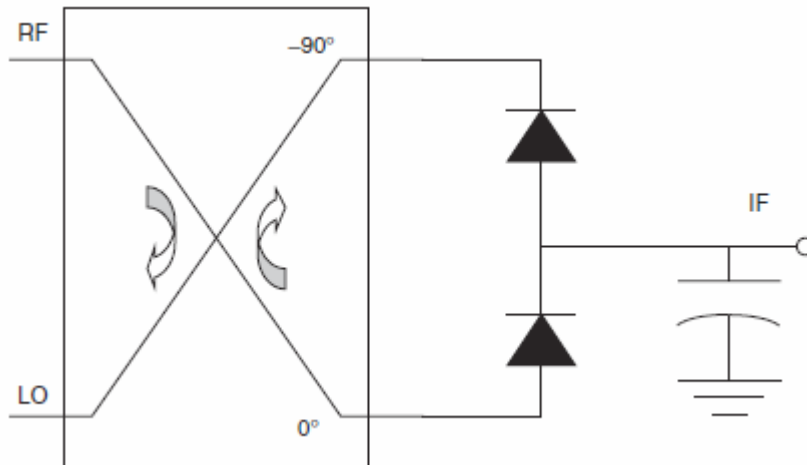


Figure 2.13: Single balanced mixer using 90° hybrid [3]

Double balanced mixers

In microwave applications the most used mixer topology is in fact the double balanced mixer. It requires at least 4 mixer diodes and 2 hybrids, while including some configurations that uses up to 8 diodes and 3 hybrids. As one can imagine, a higher number of components requires even greater LO excitation and a much more design and fabrication process. However, double balanced mixers offer better port isolation and spurious elimination features than the previously seen topologies.

In Figure 2.14 an example of double balanced mixer can be found, where transformer hybrids are used. The LO signal is applied to terminals L and L' , with RF doing the same at R and R' . Assuming that the diodes are identical, R and R' are in fact virtual grounds thus the LO

voltage is not present in the RF transformer. Something similar happens the other way around, achieving a LO to RF isolation that ranges between 30 and 40 dB.

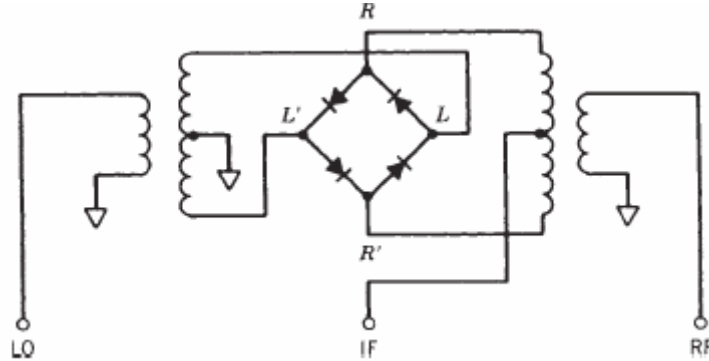


Figure 2.14: Double balanced mixer using transformer hybrids [3]

The basic behavior of the mixer diodes are not different than the previous topologies. In Figure 2.14, when the LO signal is positive, at the two upper diodes, in one of them the RF and LO signals are in phase and in the other one they are out of phase. The same happens with the two lower diodes when the polarity of the LO signal is reversed.

Applying a similar procedure to the previous cases, the forward IF currents can be summed at nodes L and L' , while the negative IF currents can be summed at nodes R and R' . In this way, no IF signal will be present at LO or RF ports. Regarding the spurious signals, being a balanced configuration, frequency components of the type $m f_{rf} + n f_{lo}$ where m and n are even integers are suppressed.

Subharmonic mixer

A subharmonic mixer, unlike the previous topologies, uses a LO excitation at ω_{LO}/n (with n typically taking the value of 2) instead of at ω_{LO} . This is interesting, as at higher frequencies a good LO signal can become more complicated to generate.

For the construction of a subharmonic mixer, an anti parallel diode pair is used, as we can see in Figure 2.15. It keeps some of the advantages of the balanced mixers, such as AM noise suppression. However, the operation concept is somehow different.

We have already seen in the previous sections that for a conventional single diode mixer, the voltage applied to the diode has the form:

$$V = V_{LO} \sin(\omega_{LO} t) + V_{RF} \sin(\omega_{RF} t) \quad (2.9)$$

Generating current at frequencies expressed by $n\omega_{LO} \pm \omega_{RF}$. However, as an antiparallel diode pair is used, the generated current frequency components are for those of $m\omega_{LO} \pm n\omega_{RF}$ only when $m + n$ is an odd integer, as for the rest of components the signal flows within the diode loop.

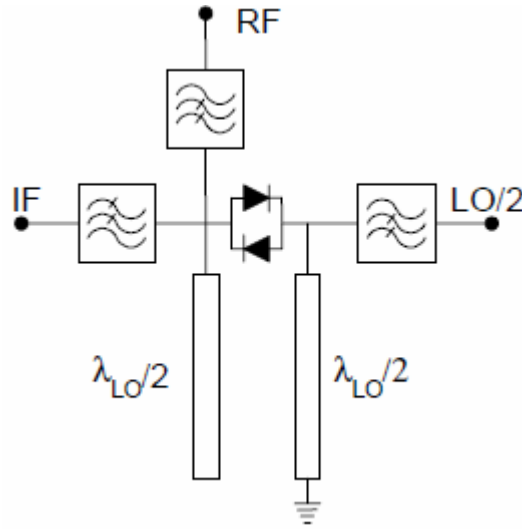


Figure 2.15: Subharmonic diode mixer block diagram

The mathematical reason is that the instantaneous current through the diodes have opposite sign. This lead to differential conductances (defined as the derivative of the instantaneous current with respect to the voltage, that is, $\frac{di}{dV}$), to have exponentials of different sign. The resulting conductance has the form

$$g = 2\alpha i_s \cosh(\alpha V_{LO} \cos \omega_{LO} t) \quad (2.10)$$

This conductance along with the applied voltage in 2.9 is used to obtain the generated current. The result is that for the components of $m\omega_{LO} \pm n\omega_{RF}$ for $m + n$ even is canceled out at the output terminal of the anti parallel diode pair.

In this way, the subharmonic mixer using anti parallel diode pair suppresses the fundamental and other odd harmonic components and the even harmonics of the LO. In addition, the diode pair is protected from large peak inverse voltage due to the anti parallel topology. Nevertheless, as the real LO excitation is at half of the desired frequency, more spurious products are generated due to the product of RF signal with $F_{LO}/2$ drivings.

2.4 Mixer circuitry overview

We are going to start off by introducing some background of the technologies that will be used to construct the mixer circuitry.

2.4.1 Mixer topology

With the MACOM mixer diode correctly characterized in computer software, a brief description of subharmonic mixer circuit that is going to be employed to construct the entire mixer

device is presented. The selected RF frequency and IF frequency are 100 GHz and 8 GHz, respectively. The LO/2 excitation selected is 46 GHz, making an effective LO drive of 92 GHz. The chosen transmission line technology is Microstrip, which will be explained in a later section.

In fact, the implementation slightly differs with the one proposed on Figure 2.15. The main discrepancy is the port allocation. In Figure 2.15 the IF and RF ports are at one side while the LO port is at the other side. However, due to implementation constraints, it is not feasible to have the IF output in the same side as the RF one, as the idea is to have a radiating element (a dipole, in fact) not too far away from the mixer. The problem of having a considerable path between the mixer and the antenna is that due to the high frequencies the losses would be very high. With the IF port in the same side of the RF port, a longer path for matching purposes would be unavoidable.

For this reason, the IF port is allocated in the same side as the LO/2 excitation. A hole in the rectangular waveguide will be made to create an exit for the IF signal. Figure 2.16 shows the block diagram of the subharmonic mixer to be designed, where M.N refers to matching network, for which single stub matching networks will be used.

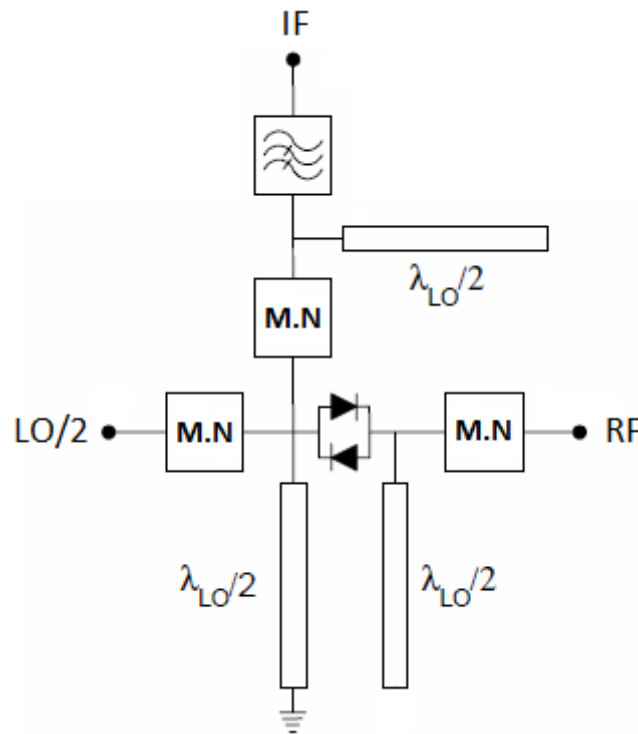


Figure 2.16: Block diagram of the subharmonic mixer to be implemented

As we can see, there are several stubs present in the circuit of Figure 2.16. The purpose of using them is explained below.

The short circuited stub of length $\lambda_{LO}/2$ at the frequency of $F_{LO}/2$ is a quarter wavelength stub thus it behaves an open circuit, allowing the LO/2 excitation to propagate correctly. How-

ever, considering that F_{RF} and F_{LO} are very close to each other, at F_{LO} it is a half wavelength stub, implying the presence of a short circuit at such frequencies and impeding RF signals to flow to the LO port. Additionally, it also behaves as a short circuit to ground for DC signals.

As for the open circuit stubs of length $\lambda_{LO}/2$, they can be found at RF port and IF port. Contrary to the short circuit stubs, the open ones behaves as short circuits at $F_{LO}/2$ and open circuits at F_{LO} . In this way, the $LO/2$ excitation will not propagate to the RF port while the RF frequency reaches correctly to the subharmonic mixer.

Regarding the IF port, it is protected in the same way as the RF port against signals of $F_{LO}/2$; however, considering that they are not ideal stubs, the signals are not fully isolated. For this end, a low pass filter will be also introduced in the IF port to attenuate the leaked $LO/2$ excitation, as well as attenuating the incoming RF signal and higher mode harmonics.

2.4.2 Transmission Line Technology

As we have already explained in Section 1, the chosen microwave transmission line topology for the construction of the mixer device is the microstrip line. Microstrip is, among the existing planar transmission line technologies, a very popular and wide used solution. The main reasons are that it can be fabricated by photolithographic processes and it carries out an easy integration with active and passive microwave devices. In fact, we will see that the the MACOM anti parallel diode pair can be simply glued on the microstrip lines.

The physical view and the fields of the microstrip is shown in Figure 2.17, as well as the field lines, both for E field and H field.

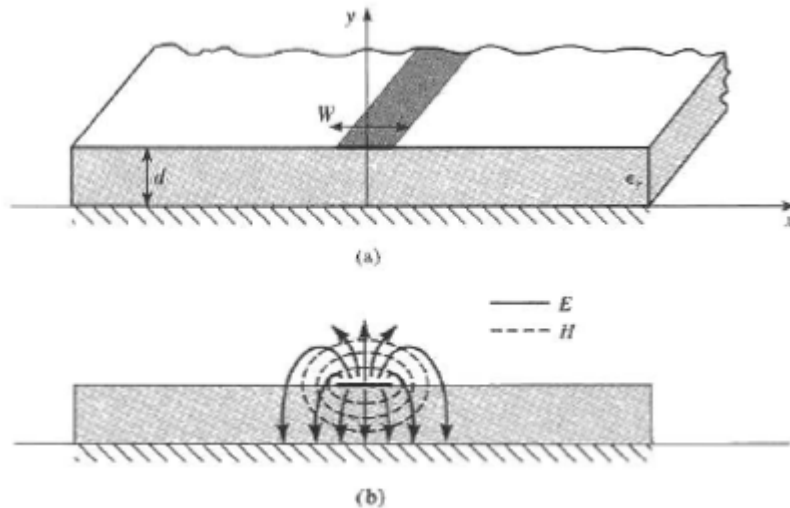


Figure 2.17: Microstrip line (a) Physical view (b) Field lines [5]

As we can see in Figure 2.17, a microstrip transmission line consists on a conductor of width W on one side of a dielectric substrate of thickness d and relative permittivity ϵ_r , with a ground plane on the other side. The thickness of the conductors is t .

In a non dielectric scenario, the microstrip structure can be assimilated by two conductors separated by a distance of $2d$ (due to image theory) where a TEM mode is propagated. However, under the presence of the dielectric only between the conductor and the ground plane, the behavior is somehow more complicated to analyze.

In Figure 2.17 (b) we can see how there are field lines inside and outside the dielectric substrate. This implies that a microstrip transmission line do not propagate a pure TEM mode wave, due to the presence of different phase velocities inside and outside the dielectric.

To be exact, a hybrid TM-TE would be propagated in a microstrip line. Considering that the dielectric is electrically thin (that is, $d \ll \lambda$), a quasi-TEM mode can be assumed. The phase velocity and the propagation constant will be:

$$v_p = \frac{c}{\sqrt{\epsilon_e}} \quad (2.11)$$

$$\beta = k_0 \sqrt{\epsilon_e} \quad (2.12)$$

Where ϵ_e denotes the effective dielectric constant of the microstrip line and it is defined (approximately) by the expression: [5]

$$\epsilon_e = \frac{\epsilon_r + 1}{2} + \frac{\epsilon_r - 1}{2} + \frac{1}{\sqrt{1 + 12d/W}} \quad (2.13)$$

Being ϵ_r the relative permittivity of the employed dielectric substrate. As for the characteristic impedance: [5]

$$Z_0 = \begin{cases} \frac{60}{\sqrt{\epsilon_e}} \ln \left(\frac{8d}{W} + \frac{W}{4d} \right) & \text{for } W/d \leq 1 \\ \frac{120\pi}{\sqrt{\epsilon_e} [W/D + 1.393 + 0.667 \ln(W/d + 1.444)]} & \text{for } W/d \geq 1 \end{cases} \quad (2.14)$$

The W/d ration is:

$$W/d = \begin{cases} \frac{8e^A}{e^{2A} - 2} & \text{for } W/d \leq 2 \\ \frac{2}{\pi} \left[B - 1 - \ln(2B - 1) + \frac{\epsilon_r - 1}{2\epsilon_r} \left\{ \ln(B - 1) + 0.39 - \frac{0.61}{\epsilon_r} \right\} \right] & \text{for } W/d \geq 2 \end{cases} \quad (2.15)$$

where

$$A = \frac{Z_0}{+0} \sqrt{\frac{\epsilon_r + 1}{2}} + \frac{\epsilon_r - 1}{\epsilon_r + 1} \left(0.23 + \frac{0.11}{\epsilon_r} \right) \quad (2.16)$$

and

$$B = \frac{377\pi}{2Z_0\sqrt{\epsilon_r}} \quad (2.17)$$

The chosen dielectric to implement both the microstrip mixer circuitry and the passive microwave circuits in further chapters is the ROGERS's RT/duroid 5880 [22]. It is a glass

microfiber with low electrical loss and comes in very thin packages, which is ideal considering the high frequencies that are employed in this project.

To be more precise, we will use substrates 0.127mm thick (0.005”) and metal cladding of $17\mu\text{m}$ (1/2 oz), which are the thinnest RT/duroid 5880 laminates that can be acquired. The reason to go with the thinnest option is due to the high frequency signals that we will have to face during this project. Under microstrip technology, there is a limit for the thickness above which the transmission line would not behave as desired. The relative permittivity ϵ_r is 2.20 and the loss tangent $\tan\delta$ is 0.0009.

2.4.3 Matching and filtering

Impedance matching networks will be required for avoid reflections at each one of the ports of the mixer. In this project, the selected matching network topology is the single stub matching network, where an open shunt stub is used. An ideal block diagram of the matching network is shown in Figure 2.18. As we can see, the variable parameters are the length and impedance (hence the width of the microstrip conductor) of the shunt open stub and the length of the series transmission line. By adjusting these three parameters it is possible to perform any kind of impedance match.

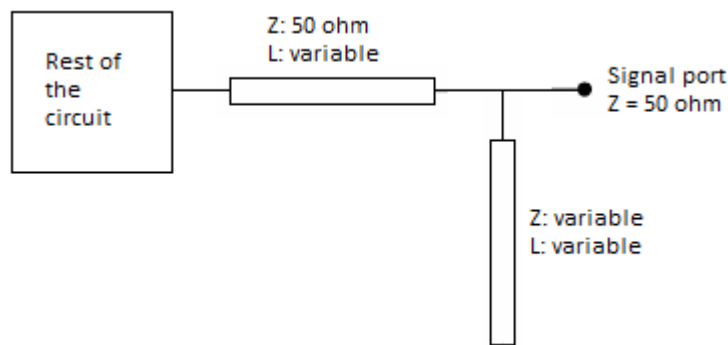


Figure 2.18: Single stub block diagram

As for the IF port, a filtering would be required to eliminate undesired frequency components. To this end, a stepped impedance low pass filter will be implemented. It consists on alternating sections of transmission line with very different impedances and of different length. This leads to reflections due to the impedance change at certain frequencies, hence obtaining the wanted behavior. It is important to notice that the structure will allow signals of some frequencies untouched, but those pass bands will be repeated periodically in the frequency domain, due to the decreasing wavelengths as the frequency goes up.

2.5 Mixer Circuit Design

After having explained all the basics, it is time to start performing simulations in AWR microwave studio. We will use 50Ω as the reference impedance at all the ports. The built in TXLINE application is used to determine the width of the microstrip transmission line to achieve the 50Ω lines, which turns out to be $375 \mu\text{m}$. It is true that the exact width to obtain 50Ω varies a little bit depending on the frequency; however the difference is so small that using a fixed width for all the frequencies does not suppose any issue.

The first step is to set up the anti parallel mixer diode pair, the open and shorted stubs (that were meant for port isolation, as explained previously), the matching network of LO port, and to check which is the optimal power excitation to obtain a better port matching. As we are treating with high power excitations for signal mixing, we will use harmonic balance ports and instead of measuring the conventional S parameters, the Large Signal S Parameter is the most appropriate one, being possible to specify the interested input and output harmonic frequencies.

Beginning with a LO power of 5dBm, the matching circuit is correctly adjusted to achieve a low reflection coefficient. Note that the optimize feature available in AWR microwave studio is used to adjust the matching networks. It could also be done manually, by obtaining the impedance of the circuit seen from the port and calculating the parameters of the single stub matching network. However, by doing so the non ideal behavior of the microstrip transmission lines are not taken into account thus the obtained results might not be the desired ones.

For this reason, the optimize feature results as a very interesting option. By selecting which are the adjustable parameters and by specifying the goals (in this case it would be to obtain a reflection coefficient better than a certain threshold during a specified range of frequencies), and the program itself will vary the selected parameters to try to achieve the goals. The matching results are, in general, much better than those obtained manually.

With the matching network correctly adjusted, now we can tune (using the AWR microwave office tool of the same name) the power of the LO excitation to see for which value the reflection coefficient is improved. Finally, the reflection coefficient was found to be optimal for a LO excitation power of 4.83 dB.

The RF and IF ports are introduced in a similar way. The RF signal is assumed to be at -10 dBm. The only constraint is that the IF port series microstrip line should be long enough to bring the rest of the elements outside of the wall of the rectangular waveguide. Note that each time an element is added to the schematic, it is necessary to redo the optimization of matching network parameters; otherwise a correct matching could be lost.

As we explained alongside Figure 2.16, there are open and shorted stubs in the circuits to obtain port isolation. However, the reality is that with the stubs alone the isolation is simply not good enough, specially at the IF port, where the down converted RF signal is supposed to be analyzed. A microwave stepped impedance low pass filter is implemented to cover this issue.

AWR microwave studio has another built in application to design filters: the iFilter Filter Wizard. It is a simple tool that by specifying some filter parameters like the order and the

cut off frequency, a model of the desired filter is generated. In order not to increase too much the complexity of the complete system, and to avoid using a very long section at the IF port, the filter order is limited at 7. In Figure 2.19 we can find the frequency response, the circuit schematic and the corresponding layout of the generated stepped impedance low pass filter.

One characteristic of the microwave filters is that they present periodic behavior in frequency. This might not be a very nice feature, but it is possible to take advantage of such situation. In Figure 2.19, we can see that while an attenuation of more than 40 dB is introduced at the frequency of the LO/2 excitation, that is, at 46 GHz, an attenuation of better than 35 dB is also introduced to the RF signal, saving the IF output from both noise sources.

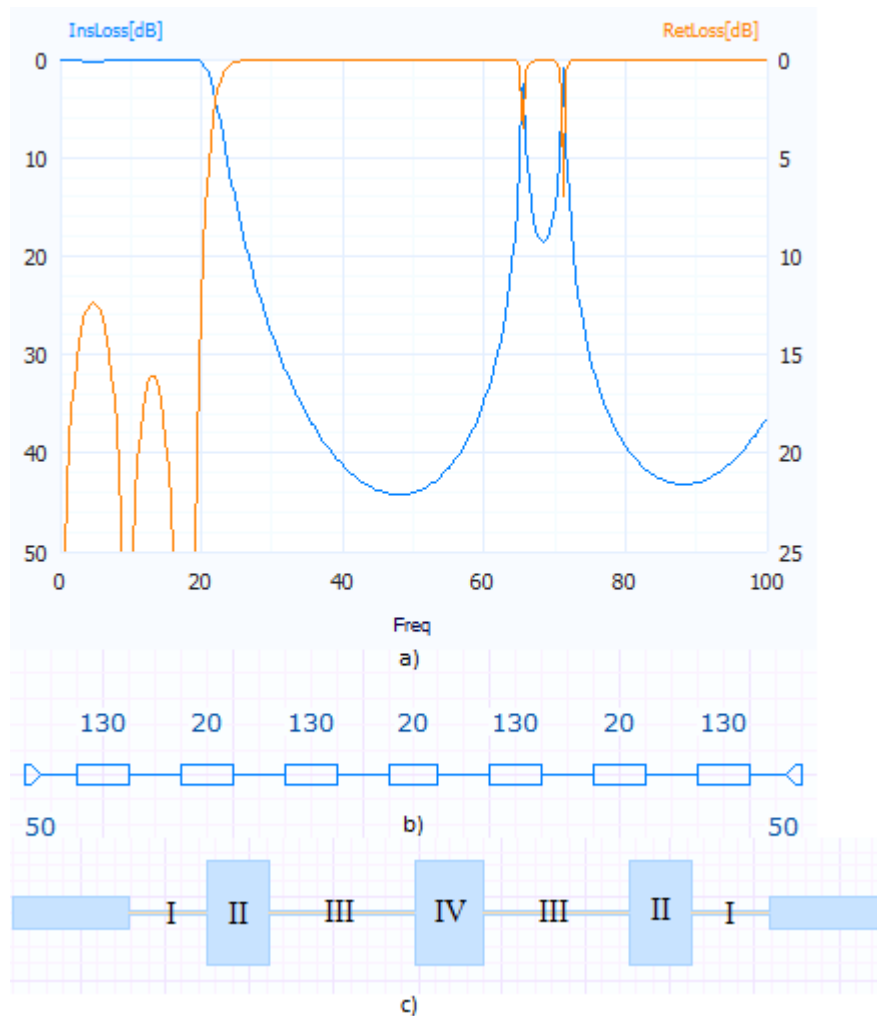


Figure 2.19: Generated LPF a) Frequency response b) Circuit schematic c) Layout

The cut off frequency of the low pass filter is 20 GHz. The impedances of the transmission lines are 20Ω for the low Z_0 and 130Ω for the high Z_0 . Using more extreme values, better attenuation can be obtained. However, it is not recommendable to use microwave conductors that are too narrow or too wide. If a certain section is too wide, undesired behavior might be

present; on the other hand, if a certain section is too narrow, construction process may result complicated. The ripple at the passband is around 0.3 dB. As we are not concerned about the bandwidth of the complete system, there is nothing to worry about the ripple.

Even though that the results in Figure 2.19 seem nice, we should not forget that the iFilter Wizard models with ideal transmission lines. It is necessary then to verify the behavior of the filter by implementing it with real microstrip lines. Again, TXLINE tool were used to convert the parameters of the ideal transmission lines (electrical lengths and impedances) into physical length and width. The length and width for each one of the microstrip sections shown in the layout of Figure 2.19, is colleted in Table 2.2. Note that the corresponding width to the lines of 130Ω is as low as 42 μm , only slightly above the minimum, which is 40 μm . If the width of a line is narrower it will break easily. The simulation results can be found at Figure 2.20.

Section	Width (μm)	Length (μm)
I	42	890
II	1290	745
III	42	1701
IV	1290	814

Table 2.2: Dimensions of the stepped impedance low pass filter

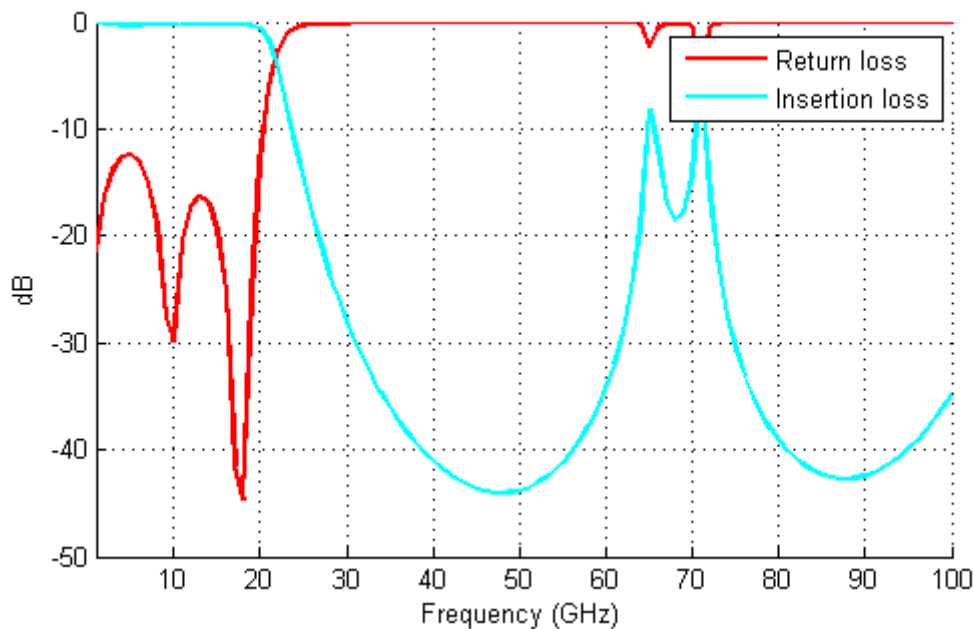


Figure 2.20: Frequency response of microstrip stepped impedance low pass filter

An insertion loss of 0.1764 dB is introduced at 8GHz, which is very low. As for the isolation, an return loss of -43.89 dB is introduced at 46 GHz, being -34.89 dB at 100 GHz. These results

are not exactly the same ones as before; nevertheless they do serve as their initial purpose.

Having designed all the elements required in the mixer circuit, a final matching network optimization is performed, and the return loss is measured for all the ports at their corresponding frequencies.

Port	Return loss (dB)
IF	-29.46
LO/2	-21.962
RF	-22.192

Table 2.3: Insertion loss for each one of the mixer ports

As we can see, the return loss for the three ports is better than -20 dB, which is good enough to ensure a correct behavior of the system. Finally, we will check for all the harmonics that would appear due to the mixer, by doing a measurement of Pharm in AWR microwave office. The result is shown in Figure 2.21.

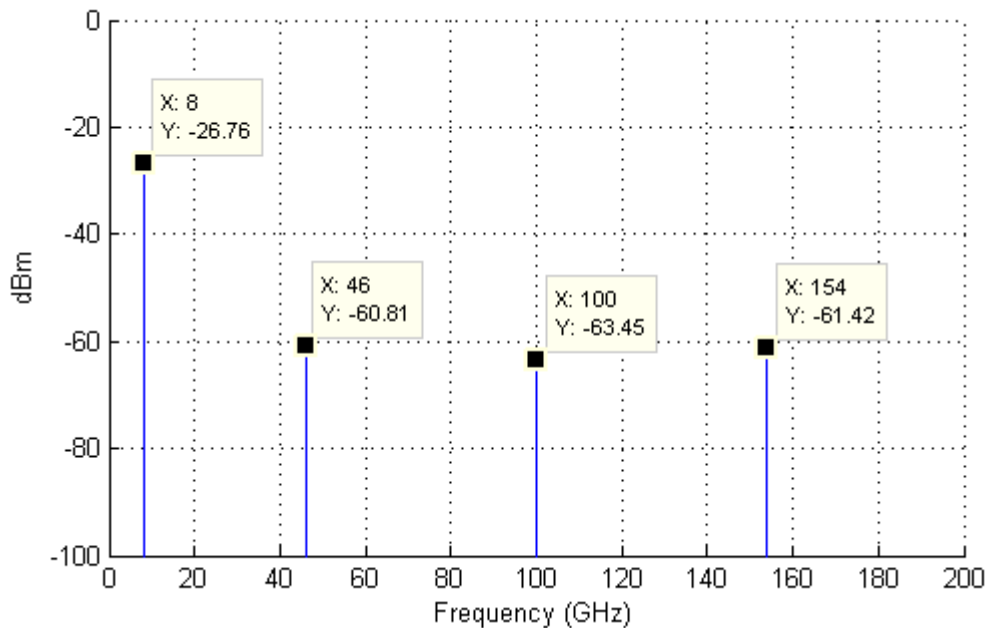


Figure 2.21: Generated frequency components at IF port

Figure 2.21 shows what is expected: apart from the IF signal, a lot of harmonics are generated. The most noticeable frequency components are marked. The IF signal at 8 GHz has a power of -26.76 dBm, meaning that from the -10 dBm RF signal, a conversion loss of 16.76 dB has been introduced. The excessive conversion loss is likely due to the fact that the mixer diode is designed to work up to 80 GHz and here we are working with frequencies of 100 GHz.

The most dominant undesired signal at the IF port is the one due to LO/2 excitation, at

46 GHz, with a power level of -60.81 dBm. Considering that it has initially a power of almost 5 dBm, an attenuation to the LO/2 excitation at the IF port of 65 dB has been introduced, thanks to both the microstrip stub and the stepped impedance low pass filter. The RF signal has been attenuated from -10 dBm to -63 dBm.

There are some more interesting data that we can extract from the mixer design, namely the conversion efficiency versus RF frequency in Figure 2.22, LO to IF isolation versus LO frequency in Figure 2.23 and RF to IF isolation versus RF frequency in Figure 2.24.

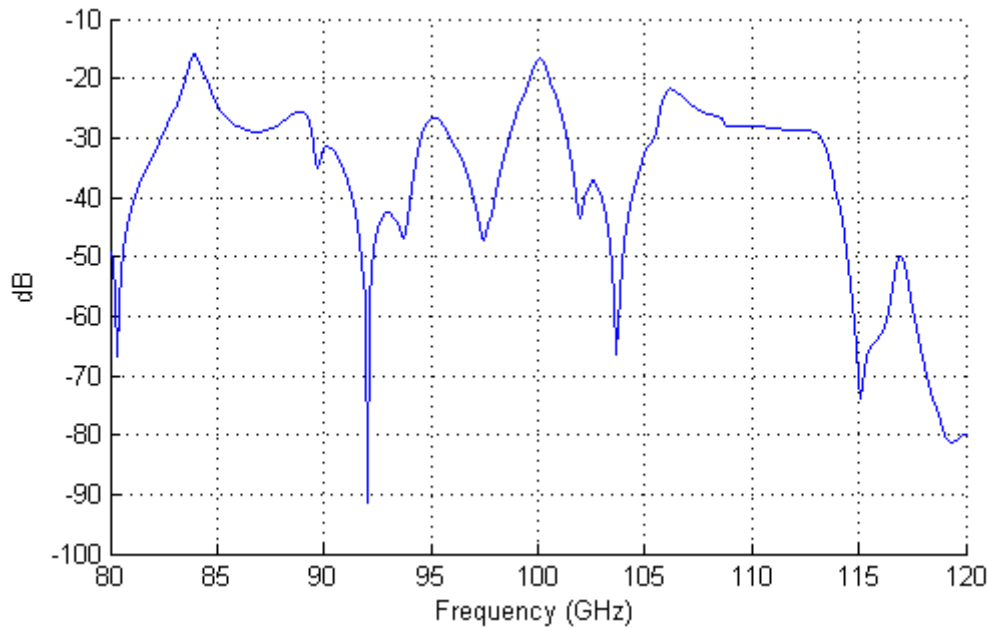


Figure 2.22: Conversion efficiency vs RF frequency

From the figures, it seems that the isolation does not impose great limitations. However, the conversion efficiency varies sharply according to the RF frequency and should be considered as the element that restricts the bandwidth of the mixer circuit. If we define the working bandwidth of the mixer to up to -10 dB with respect to the efficiency at the central working frequency of the mixer, from Figure 2.22 we would say that the circuit works for a RF input that ranges from 98 GHz to 102 GHz, resulting in a 4 GHz bandwidth.

2.6 Layout

The layout of the complete mixer circuit, along with its corresponding block diagram, is shown in Figure 2.25. The layout of the MACOM anti parallel mixer diode pair are constructed using its datasheet. The maximum dimensions of the mixer circuit is $23913\mu m \times 6841\mu m$. As the block diagram is quite extense, it is shown later by parts in Appendix A, where the dimensions of each one of the microstrip sections can be appreciated correctly.

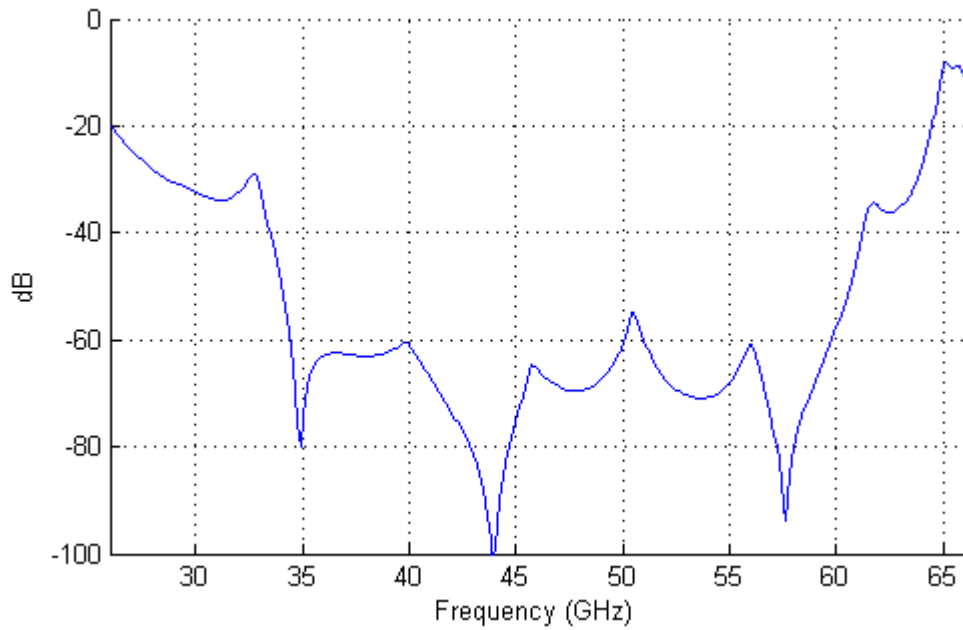


Figure 2.23: LO - IF isolation vs LO frequency

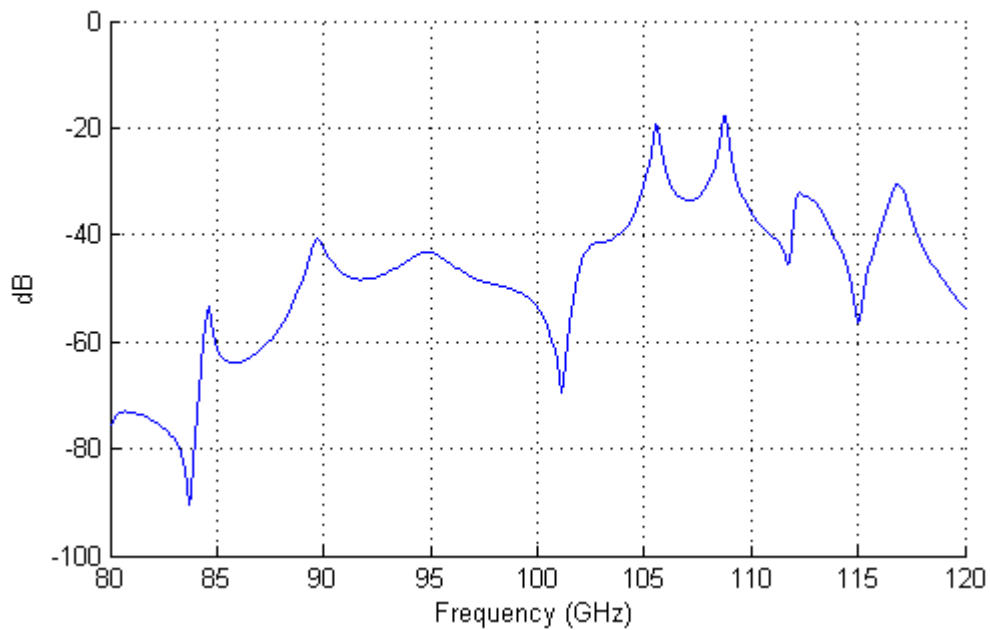


Figure 2.24: RF - IF isolation vs RF frequency

2.7 Conclusion

In this chapter, a subharmonic mixer has been designed. The RF frequency is 100 GHz. LO/2 excitation is used at 46 GHz, leading to an IF frequency of 8 GHz. A stepped impedance

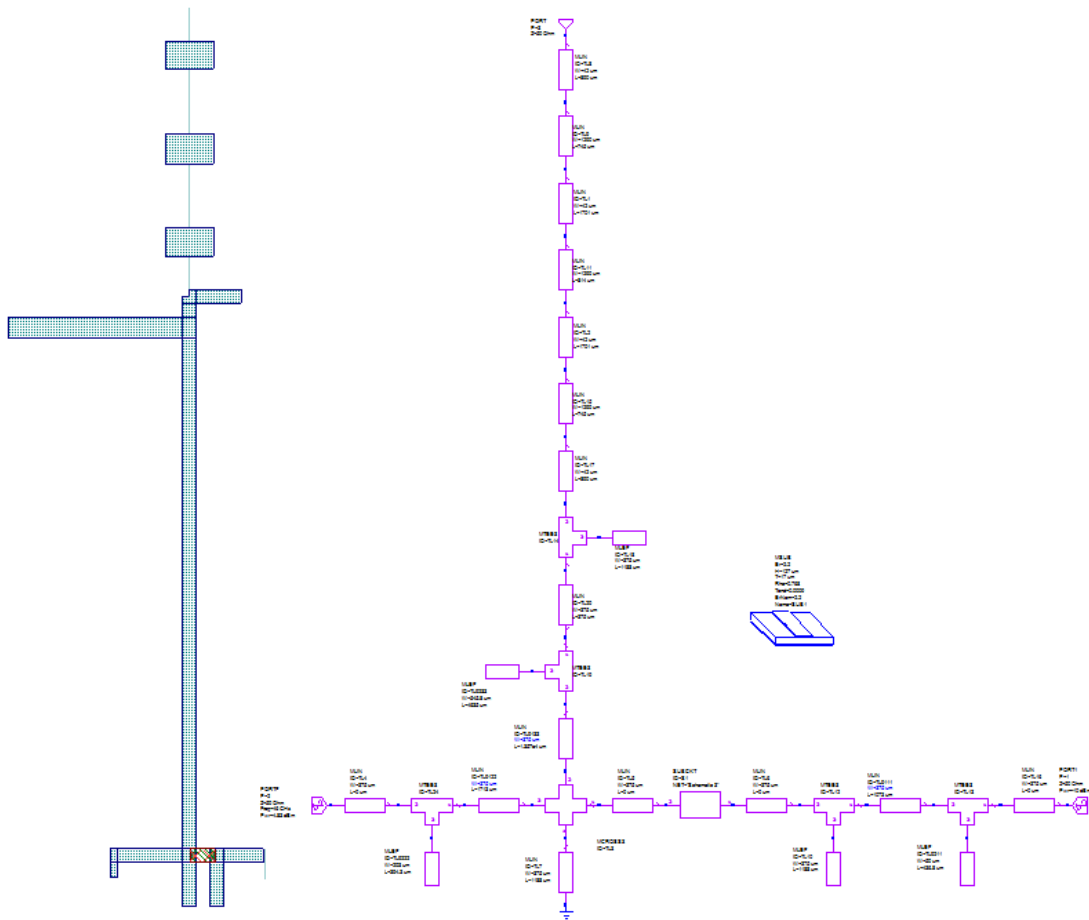


Figure 2.25: Layout and block diagram

low pass filter has been used to provide isolation of LO and RF signals at the IF port. Both isolations are found to be better than 50 dB, hence ensuring low distortion of the IF signal. All the three ports are correctly matched, with return losses better than -20 dB.

As for the conversion efficiency, the obtained conversion loss is as high as 16.76 dB. It is clear that the result is not great; the main reason for this is the fact that the used mixer in theory only works up to 80 GHz, and we are dealing with frequencies around 100 GHz. The conversion efficiency can be improved by switching the diode with a more appropriate one. The bandwidth of the mixer is 4 GHz.

In the next chapter, a set of microwave transitions are reviewed.

Microwave transitions

3.1 Introduction

Due to the wide range of microwave technologies used nowadays, it is beneficial to make use of transitions between different circuit topologies to allow inter-compatibility among elements. From Chapter 1 we learnt that several transmission line technologies will be used in this project, hence, it will be necessary to perform transitions from one technology to another. In this chapter several microwave transitions are reviewed, analyzing first the transition principles and later the simulations and experimental results obtained. In any case, not all the transition topologies shown will be used on a later stage of this project.

First of all, the transition between two coplanar technologies, the Coplanar Waveguide (CPW) and the Coplanar Stripline (CPS) is examined. This transition is very widely, specially when feeding antennas with coaxial cables.

Later on, different Microstrip to CPS baluns is studied. Among the examples reviewed, one also includes a Microstrip to Slotline transition.

Finally, rectangular waveguides are still popular due to advantages such as low propagation loss. Transitions concerning rectangular waveguides to planar technologies are examined, both to Microstrip, passing through CPS, and to CPW.

3.2 CPW to CPS Transition

The first set of microwave transition that we are going to review is devoted to convert from a Coplanar Waveguide topology into a Coplanar Stripline one. In other words, the transition should be able to transform from an unbalanced CPW feed line to a balanced CPS feed line.

The reason this kind of transitions is required is due to the fact that typically coaxial cables are used for the feeding of antennas, such as dipoles or TSAs. However, this kind of feed lines is unbalanced (asymmetrical), while antennas usually requires balanced (symmetrical) feed. Hence, several architectures of CPW to CPS baluns are analyzed in this section.

In practice, the coaxial cable is connected to the CPW end of the balun, with the antenna is attached to the CPS end. Additionally, in some applications, impedance matching is required due to the different characteristic impedances of the coaxial cable and the antenna used.

3.2.1 Wideband CPW to CPS balun

The first CPW - CPS transition that we are going to see is a simple wideband balun using a radial stub. We can see its shape in the figure below:

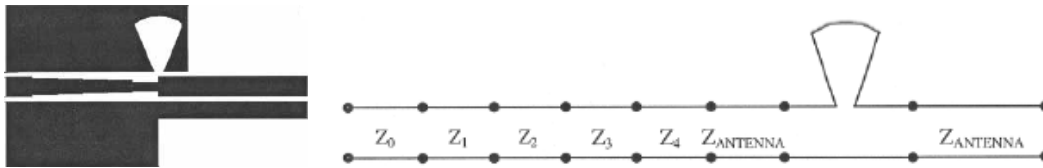


Figure 3.1: Wideband balun, layout and transmission line model [6]

The left side of the layout in Figure 3.1 is of Coplanar Waveguide topology whereas the right side is of Coplanar Stripline. In the middle, we can see a radial slot, which will be explained later.

As for the both ends of this balun, it will be necessary to match the impedances. The CPW end is usually connected to a coaxial line, thus it should have the same impedance as the used cable. In the present balun design, this impedance match is obtained by using a Chebyshev multisection impedance transformer circuit, that can be appreciated in the figure above. The number of sections depends on the ratio between the two impedances, the one of the feed line and the one of the balun. As for the CPS end, it should also have the corresponding impedance of the element to be connected, like for instance an antenna.

Back to the radial slot, it behaves as a short circuit stub, with length around $\lambda/4$, which means that both transmission lines will see that point as an open circuit. This implies that at the point where the CPS line and the CPW line is connected, due to the open circuit, the electric field of the CPW side is forced to be between the central strip and one of the ground planes without the stub, instead of between the two ground planes. In this way, the electrical field is mainly between the two conductors of the CPS, as we can see in Figure 3.2, thus power transmission is achieved.

In order to ensure that the potential on the two ground planes of the CPW is equal, two bond wires are placed at both sides of the radial slot connecting the two planes.

The reason that a radial slot instead of a rectangular slot is used is that a radial slot has smaller resonance length and wider bandwidth, that is, it does not work just at one frequency, which is the case of a rectangular slot, thus a wideband balun can be achieved. Based on experimental simulations, the optimal angle of the radial slot is found to be 45° .

The chosen substrate is a RT Duroid substrate with a relative permittivity of 10.2 and a thickness of 0.785mm. After optimizing each one of the parameters, a back-to-back balun has

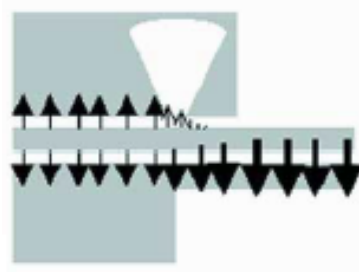


Figure 3.2: Electrical field pattern for the CPW-to-CPS balun [6]

been constructed in [6]. The simulated and experimental measurements of the parameters are shown below.

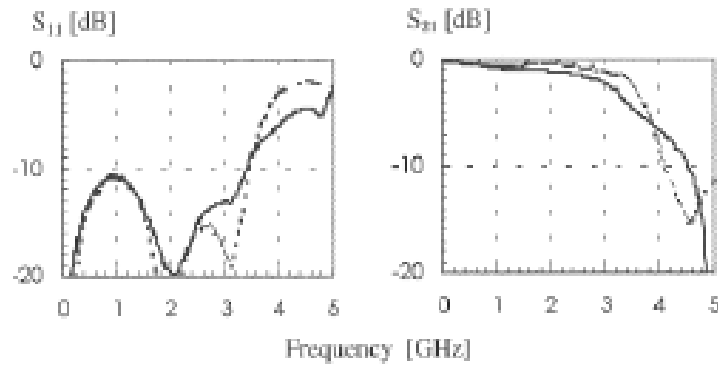


Figure 3.3: Measured (solid) and simulated (dashed) S-parameters for the back-to-back balun [6]

From Figure 3.3 we can observe how the constructed balun has a working frequency between 300kHz and 3GHz. As around a few GHz the wavelength is still large, covering a 3GHz bandwidth (with S_{11} below -10dB) implies that a wideband CPS to CPW balun has been constructed.

3.2.2 Lumped-element Transition

The main disadvantage of the previous transition is that the quarter wavelength transformer structure occupies a very large area, specially in the low frequency range, while small size is usually preferred in planar topologies. For this reason, instead of stubs, lumped elements such as inductors and capacitors are used in this CPW to CPS transition structure.

Figure 3.4 shows the layout of the proposed lumped-element CPW to CPS transition. The $\lambda/4$ short circuit stub used in conventional schemes is replaced by series and parallel LC circuits. These planar circuits are realized by short metal strips, that behaves like inductors, and interdigital capacitors. All the elements are designed to have the same resonance frequency, which is the same one of the working frequency of the transition circuit.

The capacitance of interdigital capacitor is computed using expressions under quasi-static

approximation, while the inductance values are obtained also using quasi-static close-form formulas, being all parameters dependence on the strip length, width, thickness and the conductivity of the material used.

The equivalent circuit model in Figure 3.4 can be identified as a second order bandpass filter, thus one can calculate the values of the lumped elements considering the desired center frequency, relative 3dB bandwidth and the characteristic impedance of the transmission lines.

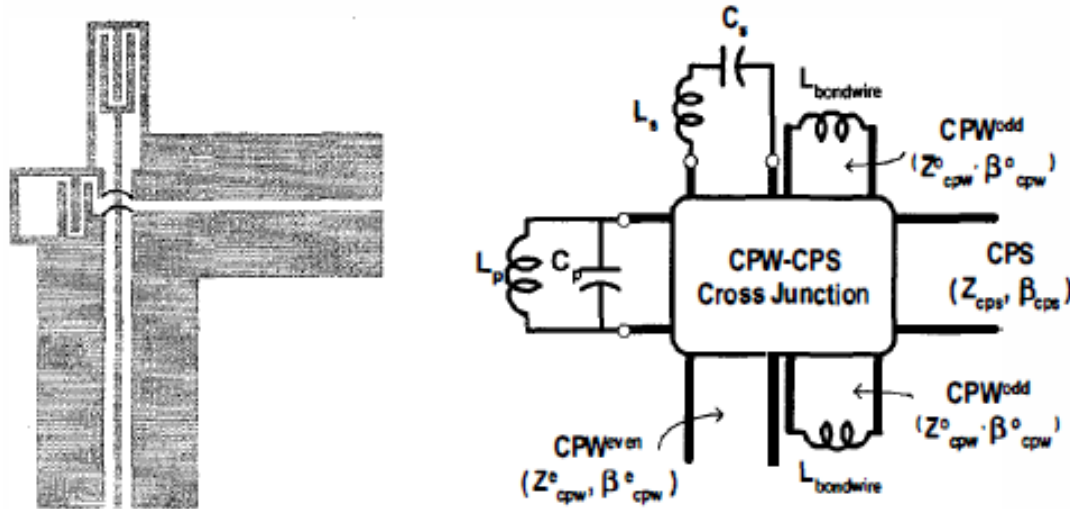


Figure 3.4: Lumped-element balun, layout and equivalent circuit model [7]

For the construction of a balun with working frequency around 3GHz, the FR4 substrate is chosen, which has relative permittivity of 4.3 and thickness of 1.6mm. The CPW and CPS lines are designed to have characteristic impedance of 100Ω . The values of the LC components are carefully chosen to obtain a maximally flat response at the pass band. The simulation and the experimental results are shown in Figure 3.5, obtaining a 2.5GHz bandwidth centered around 2.5GHz. It differs from the desired 3GHz central frequency due to the parasitic effect and the back-to-back configuration with a slotline in between.

If a metal-insulator-metal structure is used to implement the capacitor C_s , as the one shown in Figure 3.6, which has the same equivalent-circuit model as the previous circuit, a higher capacitance can be achieved employing even a smaller area than an interdigital one while having a similar performance.

In conclusion, using lumped elements it is possible to construct a CPW to CPS transition with reasonable performance and of very compact size compared to conventional transition models.

3.2.3 Very compact CPW to CPS balun

Until now we have seen two different types of CPW to CPS transition. The first one, which consists primely in a wideband balun with a radial slot, has the disadvantage of needing a very

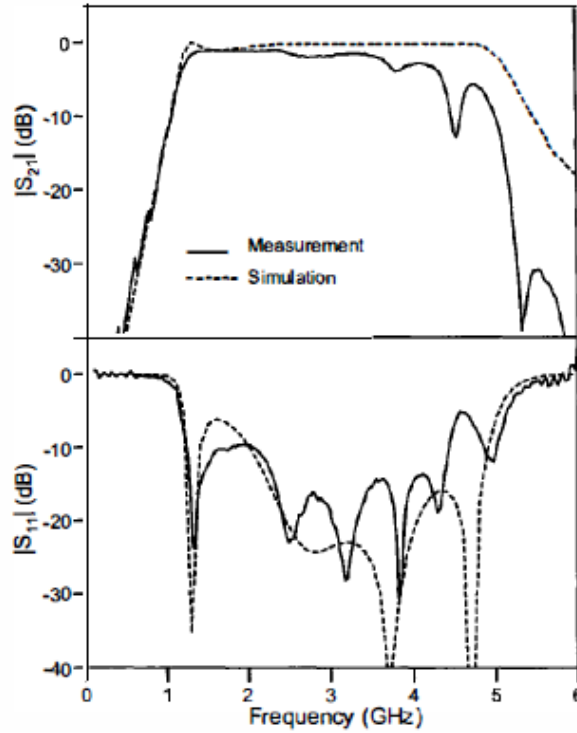


Figure 3.5: Measured and simulated results for back-to-back lumped-element transition [7]

large area, specially at lower frequencies. This is problematic when small size design is required. The second type of transition uses lumped element that allows the construction of a balun of similar characteristics, but occupying less area. However, this solution is not optimal neither, as it is complicated to design and thus it is not an easy task to achieve the exact desired working frequency, due to the presence of parasitic effects from the different lumped elements used.

In this paper, the authors try to reduce the total size using another approach: to use an additional ground plane. The topology is the basically same one as in section 3.2.1, using a Chebyshev impedance transformer for impedance matching, and a radial slot for the balun. Nevertheless, the noticeable difference is that a ground plane is plated under the substrate, leading to a double layer balun design.

The presence of a ground plane at the bottom of the balun gives rise to even modes in the CPS line, while in the uniplanar balun it supports mainly odd mode propagation. The even and odd modes in coupled microstrip lines have different characteristic impedance, thus by optimizing them size reduction of the double layer balun can be achieved. The required number of sections of the Chebyshev transformer is reduced, as well as the dimensions of the rest elements of the balun. Thanks to this behavior, the total size of the balun can be cut down to even below 60% of the original size, as well as obtaining a reduction of the insertion loss.

One problem encountered is the appearance of slotline mode at the side of the element to be connected to the CPS line. In practice, this slotline mode is suppressed by connecting the

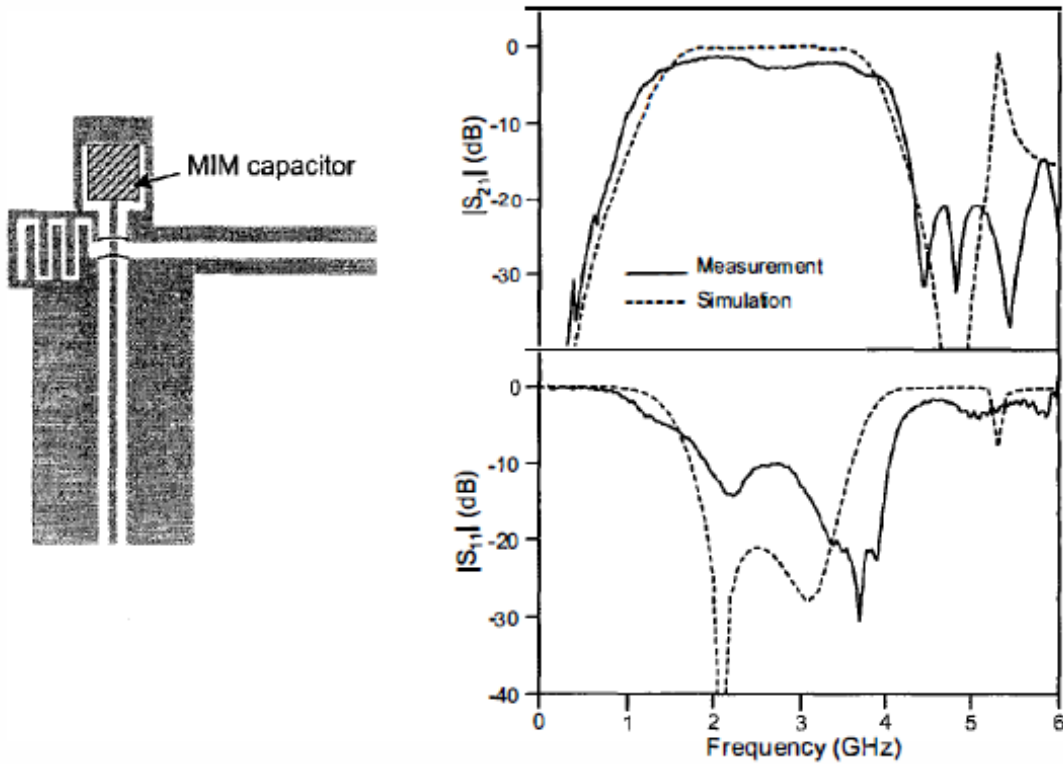


Figure 3.6: Layout of Lumped element transition implement with a MIM capacitor, along with measured and simulated results [7]

two ground planes of the feeding line, that is, the CPW section, with bond wires to ensure the continuous propagation of the fundamental coplanar mode. The position and length of the bond wire have a big influence on the resonant frequency, thus they have to be chosen carefully. We can see the size difference on Figure 3.7.

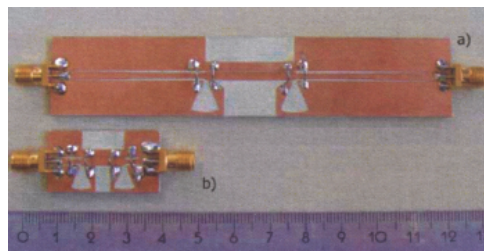


Figure 3.7: Back-to-back balun configuration: a)uniplanar b)double layer [8]

The substrate used is the RO4003C, with relative permittivity of 3.38 and thickness of 1.524mm. The simulation results, as well as the measured performance of the double layer design can be seen in Figure 3.8. S_{11} is below -10dB between 7GHz and 8.5GHz.

In this way, a uniplanar balun is miniaturized by adding a second metalization layer, provid-

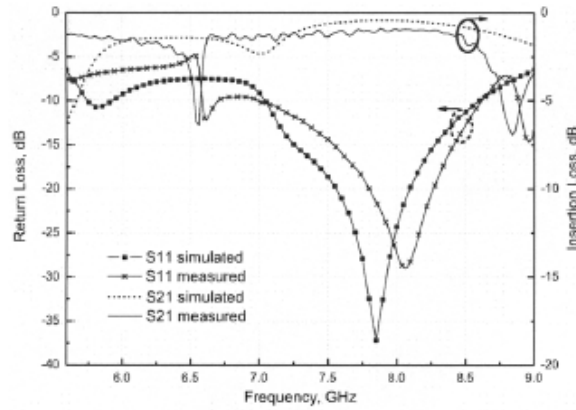


Figure 3.8: S-parameter for double layer design in back to back configuration [8]

ing additionally a lower insertion loss by suppressing the unwanted radiation of the ungrounded CPS line that would take place at the uniplanar topology. The size is significantly smaller and thus not suitable for applications requiring reduced areas.

3.2.4 Coplanar Waveguide to Coplanar Stripline Transition

We have seen three different types of CPW to CPS transition schemes. However, the ones that uses radial slots as quarter wavelength stubs faces the problem that the bandwidth might be limited by the imperfect open stub termination. In this paper the authors analyze theoretically and experimentally another kind of CPW to CPS transition. The circuit layout and its equivalent circuit model is shown in Figure 3.9.

This transition structure is decomposed into six parts: the symmetric coplanar waveguide (SCPW), the asymmetric coplanar waveguide tapered linearly in the lower slot (TCPW), the asymmetric coplanar waveguide tapered linearly in the upper ground plane (ACPW), the unterminated slotline open (TSLO), the asymmetric coplanar stripline tapered linearly in the upper strip (TCPS), and the symmetric coplanar stripline (SCPS).

The lower slot width of TCPW is tapered from SCPW to ACPW and then kept constant until the other end of the transition in order to minimize the discontinuity effects. By narrowing the lower slot width gradually and terminating the open stub on the upper slot, the electromagnetic power on the upper slot may efficiently couple to the lower one. The upper strip of the TCPS is also gradually tapered to obtain the necessary impedance matching.

The equivalent model of the circuit is studied for the purpose of computing the dimensions of each one of the sections of the present transition. Additionally, FDTD method is used to simulate and to optimize the behavior of the transition. The $635\mu\text{m}$ thick alumina substrate is selected, with a relative permittivity of 9.8, to construct a back to back configuration of the designed balun for its later measurements. It has been observed that the inclined angle θ associated with the TSLO and TCPS sections in Figure 3.9 is essential to optimize the transition

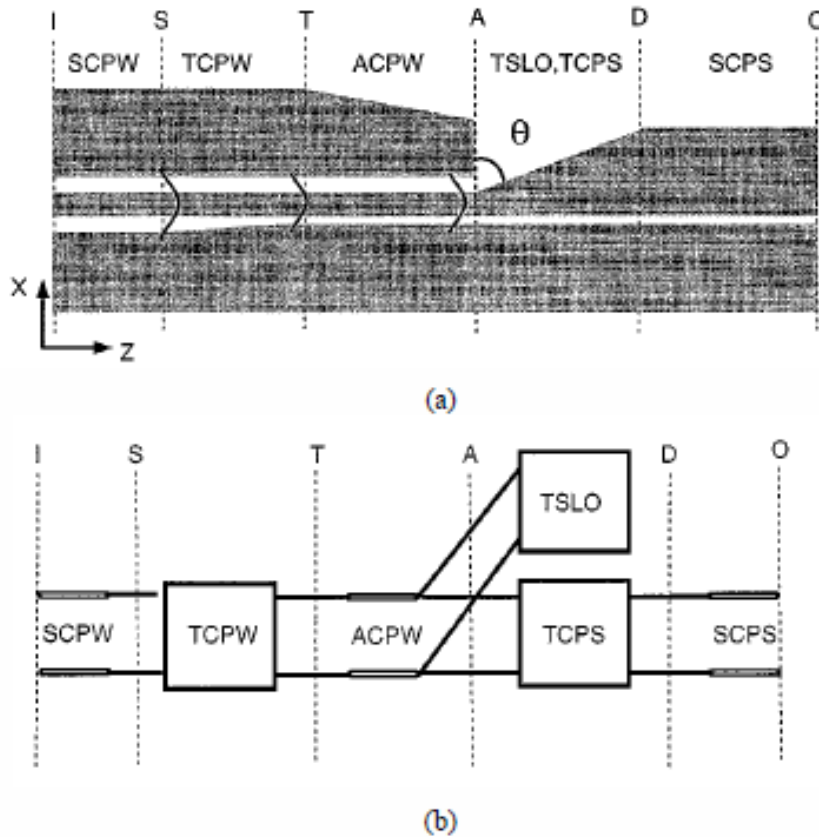


Figure 3.9: (a) Physical configuration (b) equivalent circuit model [9]

response. An example of the behavior of the balun, using $\theta = 60^\circ$, can be seen in Figure 3.10.

In conclusion, a very wide band CPW to CPS transition has been designed and constructed. The overall results are not great, as the measured transmission coefficient is -2 dB. By optimizing some parameters such as the inclined angle, as well as other dimensions of the transition, the performance can be improved obtaining broader bandwidth and lower insertion loss.

3.3 Microstrip to CPS Transition

The Coplanar Stripline has advantages such as lower cost, efficient use of area and small circuit size. Additionally, its propagation parameters are relatively independent of the substrate thickness which simplifies the designing process. Besides, its popular usage in areas of antenna feeding has made it necessary in a wide range of applications.

By the other hand, microstrip transmission line has also a very broad range of applications, such as couplers, dividers, and amplifiers. For that reason, five microstrip to CPS transitions are reviewed within this section, from which one also includes a microstrip to slotline transition.

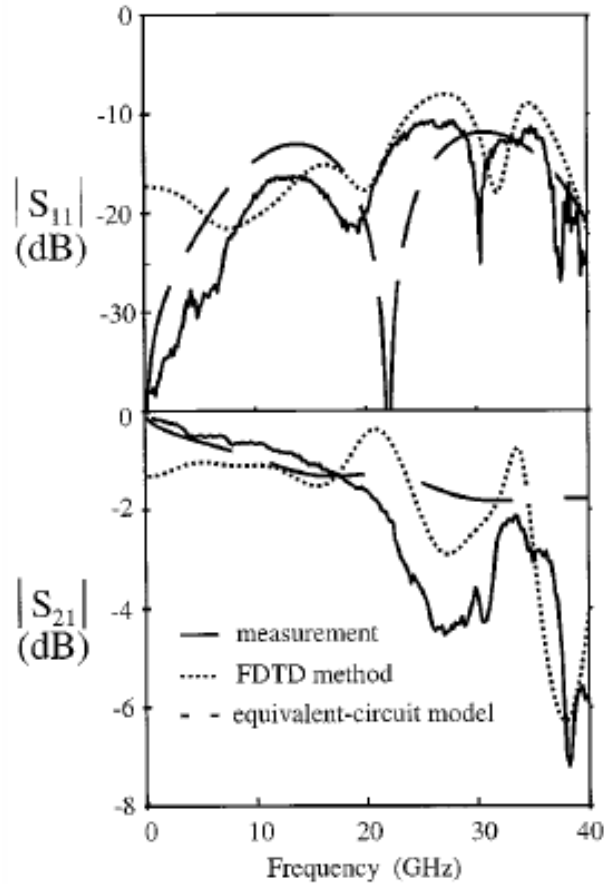


Figure 3.10: S-parameters of back to back CPW to CPS transition with $\theta=60^\circ$ [9]

3.3.1 Coplanar Stripline to Microstrip Transition

The first CPS to microstrip transition that we are going to analyze consist in the utilization of a radial stub. Its layout, under back to back configuration, can be seen in Figure 3.11. The area surrounded by dashed line indicates the presence of the microstrip ground plane.

Note that in the CPS line, the electric field is across the strip conductors and parallel to the substrate; by the contrary, in the microstrip, the electric field is normal to the substrate, thus a rotation of the electric field by 90° is needed. For that end, the radial stub is used. The resonance frequency of the radial stub depends on the radius R and the angle φ . At that frequency, the radial stub provides a virtual short circuit between the CPS strip conductor and the microstrip ground plane. The angle θ , that is, the angle corresponding to the edge of the ground plane, determines the rotation of the electric field.

In this paper, a design for a center frequency of 5.5GHz using RT Duroid 6010 substrate is constructed. The FDTD simulation results, as well as the measurements is shown in Figure 3.12, obtaining a passband between 5.1GHz and 6.1GHz for a return loss below -10dB.

Additionally it has been proven that at the double of the designed frequency, that is, 11GHz,

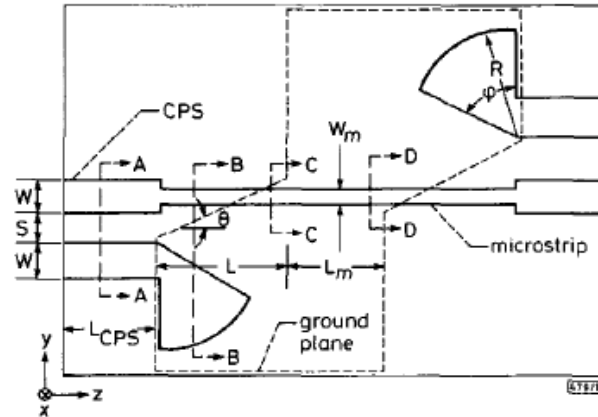


Figure 3.11: Layout of back to back configuration of the proposed CPS to microstrip transition [10]

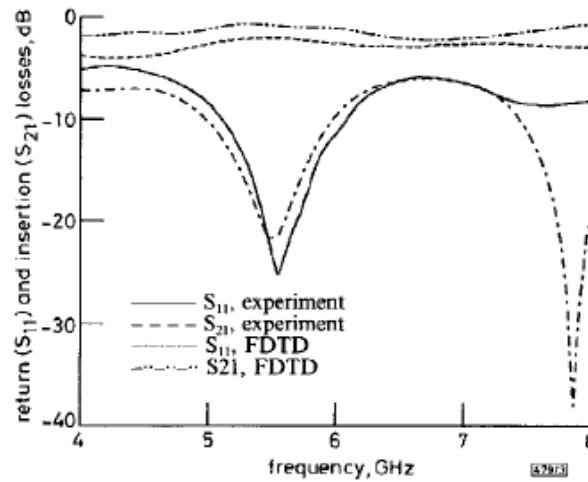


Figure 3.12: FDTD simulation and measurement of back to back configuration of the CPS to microstrip transition [10]

the radial stub behaves as an open circuit, thus the return loss is very high at that point. In conclusion, a CPS to microstrip transition with a relative bandwidth of 18% has been successfully constructed.

3.3.2 A Wideband Microstrip to CPS Transition

The topology of this CPS to Microstrip is very similar to the previous one, which is illustrated in Figure 3.13. The difference is that the designed transition is in reverse order, thus the layout of the back to back configuration is slightly different, specially the ground plane. In any case, the transition principles of this balun is pretty much the same ones.

The rotation angle ϕ , devoted to change the electric field orientation, is optimized as 30° .

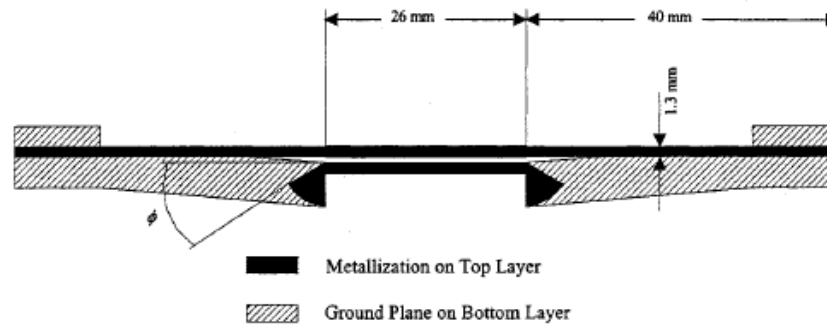


Figure 3.13: Microstrip to CPS back to back transition structure [11]

Since none quarter wavelength transformer is used, wideband performance is achieved, that can be seen in Figure 3.14. The substrate used is RT Duroid 5870, of relative permittivity 2.33 and 20 mil thick.

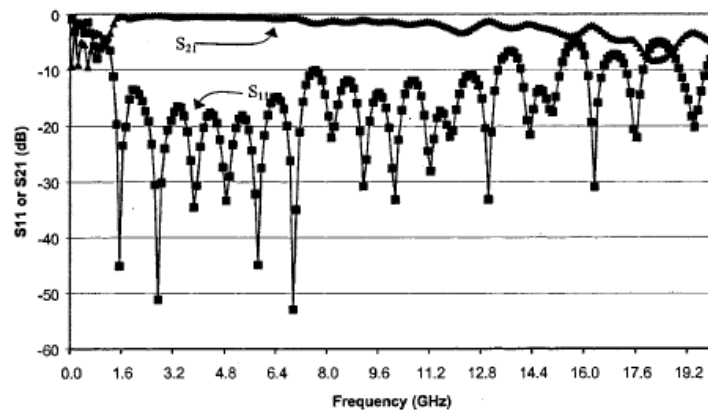


Figure 3.14: Measured return and insertion loss of the proposed transition [11]

The reason of the increase in terms of the bandwidth with respect to the previous transition is likely to be produced by the difference ground planes. Here, a return loss better than 10dB is achieved from 1.3GHz to 13.3GHz, while the 1dB insertion loss is obtained from 1.4GHz to 7.3GHz, both for back to back configurations, which leads to a simple design with great bandwidth of a microstrip to CPS transition.

3.3.3 A Broadband Transition Between Microstrip and Coplanar Stripline

In this paper, the authors try to improve the performance obtained in section 3.3.1 and section 3.3.2. To this end, broadside coupled strips are used instead of the radial stubs, thus the transition area is reduced while broadband response can be achieved. The shape of the overlapping strips is taken over in order to avoid disruption of the strip edge currents. The layout is shown in Figure 3.15, where the overlapping area is highlighted.

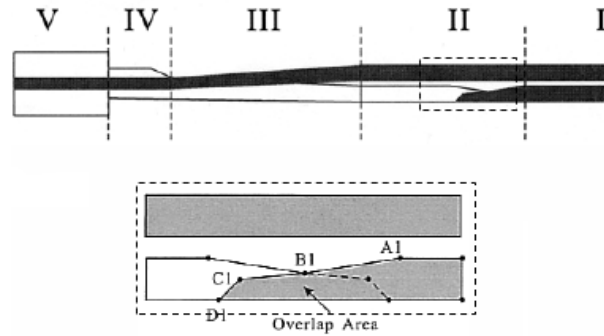


Figure 3.15: Layout of the proposed transition, including a highlighted area [12]

In order to produce a virtual short circuit between the coplanar and the strip continuation to the microstrip ground plane, the overlapping area shown in Figure 3.15 should be large enough to provide the required electromagnetic coupling. However, as most of the current distributes along the edges of the strips, those edges of the both strips have to be trimmed to avoid abrupt discontinuities. Note that the overlapping area is symmetric with respect to the middle.

As it is explained in the previous sections, the key point at a microstrip to CPS transition is to rotate the electric field by 90° , which is performed during section II in Figure 3.15. The section IV also plays an important role, as it tries to concentrate the current distribution in the edges of the strips instead of between the strip and the ground plane. In other words, it guides the edge currents of the CPS to the middle region of the ground plane of the microstrip end. A disruption of the edge currents from part III to part V would imply an increase of the return loss.

A transition for X-band has been designed using Arlon 25N, which has dielectric constant of 3.25 and thickness of 18mil. The simulated and measured S parameters can be found in Figure 3.16.

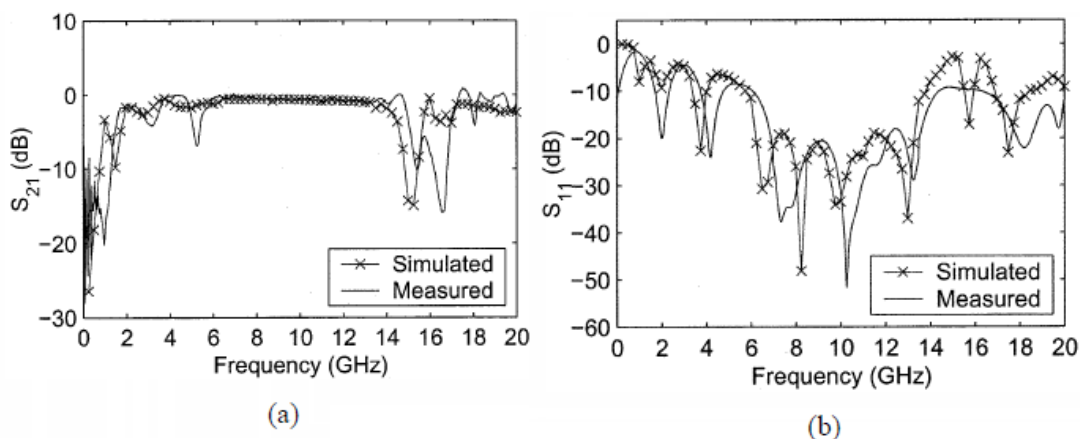


Figure 3.16: Simulated and measured (a) insertion loss and (b) return loss of back to back configuration [12]

The bandwidth corresponding to 1dB insertion loss and 15dB return loss ranges from 6.5GHz to 13.8GHz. It also has been found that the longer is section III, the better return loss of the transition can be achieved, depending on the application requirements to reach the necessary size-performance compromise.

3.3.4 Wideband Microstrip to CPS/Slotline Transitions

One issue that has not been dealt within the previous sections is the one concerning the impedance matching between the different transmission line technologies. To include that feature, a microstrip multisection matching transformer is used. Additionally, a microstrip to slotline transition is proposed.

The problem of the design in section 3.3.3 is that it requires the precise construction of a certain structure at both sides of the substrate (the overlapping strips) and in practice it is not easy at all to fabricate. In this paper, the slots are recurred again. The topology is shown in Figure 3.17, where both rectangular stub and radial stub are compared.

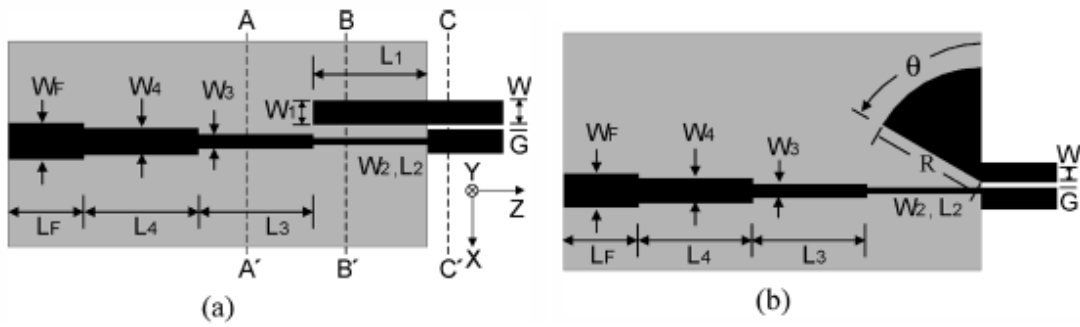


Figure 3.17: Microstrip to CPS transition using (a) rectangular stub (b) radial stub [13]

The transition principle is the same one: by using a quarter wavelength stub, the electric field is rotated by 90°. In Figure 3.18 we can appreciate the resulting electric distribution at each one of the lines marked in Figure 3.17. The purpose of the stubs is to avoid concentrating the total electric field between the strip and the ground plane, or between the two strips. The impedance matching is obtained by varying the width of the strip at the microstrip section.

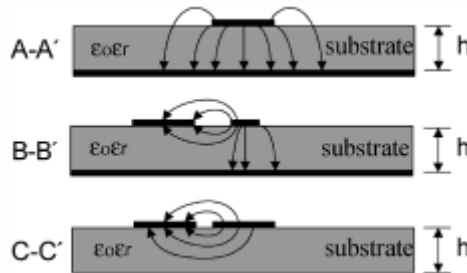


Figure 3.18: Cross section view of electric distributions [13]

The experimental measurements of back to back configuration of the proposed transition, built on a RT Duroid 5870 substrate of 0.508mm thick is shown in Figure 3.19. It has been verified that the optimization of the radial stub allows to obtain a wider bandwidth than the rectangular stub.

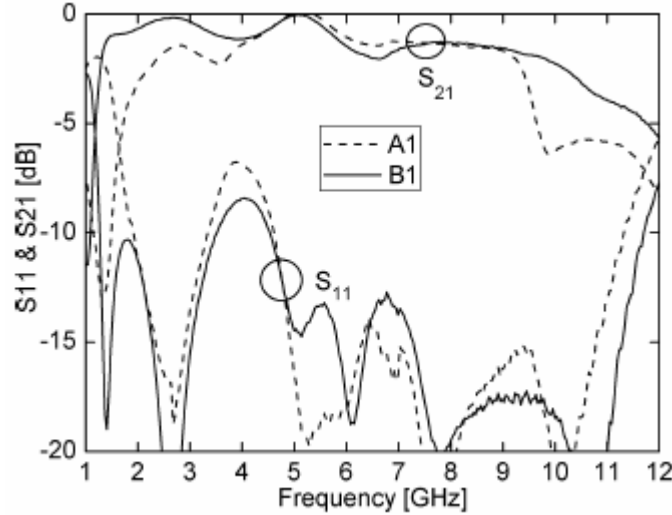


Figure 3.19: Measured S parameters for back to back transition using (A1) rectangular stub and (B1) radial stub [13]

However, there are still parasitic effects and discontinuities thus the transitions constructed fully based on equations can be improved. For this purpose simulations are employed, obtaining an optimized design whose simulation and experimental results can be found in Figure 3.20. Here, an insertion loss better than 3dB is achieved between 1.1GHz to 10.5GHz, of which from 1.4GHz to 6.6GHz the insertion loss is better than 1dB, resulting a much better performance than the non optimized version of the transition.

The microstrip to slotline transition is shown in Figure 3.21. It uses the optimal microstrip to CPS transition as a building block, and using tapered lines it is transformed into slotline topology, while maintaining the gap width. The optimal radial stub is found to be slightly different as the one used for the microstrip to CPS transition. The simulation and experimental results can be seen in Figure 3.22, where an insertion loss better than 3dB is achieved from 2.7GHz to 10.4GHz.

3.3.5 Compact Microstrip to CPS Transition

Finally another microstrip to CPS transition is reviewed briefly, which consists in splitting a microstrip line into two orthogonal paths with an out of phase to form the CPS line. The functionality principle is basically the same one as in section 3.3.3; however, as we can see in Figure 3.23, there is a perpendicular path between the microstrip section and the CPS section, achieving a two pole transmission characteristics. The measured S parameters is shown in

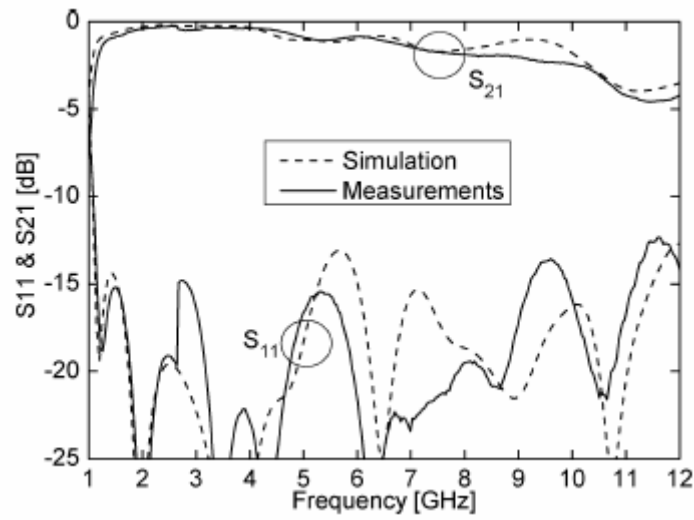


Figure 3.20: Simulated and measured S parameters of the optimal design [13]

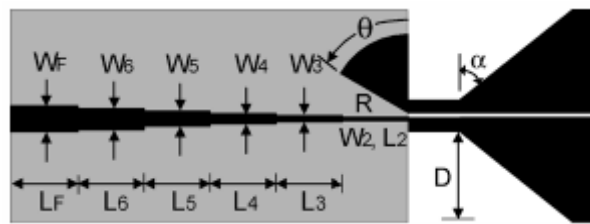


Figure 3.21: Microstrip to slotline transition [13]

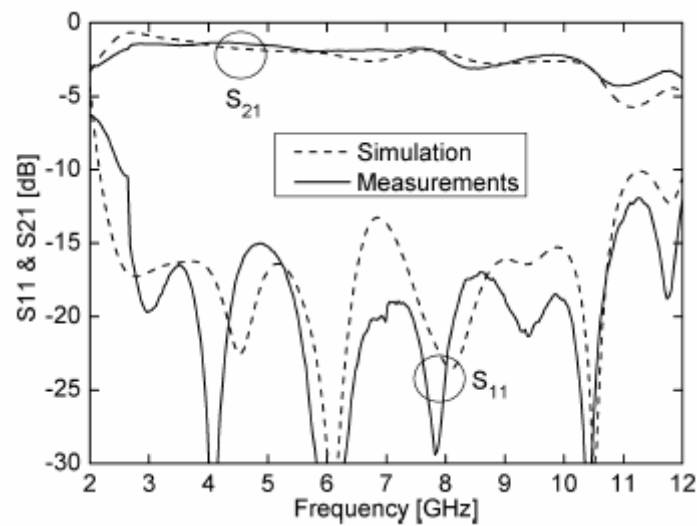


Figure 3.22: Simulated and measured S parameters for microstrip to slotline back to back transition [13]

Figure 3.24, where good transmission performance is obtained from 3.5GHz to 10.0GHz.

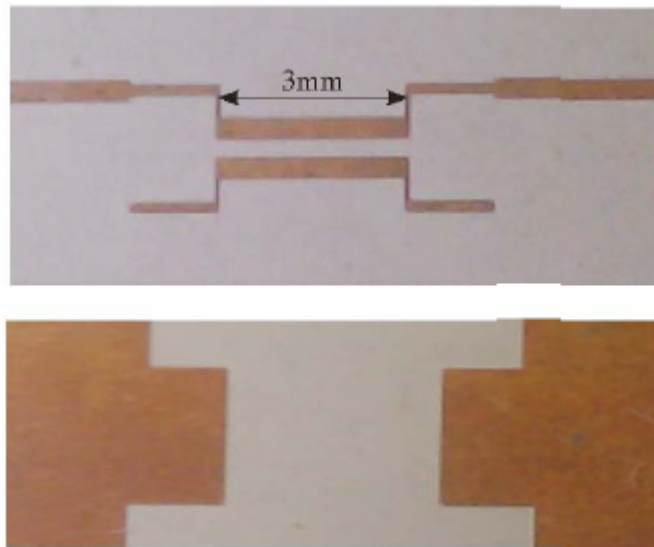


Figure 3.23: Top and bottom view of constructed back to back microstrip to CPS transition [14]

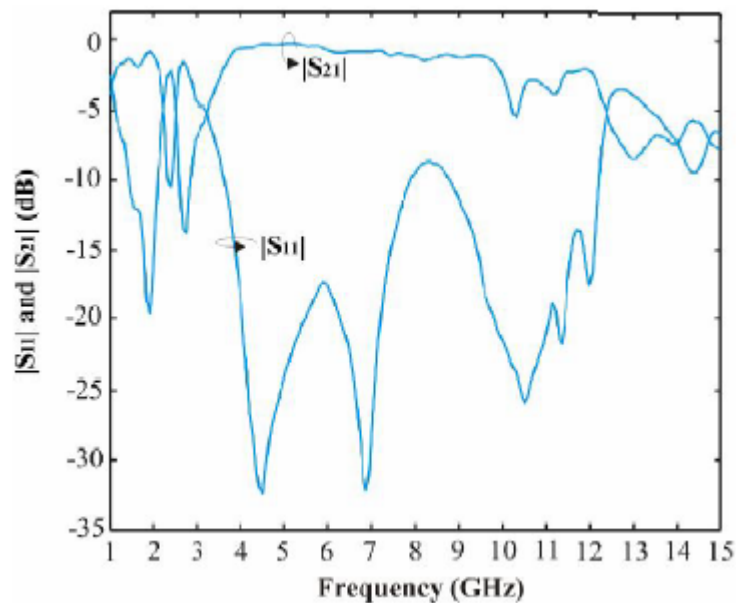


Figure 3.24: Measured S parameters of the transition shown in Figure 3.23 [14]

3.4 Waveguide Transitions

Due to their low loss characteristics, metallic waveguides still have a broad presence in microwave application systems, such as local oscillators or with the use of generators. Since

nowadays most devices are based on planar technologies, such as CPS or CPW, it is very handy to have a waveguide to CPS/CPW/microstrip transition with good performance. In this section, we are going to review through some of them analyzing the different circuitry used.

3.4.1 Microstrip to Waveguide Transition Using Quasi-Yagi Antenna

A microstrip to waveguide transition is proposed using a quasi Yagi radiator, passing through a section of CPS line. The scheme of the transition, including the waveguide, is shown in Figure 3.25, where the key point of the transition, that is, the connection of the CPS Yagi-like antenna to the microstrip line, is shown in Figure 3.26.

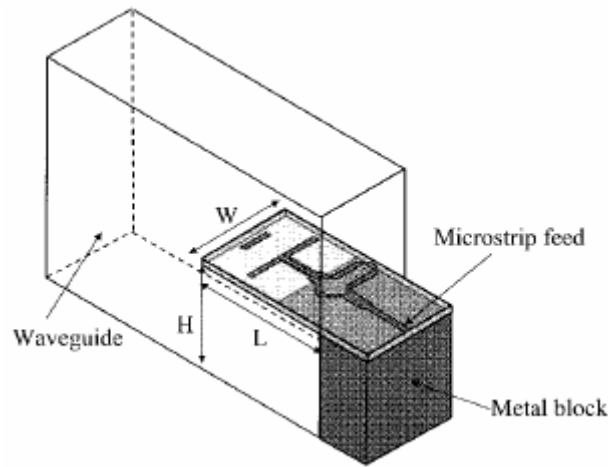


Figure 3.25: Proposed microstrip to waveguide transition [15]

As we can see, the antenna is inserted in the E plane of the waveguide. The ground plane of the microstrip section is in contact with the waveguide, while the other strips are placed apart from it. It is useful to analyze each of the sections of this transition separately.

Regarding the CPS antenna, it consists in a dipole antenna of length $\lambda_d/2$, where λ_d is defined as $\lambda_0/(\sqrt{\epsilon_r} + 1)$. The distance between the dipole and the truncated ground plane is approximately $\lambda_d/4$. As the dipole is aligned in the same direction as the E plane of the waveguide, it is able to excite the dominant mode of the rectangular waveguide, that is, the TE_{01} .

In order to improve the directivity of the antenna, and to prevent problems such as a poor front to back ratio, a shorter dipole element is added as the director of the Yagi antenna, that improves the front to back ratio as well as allowing to obtain a broader operation bandwidth. In this way, a three element Yagi antenna, including a driver, a reflector and a director is obtained.

As for the size and the position of the director, it is found that optimal behavior can be obtained with director length slightly lower than the ones that can be found in conventional Yagi antenna design tables. The same thing happens with the distance between the director and the driver, in order to achieve broadband characteristics. The simulated of the waveguide

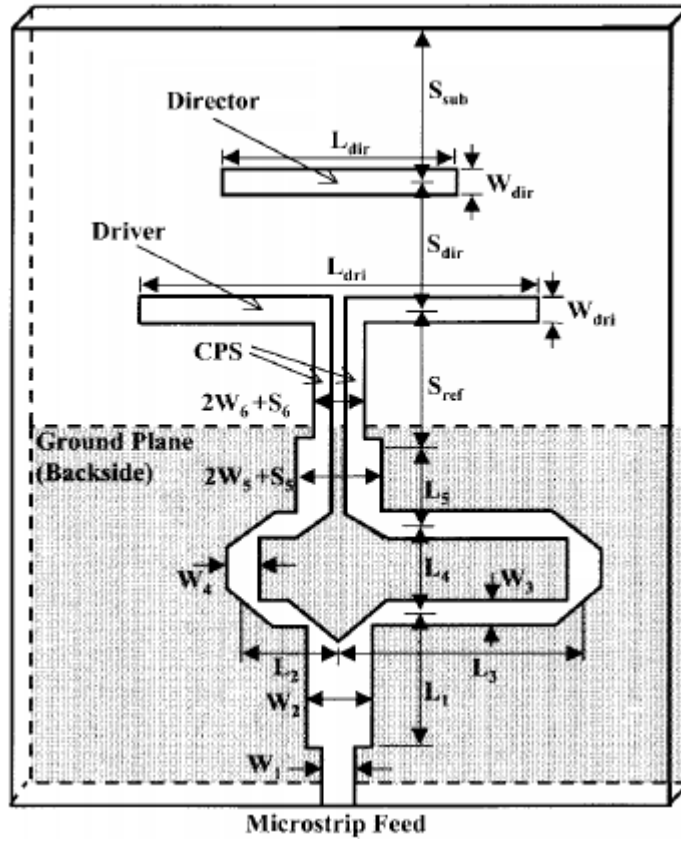


Figure 3.26: Schematic of the quasi Yagi antenna [15]

to CPS transition can be viewed in Figure 3.27.

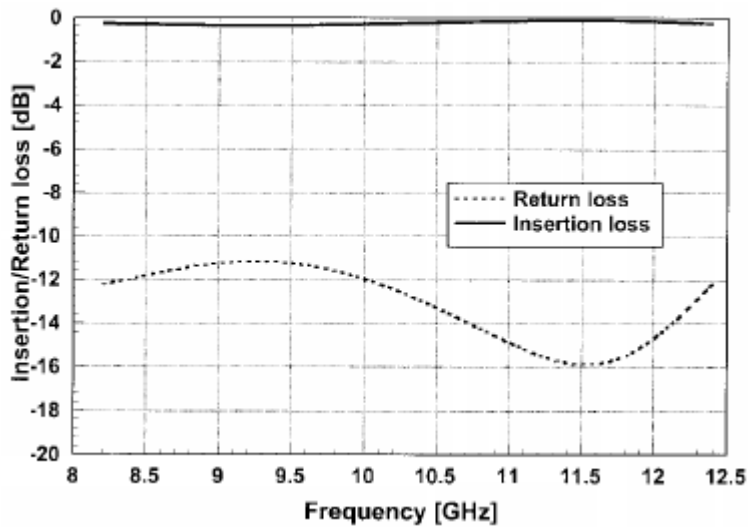


Figure 3.27: Simulated S parameters of waveguide to CPS transition [15]

The microstrip to CPS balun used for this design is different than the ones that we have

reviewed in the previous sections. The circuit in Figure 3.26 is devoted to create a 180° between the two coupled strips. Note that the CPS section can only support mainly odd modes, thus even modes are suppressed thanks to the ground plane and the phase difference.

The measurement results of the proposed transition, constructed over a Duroid substrate with relative permittivity of 10.2 and thickness of 0.635mm, is shown in Figure 3.28. In this case the back to back configuration of the transition is not recurred, but the S parameters is measured using a SMA connector to the microstrip end and a W/G adapter to the waveguide end.

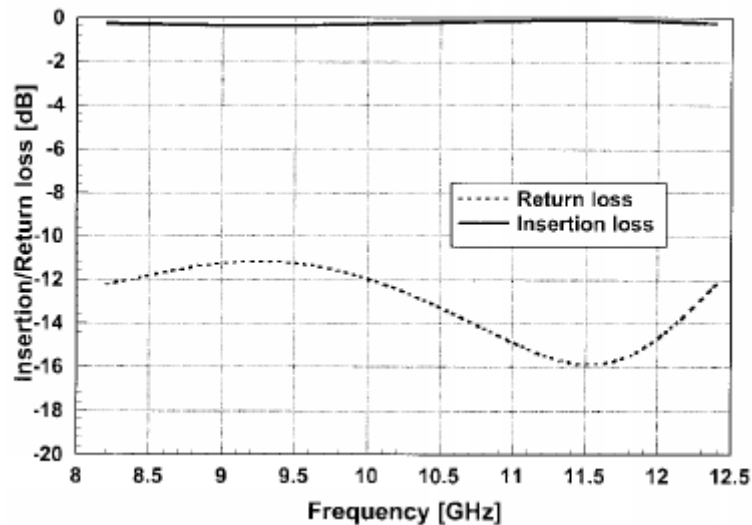


Figure 3.28: Measured S parameters of waveguide to microstrip transition [15]

Here we can see that a good transition performance is achieved over a wide frequency range. From 8 to 12 GHz the return loss is better than 10dB. A return loss better than 12dB and insertion loss better than 0.9dB is achieved over a 39% bandwidth around the center frequency.

3.4.2 CPW to Rectangular Waveguide using Fin-Line Taper

A wideband coplanar waveguide to rectangular waveguide uniplanar transition based on a fin-line taper and fin-line-to-CPW is presented. The overall picture of the complete proposed system can be found in Figure 3.29, while the layout of the transition is shown in Figure 3.30.

The fin-line taper converts the TE_{10} mode of the rectangular waveguide to a unilateral fin-line mode. Different types of fin-line tapers can be applied, such as exponential, parabolic or linear, depending on the obtained performance for a given application. The end of the tappers make contact with the walls of the rectangular waveguide, right in the center where the E-field is at its maximum for the interested propagation mode. Sometimes, specially when high permittivity substrate is used, it might be necessary to use an impedance transformer in front of the taper section, as can be seen in Figure 3.30.

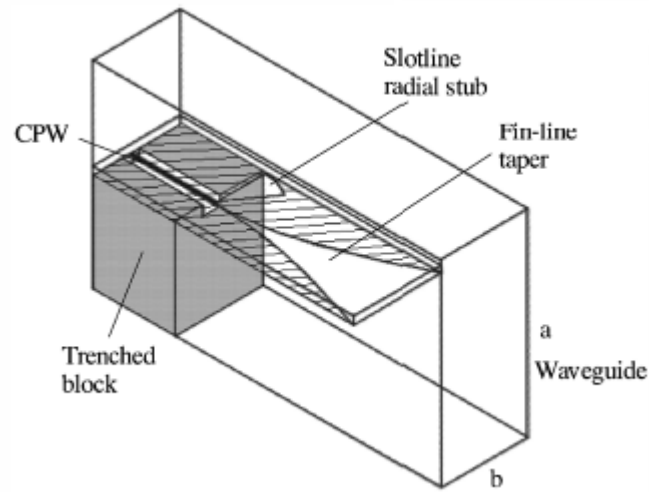


Figure 3.29: Overall picture of the proposed transition [16]

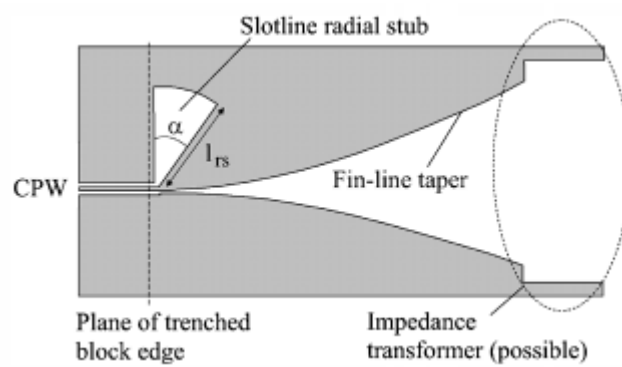


Figure 3.30: Circuit layout of the proposed transition [16]

What is remaining is to transform the fin-line taper into CPW. This can be done using a wideband slotline to CPW transition with a radial stub, after which the coupled slotline mode is suppressed.

The proposed transition, designed for the X-band, is optimized for two different substrates, one of relative permittivity 2.33 and another of 10.8, both under back to back configurations. The simulation results, as well as the experimental measurements, are presented in Figure 3.31.

For the low permittivity substrate, the obtained behavior is quite acceptable over the complete interesting band. However, for the case of the high permittivity substrate, the measured behavior differs from the simulated one. The authors attributes this behavior to their low quality fabrication process. In any case, it has been demonstrated the functionality of the proposed CPW to rectangular waveguide transition, which has as its main advantage its simplicity to design and fabrication, while achieving acceptable performance.

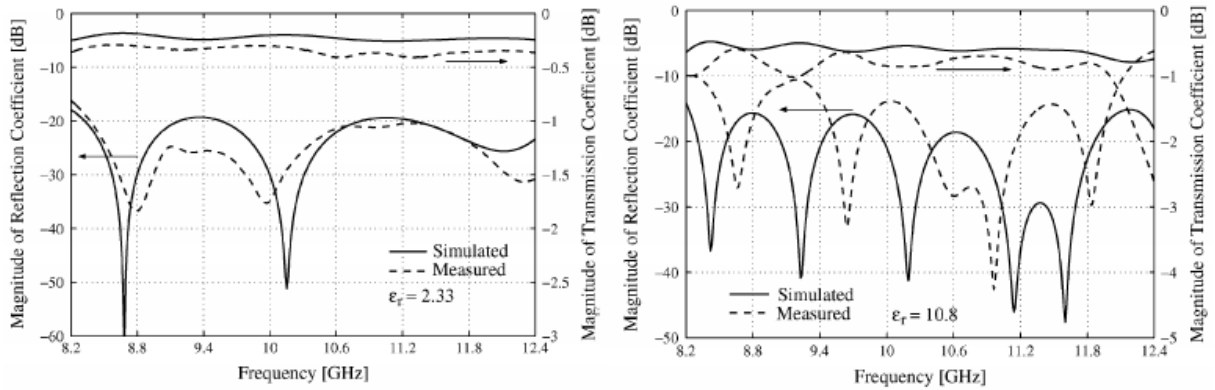


Figure 3.31: Simulated and measured S parameters of CPW to waveguide transition [16]

3.4.3 Wideband CPW to Rectangular Waveguide Transition

The problem of the previous transition is that it makes use of an additional fin-line taper to CPW balun where a radial stub is involved, as well as having a long transition structure. This implies a high loss from one end to another, not to mention that the working bandwidth is also affected by the additional balun. In this paper the authors proposes another version of the request transition, which overall scheme can be found in Figure 3.32. The top view of the transition circuit is shown in Figure 3.33.

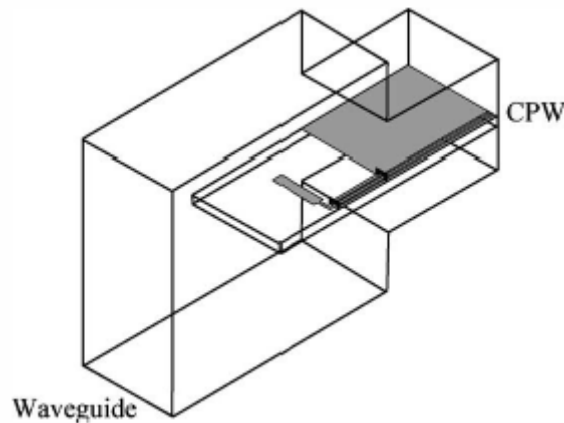


Figure 3.32: Overall view of the proposed CPW to waveguide transition [17]

The TE_{10} mode of the waveguide is coupled to the CPW with a rectangular E-plane probe, situated at the center of the rectangular waveguide. This probe forms 90° with the center conductor of the CPW. The CPW line is introduced inside the rectangular waveguide and placed in conduction with one of the rectangular waveguide walls. The substrate is extended beyond the rectangular probe acting as an impedance transformer between the rectangular waveguide and the probe. The CPW dimensions has to be chosen carefully and to be only slightly asymmetrical

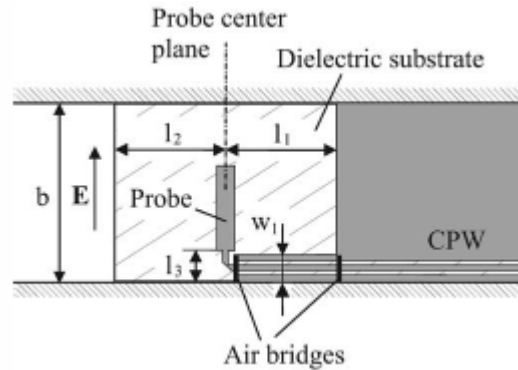


Figure 3.33: Top view of the proposed transition [17]

electrically, considering the undesired effects produced by the waveguide wall.

Even though some theoretical parameters is assigned to the different elements present in the transition, it is always better to run simulations in order to optimize the resulting behavior. Moreover, it is important to note that an undesired mode can propagate in a CPW line: the coupled slotline mode. To avoid this behavior, air bridges are used, as can be seen in Figure 3.33, that connect the side strips of the CPW. One is placed in the end of the CPW and the other one at the short plane.

The transition designed for X band has been constructed over a RT Duroid 5870, under back to back configuration. The waveguide narrowing, that can be seen in Figure 3.32, is used to suppress even more the coupled slotline mode that appears in the CPW. The simulated and measured S parameters is presented in Figure 3.34.

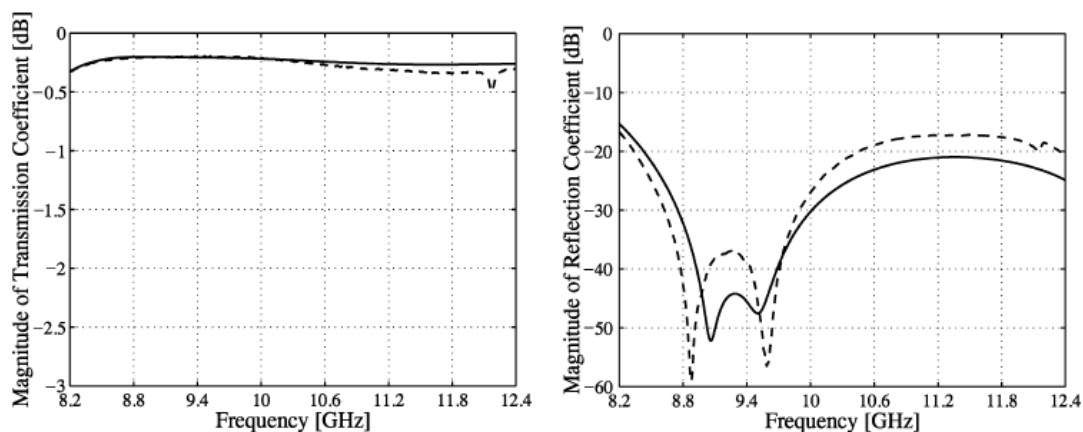


Figure 3.34: S parameters of the proposed transition. Solid: simulated results; Dashed: measured results [17]

An insertion loss less than 0.3dB is measured almost over the whole X band. A small resonance peak can be found at 12.2GHz, where the insertion loss is worsen to 0.5dB. Taking into account that the measurements are done to a back to back configuration of the transition,

real insertion loss of the design is in the range of 0.1dB. In conclusion, a wideband, low insertion loss CPW to waveguide transition design has been demonstrated.

3.5 Conclusion

In this section we have analyzed many microwave transitions. The Wideband Microstrip to CPS/Slotline transition covered in Section 3.3.4 is chosen to implement the required microstrip to CPS transition. One part of the Microstrip to Waveguide Transition Using Quasi Yagi Uda Antenna will be used to design a rectangular waveguide to CPS transition.

In the next chapter, we will aim to design a microstrip to CPS transition.

Microstrip to coplanar stripline transition

4.1 Introduction

In Section 1 we explained the purpose of this whole project, that briefly consists on an heterodyne receiver with a radiating element, that involves a waveguide to microstrip transition with a mixer circuit, as well as IF filtering. To achieve such goal, designing a transition between microstrip transmission line and a coplanar stripline is unavoidable, since there are different technologies available in the project.

The microstrip line is used for implementing the active mixer scheme, as explained in previous sections. The coplanar stripline (CPS) is employed as it offers an easy integration with some of the radiating elements, such as the simple dipole antenna and the Yagi antenna. The Yagi antenna will be used to construct a microwave transition from rectangular waveguide to planar technologies and it will be reviewed in the next chapter.

For the simulation of these microwave elements, we will use the CST Microwave Studio. The circuitry components will be modeled in the software and full-wave electromagnetic simulations will be performed to judge the performance of the implemented solution.

Let us recall the physical properties of the materials that are going to be used to construct the aforementioned transition, listed in Table 4.1:

Conductor type	Copper
Conductor thickness	$17 \mu m$
Substrate relative permittivity	2.2
Substrate thickness	$127 \mu m$

Table 4.1: Component physical properties

The chapter is organized as follows. First, we will go through some coplanar stripline basis. Later on, each one of the steps taken to design the corresponding transition is explained. Finally,

a back to back transition that consists on microstrip to cps to microstrip at 46 GHz is constructed to measure the actual performance of the transition.

4.2 Coplanar stripline theory

The coplanar stripline (from now on CPS) is a planar microwave technology that consists of two parallel strip conductors laid on a dielectric substrate and separated from each other. It presents advantages such as the possibility of series and shunt mounting of devices, and being a balanced transmission line. It is ideal for implementing feeding networks of balanced antennas, such as dipoles or LTSAs. However, it has a main drawback. In absence of a ground plane, CPS supports, besides the fundamental CPS mode, other two parasitic modes, one TE_0 and one TM_0 , which do not have cut off frequency [18]. The electric field of the fundamental mode of the CPS is perpendicular to the striplines and suffers interference from the TE_0 parasitic mode.

There exist several implementations of CPS, each one with its own layout and transmission characteristics. Only the most basic one is discussed here, which consists on two identical striplines on a homogeneous dielectric substrate of finite thickness. A cross section is shown in Figure 4.1, where all the relevant parameters are displayed.

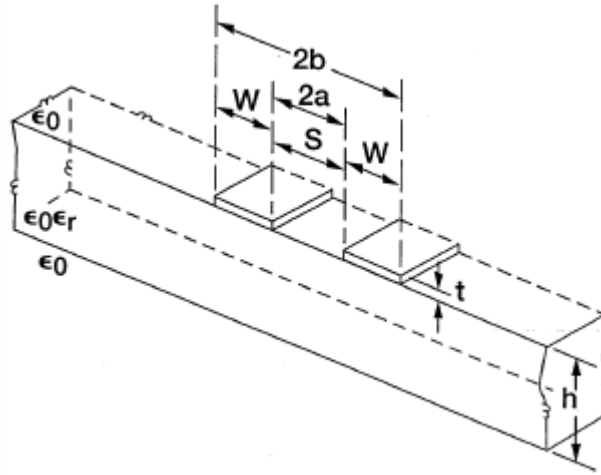


Figure 4.1: Cross section of a standard CPS line [18]

The width of each one of the conductor striplines is W and S denotes the gap between the two strips. The fundamental propagation mode is the quasi-static TEM mode. The effective dielectric constant is given by the following expression [18]:

$$\epsilon_{eff}^{CPS} = 1 + \frac{1}{2}(\epsilon_r - 1) \frac{K(k)}{K(k')} \frac{K(\kappa')}{K(\kappa)} \quad (4.1)$$

In which K is the complete elliptical integral of the first kind:

$$K(k) = \int_{\pi/2}^0 \frac{d\theta}{\sqrt{1 - k^2 \sin^2 \theta}} \quad (4.2)$$

k, k', κ and κ' are defined respectively as [18]:

$$k = \sqrt{1 - \left(\frac{a}{b}\right)^2} \quad (4.3)$$

$$k' = \sqrt{1 - k^2} = \frac{a}{b} = \frac{S}{S + 2W} \quad (4.4)$$

$$\kappa = \sqrt{1 - \frac{\sinh^2(\pi a/2h)}{\sinh^2(\pi b/2h)}} \quad (4.5)$$

$$\kappa' = \sqrt{1 - \kappa^2} \quad (4.6)$$

The phase velocity and the characteristic impedance would be [18]:

$$v_{ph}^{CPS} = \frac{c}{\sqrt{\epsilon_{eff}^{CPS}}} \quad (4.7)$$

$$Z_0^{CPS} = \frac{120\pi}{\sqrt{\epsilon_{eff}^{CPS}}} \frac{K(k')}{K(k)} \quad (4.8)$$

Figure 4.2 represents the relationship between the characteristic impedance and the factor defined as $S/(S + 2W)$, where the normalized substrate h/b is also a conditioning parameter. As we can see, CPS lines generally have high impedances, that should be kept in mind when working with such transmission lines.

4.3 CST set up

Before getting into the transition design, there are two issues regarding the CST software that should be analyzed beforehand: CST mesh specification and CST waveguide port definition.

4.3.1 CST mesh specification

When a certain component is defined within CST microwave studio, the software generates a set of mesh cells to represent the corresponding electromagnetic structure, that is used for system simulation. The greater is the density the generated cells, the better should be the quality of the simulation results. However, one should remind that as the number of created mesh cells increases, the complexity of the simulation arises as well, meaning that more computational power will be required.

In this way, the generation of the mesh cells should be taken into account so as to have enough simulation quality (in other words, to ensure that the obtained simulation results are

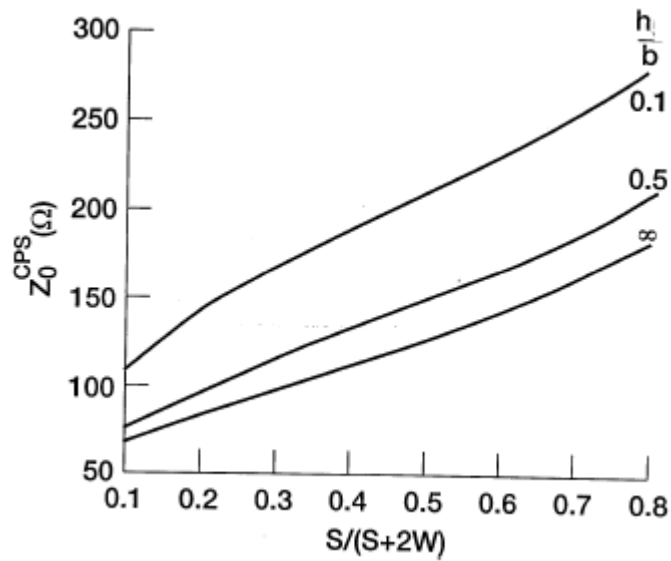


Figure 4.2: Characteristic impedance of CPS as a function of S and W [18]

reliable and consistent), while avoiding an excessive number of mesh cells that slows down the simulation process.

For this reason, a parametric sweep varying the cell generation parameters had been launched. The results for the return loss of a not optimized microstrip to CPS transition are shown in Figure 4.3.

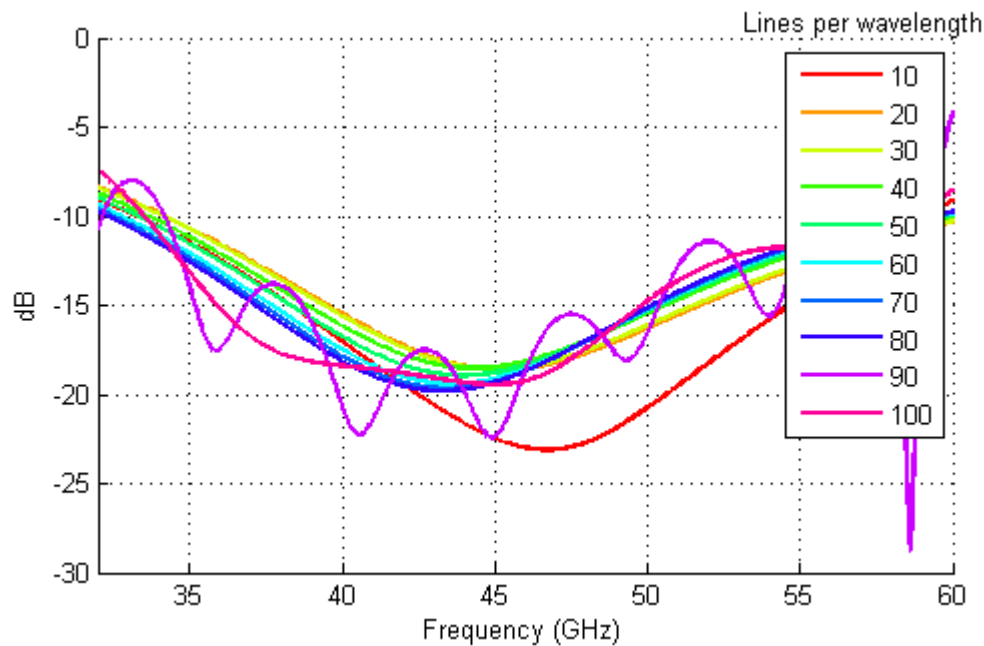


Figure 4.3: Return loss varying mesh configuration

It is easy to notice that the simulation results depend on the mesh settings. As we can see, at lower mesh definitions, specially when only 10 or 20 lines are generated per wavelength, the simulation results are very susceptible to the mesh configurations and, thus, to the number of generated cells. At medium mesh definitions the obtained curves seems to converge, while still small variations can be appreciated. For very high mesh settings, sometimes it happens that modeling an excessive number of cells leads to instability in the simulation results.

A compromise is made between the simulation quality and the required computational power. The settings used can be found in Table 4.2. Lines per wavelength defines the minimum number of mesh lines in each coordinate for a distance equal to the wavelength corresponding to the highest simulation frequency. Lower mesh limit defines the maximum mesh step to be used for the mesh creation. Mesh line ratio limit forces the automesh module not to surpass a certain ratio between the minimum and maximum distance between mesh lines.

Lines per wavelength	40
Lower mesh limit	20
Mesh line ratio limit	20

Table 4.2: Mesh properties used in CST microwave studio

With the configuration above, roughly 400 thousand mesh cells are generated for a standalone CPS to microstrip transition, and around 2.5 million cells for the complete rectangular waveguide to microstrip transition. This allows a much more reasonable computation time while performing simulations.

4.3.2 CST waveguide port definition

Once it has been defined the electromagnetic structures in software, their behavior has to be analyzed, for which simulations are performed. Generally, what we want to obtain and analyze from the simulation results is the S parameters of the defined structure. S parameters usually refers to the transmission properties between certain ports (one or more), which has to be specified within the software yet.

In CST microwave studio, defining waveguide ports is a flexible way to specify where the ports are supposed to be measured. By establishing different sizes of the waveguide port, a wide range of microwave technologies can be simulated. For instance, for a microstrip transmission line, the recommended port size is registered in the manual of the CST program. In this project, we will use, for the microstrip side, a waveguide port of the same width as the substrate along with a height that is 6 times the thickness of the substrate.

However, there is not recommended port size for CPS lines. To ensure that the obtained simulation results are consistent, we will have to find out the correct waveguide port definition for the CPS lines. For this end, a parametric sweep regarding the port size has been launched.

The result for the port impedance of a CPS line is shown in Figure 4.4. The size of the port is initially set as Table 4.3, and varied to $\pm 0.2\text{mm}$ both vertically and horizontally.

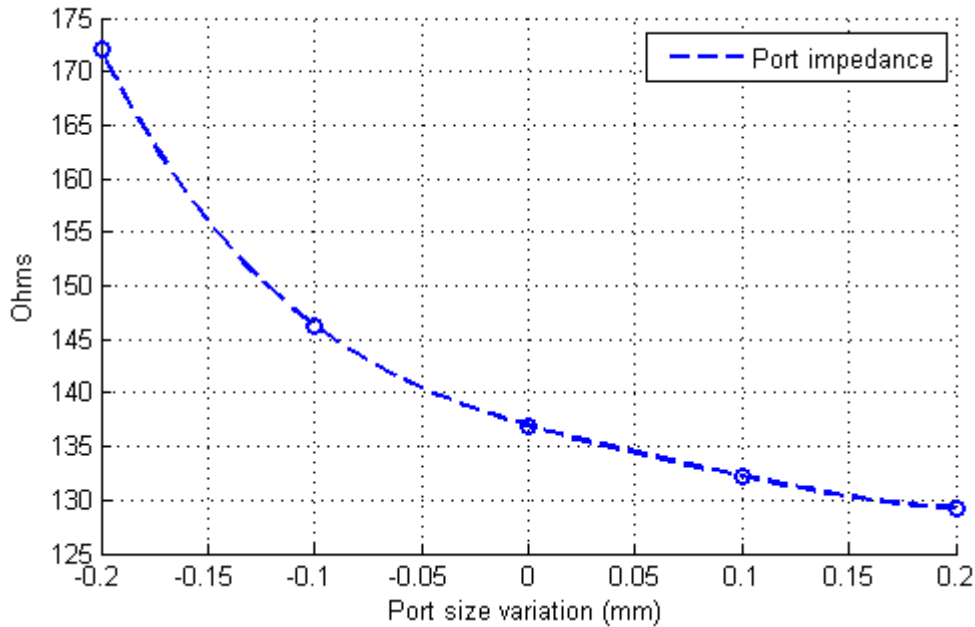


Figure 4.4: Calculated port impedance varying its size

Basically, the bigger is the defined waveguide port, the smaller is the port impedance calculated by CST microwave studio, although the relation is not linear but converges as the port size increases. The criterion to select the waveguide port size is the one for which an increase on the port size does not translate to a noticeable change in the port impedance. The resulting waveguide port size for a CPS line is:

Port width	4 times the width of a conductor strip
Port height	0.7 mm

Table 4.3: Selected waveguide port size

4.4 CPS parametrization

As stated in Section 4.2, the characteristics of a CPS line depends on its parameters, mainly the width of the strip conductor and the gap between the two strips. While the transmission properties are usually acceptable, the line impedance strongly depends on these two aforementioned elements. Before hurrying up into the design of the proposed transition, we should define the dimensions of the CPS to be used.

For this reason, simulations have been launched to observe the dependence of the transmission line impedance when varying the parameters. A parametric sweep regarding the conductor width W , as seen in Figure 4.1, is shown in Figure 4.5. The counterpart, varying the gap between the two conductors, S , is shown in Figure 4.6.

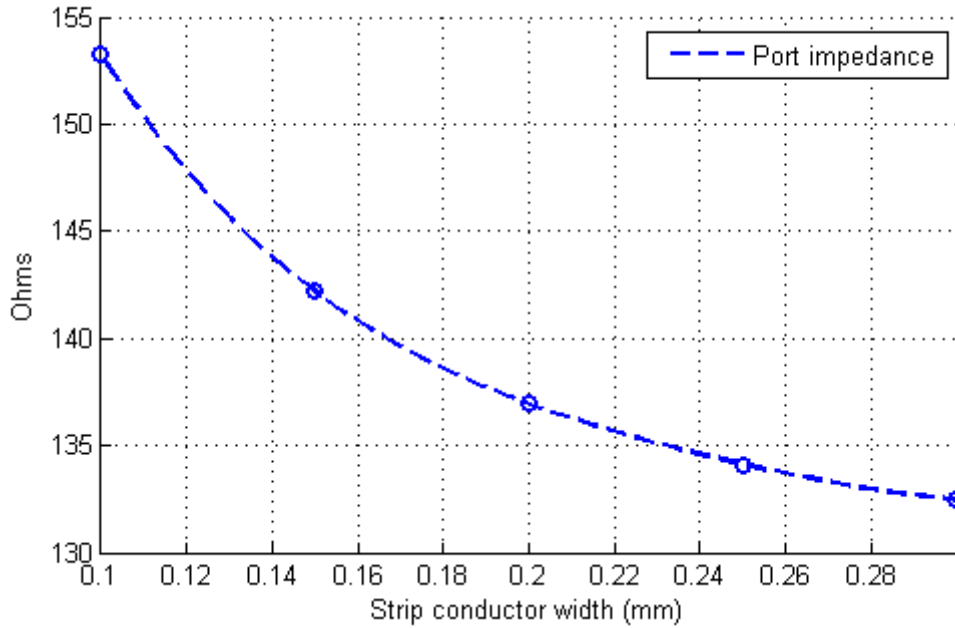
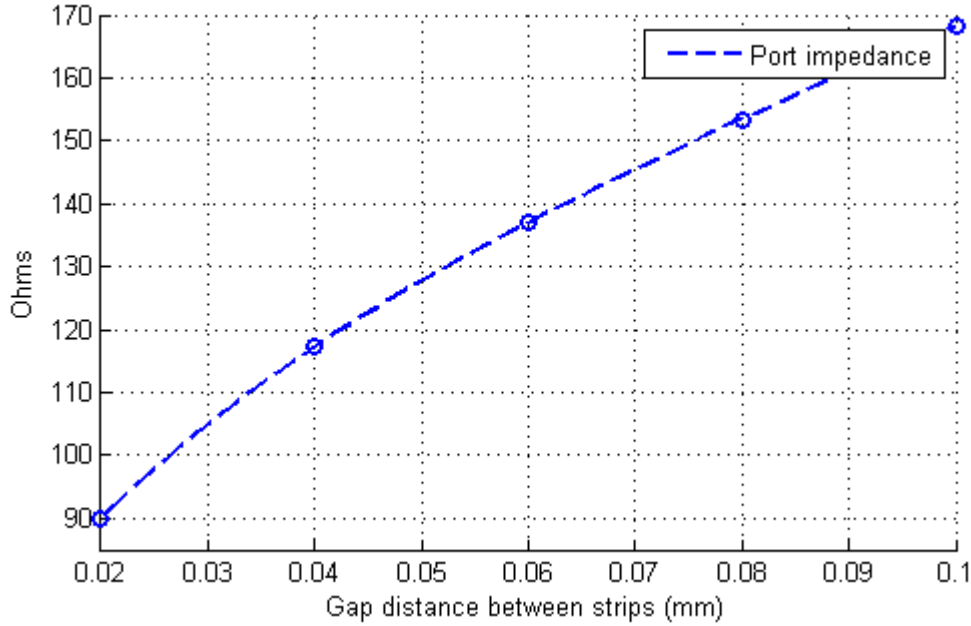


Figure 4.5: Variation of W , fixing S to 0.06 mm

As we can see, the line impedance is inversely proportional to the width of the conductors and to the separation between them. In the active element circuitry, we have worked with reference impedances of 50Ω , thus we are interested in using a CPS line with a low impedance. However, there are two constraints that we have to take into account:

- The maximum width of the substrate and hence the circuitry on it is restricted to 2.8448 mm, due to the inner dimensions of the rectangular waveguide WR22. Therefore, the width of the CPS line should be limited to something narrow compared to the maximum width.
- There are also constraints in the fabrication, as the thinnest laser beam available in the labs is $50 \mu m$ width. For this reason, the gap between the two strip conductors, S , cannot be less than 0.05 mm.

It is clear then, that a compromise between the line impedance and the CPS parameters has to be made to fulfill all the requirements. Table 4.4 shows the final result.

Figure 4.6: Variation of S , fixing W to 0.20 mm

Strip width W	0.02 mm
Gap S	0.06 mm
Line impedance	136 Ω

Table 4.4: Selected CPS parameters

4.5 Microstrip to CPS transition

In the previous Chapter, we have already discussed several microstrip to CPS implementations. The transition presented in Section 3.3.4 [13], with a rectangular stub, is chosen to be used. Figure 4.7 indicates the overall view of such transition, where the gray area represents the ground plane of the microstrip.

The main reasons for picking this implementation of microstrip to CPS transition resides in its simplicity, both in the design stage as well as in the fabrication process. In Section 3.3 there were many other transition implementations that possess greater complexity or require precise beaming at both sides of the substrate.

In Figure 4.7 we can see that the transition mainly consists of two parts: a quarter wavelength rectangular stub in CPS and a multi section impedance transformer under microstrip topology.

The purpose of the open circuit quarter wavelength rectangular stub is to make the microwave field lines to concentrate in the other strip line and passing to the microstrip section, instead of continue propagating in the way a CPS line does. It behaves like a ground connection in the frequency of interest, hence reflecting all the incident power.

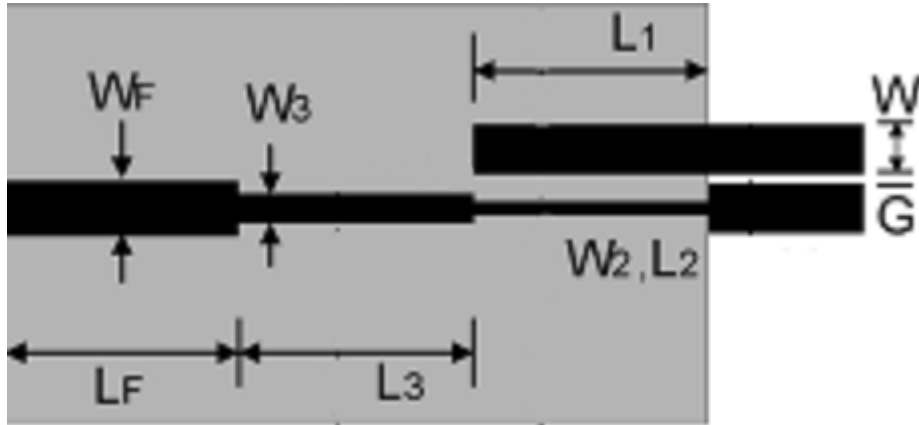


Figure 4.7: Microstrip to CPS transition using a rectangular stub [13]

In [15] we can find an approximation to the expression of the wavelength for the CPS technology, which is $\lambda_0/(\sqrt{\epsilon_r} + 1)$. Using this formula, the equivalent wavelength at 46 GHz, which is the interested frequency for the transition, is 2.6263 mm. In this way, a theoretical quarter wavelength stub should be 0.6566 mm long.

As for the multi section impedance transformers, there are several possible implementations. In this project, we are going to use a quarter wavelength Chebyshev transformer of one section, whose equivalent circuit can be found at Figure 4.8. The impedance Z_1 will take the value of $\sqrt{Z_0 Z_L}$, where Z_0 is the impedance of the microstrip, 50 Ω , and Z_L the impedance of the CPS, which were found to be about 136 Ω in Section 4.4. Only one section is used mainly to reduce the total length of the transition, as it will result beneficial when integrating with the rectangular waveguide.

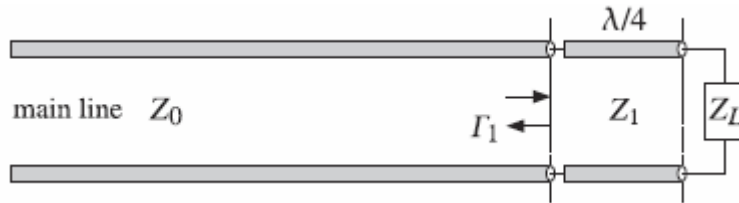


Figure 4.8: One section quarter wavelength Chebyshev impedance transformer [19]

In Figure 4.7 we can appreciate how the multi section impedance transformer is implemented under microstrip. The thinnest section, with width W_2 , will have the same impedance as the CPS line, while the section with width W_F will be of 50 Ω , so as to connect later with the active element circuitry. The section of width W_3 will be of impedance $\sqrt{136 \times 50} = 82.4621\Omega$.

The microstrip width corresponding to these impedances are again obtained using the TX-Line tool of AWR Microwave Studio. The equivalent quarter wavelength can also be obtained using this tool. The theoretical values for the parameters shown in Figure 4.7 can be found in the following table (actually the value of L_F is irrelevant):

W	0.200 mm
G	0.060 mm
L_1	0.657 mm
W_2	0.035 mm
L_2	1.270 mm
W_3	0.151 mm
L_3	1.225 mm
W_F	0.375 mm
L_F	1.000 mm

Table 4.5: Theoretical Microstrip to CPS transition parameters

However, these are merely theoretical values and must be verified and adjusted in simulations. One possible factor of error is that the assumed Z_L is the one of the CPS line. In reality, the transition is done between a microstrip line and one of the strips of the CPS line, therefore the actual impedance that should have the microstrip line of width W_2 and length L_2 might be different from the one stated in Table 4.5, hence the middle section of the impedance transformer would have the same problem.

For this reason, numerous parametric simulations about each one of the relevant parameters of the transition (that are L_1 , W_2 , L_2 , W_3 and L_3) have been done. With the objective of achieving a low insertion loss at the frequency of 46 GHz, as well as good return losses at both ends of the transition, the values for all the parameters have been chosen. A fine adjustment involving all the parameters were done to optimize as much as possible the obtained S parameters. The optimized values are shown in Table 4.6.

L_1	0.730 mm
W_2	0.060 mm
L_2	0.630 mm
W_3	0.220 mm
L_3	0.640 mm

Table 4.6: Optimized Microstrip to CPS transition parameters

The modeled layout of the proposed transition can be seen in Figure 4.9, where the size of the two ports are also shown. A ground plane is in the backside, covering all the microstrip region. The blue line on the figure indicates the boundary from which, at its right side the ground plane is present.

The S parameters are shown in Figure 4.10. As we can see, it provides good matching at 46 GHz in both ports, as well as good transmission parameter. The main features are listed in

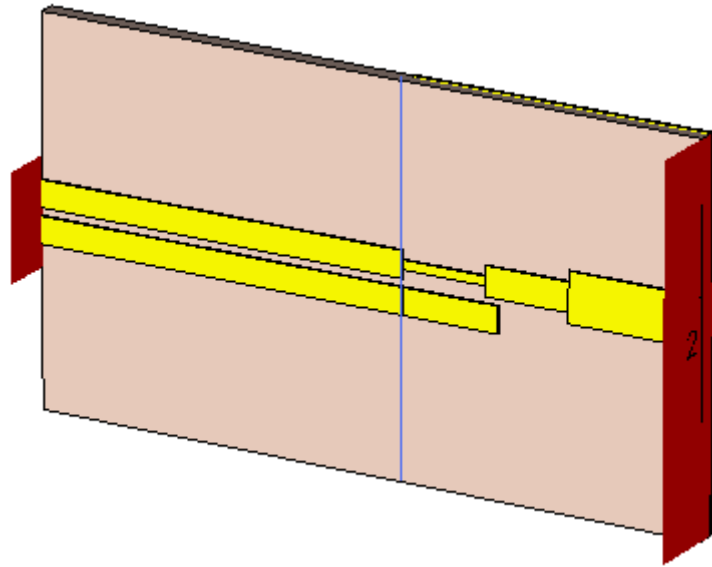


Figure 4.9: Microstrip to CPS transition

Table 4.7.

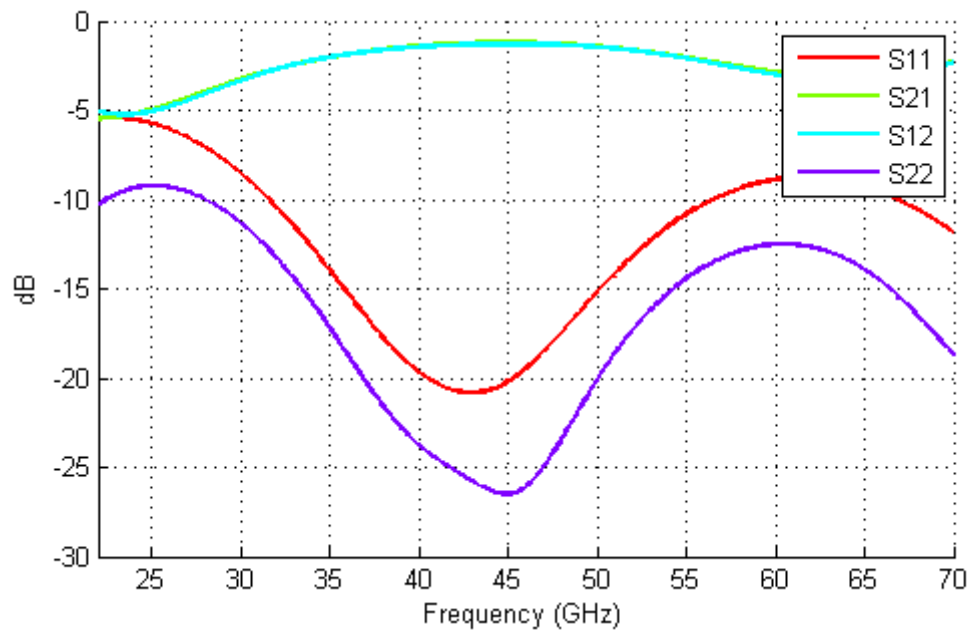


Figure 4.10: Simulated S parameters of Microstrip to CPS transition

The convention for the bandwidth is to have an insertion loss better than 3 dB at the same time of having return losses lower than -10 dB.

Insertion loss at 46 Ghz	1.25 dB
Microstrip return loss at 46 Ghz	-26.09 dB
CPS return loss at 46 Ghz	-19.48 dB
Bandwidth	25 GHz (from 31 GHz to 56 GHz), 57.47%

Table 4.7: Microstrip to CPS transition

4.6 Back to back transition

It is interesting to perform physical measurements to verify the real performance of the designed microstrip to CPS transition. However, there is no direct way to connect a CPS line to a network analyzer since the required CPS probes are not available in the laboratory. For this reason, what we are going to do is to construct a back to back transition, where the both ends are of microstrip technology. In this way, ports can be mounted easily at both ends of the back to back transition and the connection to the network analyzer would be straight forward.

The back to back transition is obtained by simply mirroring the designed transition of Section 4.5. First we will simulate only the back to back transition, in order to check if the transition behavior is still correct. The transition layout is shown in Figure 4.11, and the corresponding results in Figure 4.12. In appendix A we can find detailed layouts of the back to back transition.

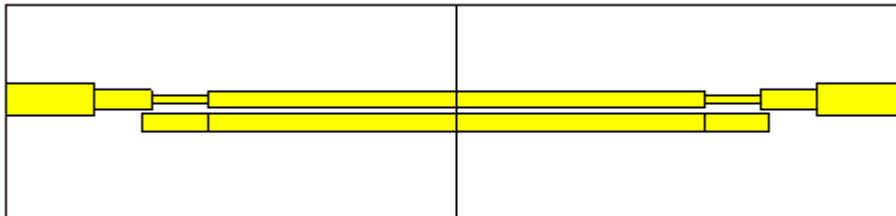


Figure 4.11: Back to back topology of Microstrip to CPS transition

The transition still works well over a wide range of frequencies. However, the circuitry shown in Figure 4.11 is not the real one, as more space should be left in the back to back transition for the allocation of physical ports. It would be interesting to simulate the actually physical structure that is going to be constructed. The used port is the RPC-2.40 RIGHT ANGLE JACK PCB from Rosenberger, that theoretically works up to 50 GHz. It is physically very big in comparison with the designed transition. Since the ports should be clipped to the substrate, a much bigger substrate should be employed instead of the one of Figure 4.11. For this reason, the length of the $50\ \Omega$ microstrip section has been extended from 1 mm to 10mm. The resulting scheme can be seen in Figure 4.13, where the ports are also modeled physically so as to indicate the dimensions of the ports with respect to the ones of the transition.

One realizes at the first glance that the ports are actually much bigger than the transition itself. This introduces a set of undesired behaviors and will affect negatively to the quality

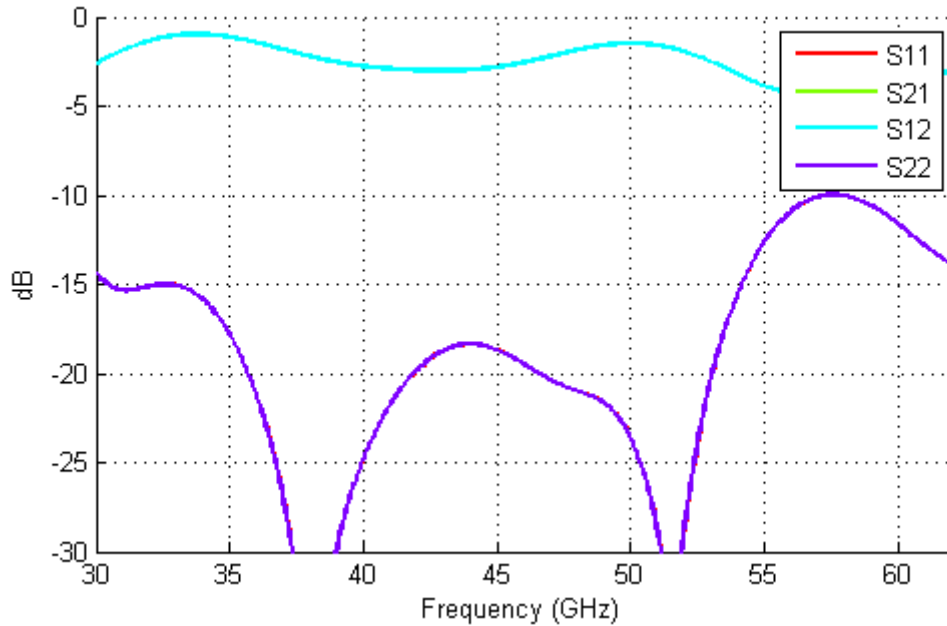


Figure 4.12: Simulated S parameters of back to back Microstrip to CPS transition

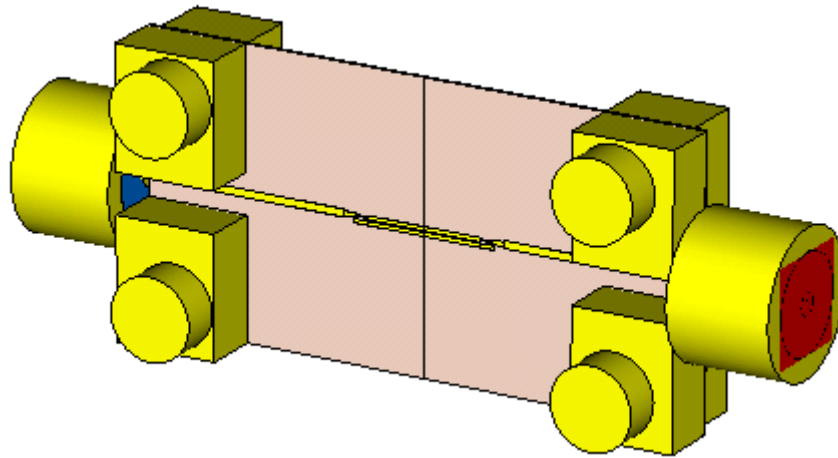


Figure 4.13: Back to back topology of Microstrip to CPS transition with ports

of simulation, mostly due to incorrect mesh generation. In addition, the distance between the two ground connectors of the port is 2 mm, which is something close to the wavelength around the frequency of interest. Resonance may appear in the ports influencing the behavior of the transition.

In Figure 4.14 we can appreciate how the fabricated back to back transition looks like. As the substrate is extremely thin, a thicker substrate had to be placed below the ports in order to avoid any stress that can be applied in the transition. In fact, the model had been constructed several times as the substrate is often wrinkled and the strips did not have flat shape. Note that

the thicker substrate is not in contact with the dielectric of the transition, but works only as a support.

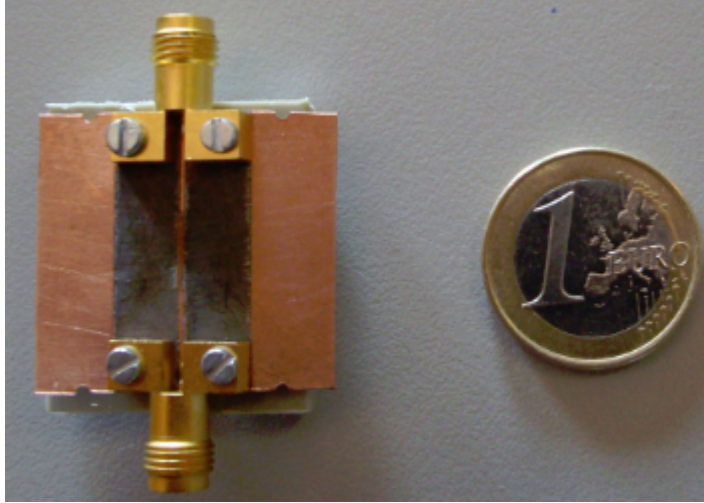


Figure 4.14: Back to back topology of Microstrip to CPS transition

Additional copper layering were deployed in the sides of the transition to give more consistency to the entire structure. The measured insertion loss and return loss, along with the simulation results of Figure 4.13, are shown in Figure 4.15.

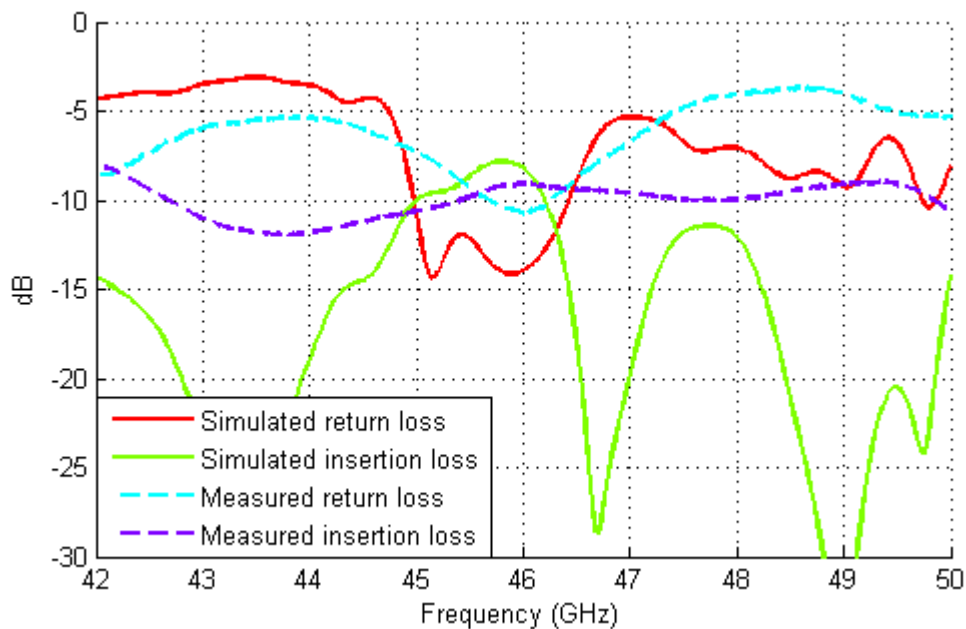


Figure 4.15: Simulated and measured S parameters

The return loss, both simulated and measured, take pretty much the same order, being above -10 dB but for frequencies around 46 GHz. The simulated insertion loss has a lot of variations,

while the measured one is much more stable. The simulated insertion loss is around 8 dB with its corresponding measured value degraded to around 9 dB.

A wide range of reasons can explain the encountered performance degradation, specially the undesired behavior that might have been introduced with the much bigger ports. The additional support and copper layers in the constructed prototype also contributes to a deterioration of the designed transition. In any case we can see how the transition is well matched at 46 GHz, and a relatively poor insertion loss probably due to the ports used. It might result interesting to perform simulations only with the ports and a microstrip line, just to verify their influence in the propagation of signals.

4.7 Dipole prototype

In order to check the functionality of the proposed microstrip to CPS transition, we are going to integrate a radiating element to analyze how does it behave. A dipole is one of the simplest antenna topologies that can be found. It offers the advantage of easy design process (the dipole length is basically the only parameter to be adjusted) and it can be directly connected to a CPS line.

In this way, a dipole antenna has been directly attached to the designed microstrip to CPS transition. In Figure 4.16 we can see an example of the physical view of that structure. The length of the CPS line is the same one as in the transition prototype, that is, 2.8 mm. Extra substrate is added to both ends of the dipole to avoid field discontinuity at those points.

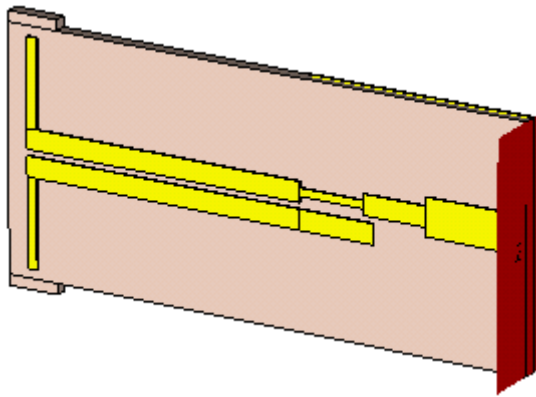


Figure 4.16: Physical overview of a dipole antenna attached to the proposed microstrip to CPS transition

The CPS line has a quite high impedance while $\lambda/2$ dipole offers a much lower impedance. In order to achieve impedance matching, we can increase the dipole length until achieving the desired impedance, thus actually matching is not a problem. As the transition works around 46 GHz, the intention is to achieve a good radiation pattern along with a low return loss at the same frequency. However, for the circuit of Figure 4.16 the obtained radiation pattern is shown

in Figure 4.17.

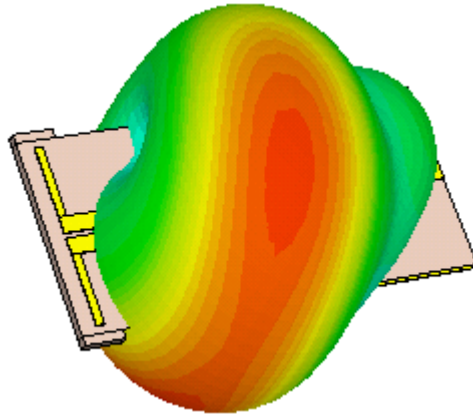


Figure 4.17: Radiation pattern for the circuit in Figure 4.16

The structure does not radiate in a broadside shape at all. Several simulations were launched to locate the source of this undesired effect, isolating each one of the elements present to find out which one is distorting the radiation pattern of the dipole. It was found that the ground plane of the microstrip was affecting the default radiation pattern of the dipole and producing the strange behavior that can be seen in Figure 4.17.

A solution to this problem is to vary the distance between the dipole and the ground plane of the microstrip line, hence varying the length of the CPS line. We can see the evolution of the radiation patterns in the E plane cut, in Figure 4.18, and H plane cut, in Figure 4.19, varying the length of the CPS from 1 mm to 2 mm in steps of 0.2 mm.

According to the graphs, if the length of the CPS line is too short, the radiation pattern of the structure in the broadside direction is very poor and its main lobe is located elsewhere. As the length of the CPS line increases, the radiation pattern is improved in the sense that the dipole radiates a nicer beam in the opposite direction to the ground plane.

It was found that the best radiation pattern corresponds to the case where the CPS line is 1.6 mm long, where the main lobe has minimum beam width in both E and H planes and has maximum amplitude in the broadside direction.

As for the length of the dipole, it was found that to achieve the best matching around 46 GHz, the length of the dipole should be around 3.1 mm. In Figure 4.20 we can find out that the return loss at 46 GHz is around -22 dB. The bandwidth is not very broad, as the reason resides in the fact that a dipole is not a broadband device. Still, an return loss better than -10 dB can be achieved covering more than 10 GHz.

The resulting radiation pattern is shown in Figure 4.21. As we can see, the desired radiation pattern has been achieved after analyzing previously parametric simulations, although a slight tilt is still present. The directivity is close to 4 dB. It is a little bit away from its ideal value (a dipole alone has 2.15 dB and an ideal ground plane should add 3 dB). The main reason is that the the available ground plane, which is not infinitely big, is not placed in the correct angle to

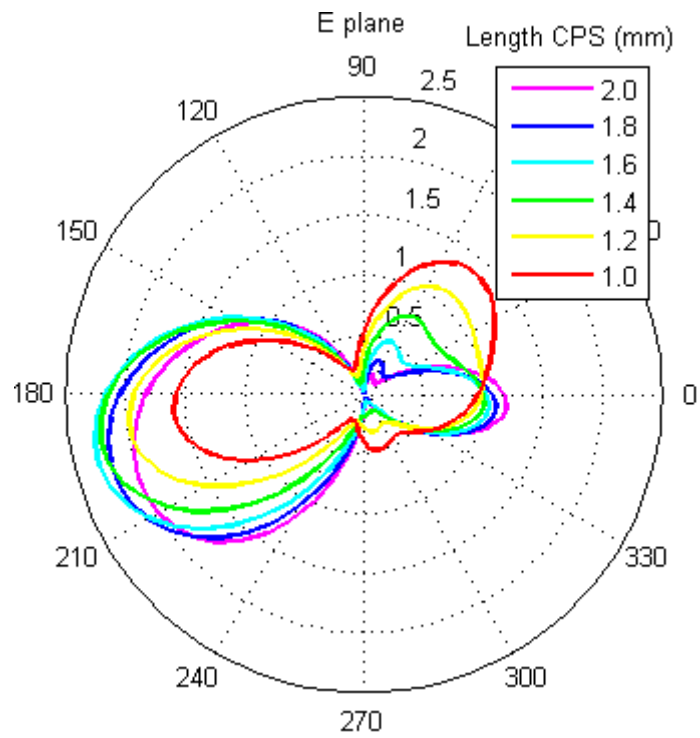


Figure 4.18: E plane cut radiation pattern

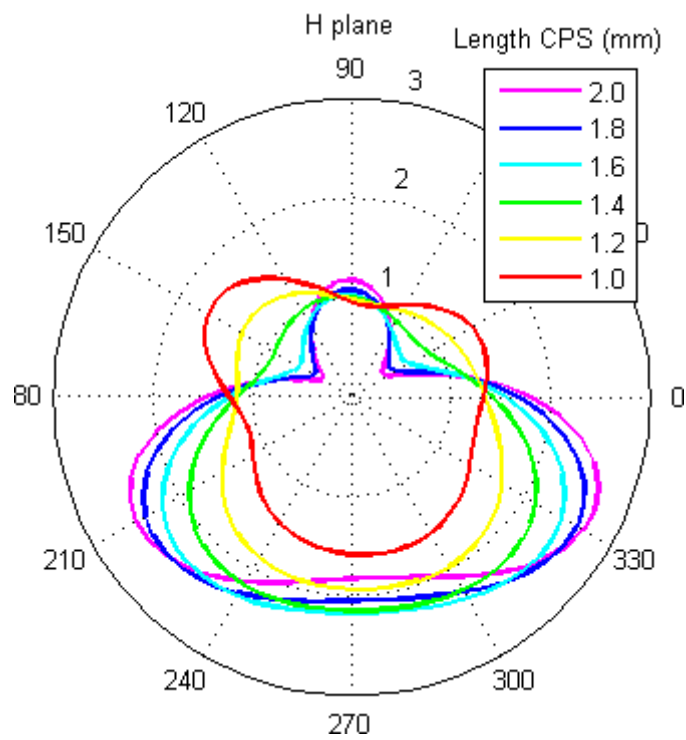


Figure 4.19: H plane cut radiation pattern

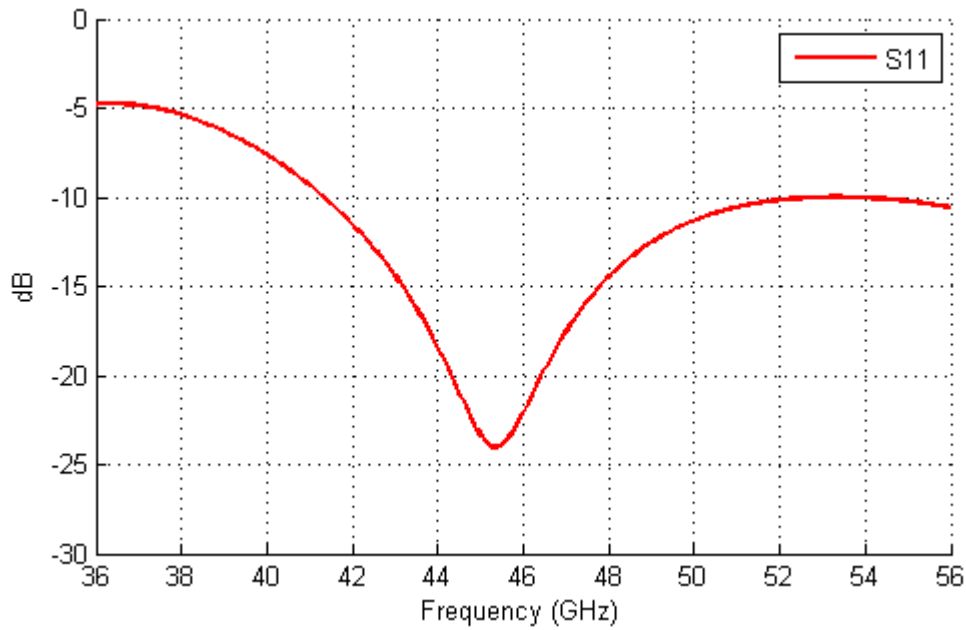


Figure 4.20: Insertion loss

reflect the radiations of the dipole in the most efficient way.

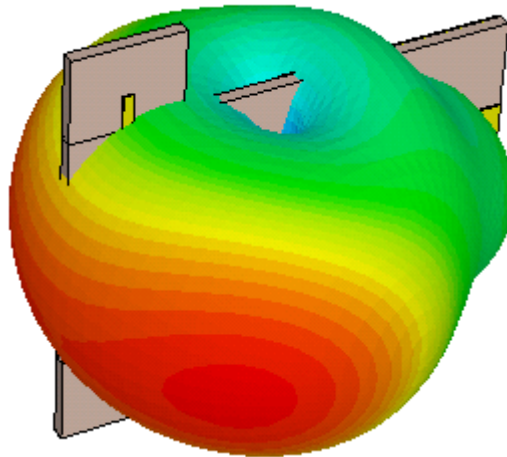


Figure 4.21: 3D radiation pattern

4.8 Conclusion

In this chapter we have developed a microstrip to CPS transition. Back to back topology of the transition has been designed and constructed. However, the simulated and measured S parameters does not agree. To begin with, the simulation results have already been worsened when

the ports are included in back to back simulations. As we have already explained, additional support are attached to the constructed model to enhance its integrity and at high frequencies their behavior should not be disregarded.

A dipole prototype has been tested in simulation. It was found that the microstrip ground plane produces undesired effects in the radiation pattern of the dipole antenna. By varying the distance between the dipole and the ground plane it was possible to obtain a good radiation pattern at the same time as a return loss better than -20 dB.

In the next chapter we will make use of the microstrip to CPS transition to design the rectangular waveguide to microstrip transition.

Rectangular waveguide to microstrip transition

5.1 Introduction

With the microstrip to CPS transition properly designed, now it is time to make use of it to achieve the rectangular waveguide to microstrip transition. As stated in the Section 1, the local oscillator input of the mixer circuit will be fed through a rectangular waveguide due to its low loss characteristics. In Section 2 we explained that the mixer circuit will be constructed under microstrip technology, hence the necessity to use the aforementioned transition.

In order to achieve the rectangular to microstrip transition, we will make use of a Yagi Uda antenna. However, the natural way to connect to the Yagi Uda antenna is by means of a balanced technology, such as the Coplanar Stripline (CPS). For this reason, the transition will be first from a rectangular waveguide to a Yagi Uda antenna connected to a section of CPS. Later on, the microstrip to CPS transition developed in the previous section will be attached to the CPS section, finally accomplishing the proposed rectangular waveguide to microstrip transition.

In this chapter, we will first look at the basics of the rectangular waveguide, as well as the Yagi Uda antenna used as a radiating element to construct the transition. Later on, the theory is applied to design a rectangular waveguide to CPS transition. After that, the microstrip to CPS transition is incorporated. Then, an early prototype of the complete system is shown, indicating its working frequency and transition characteristics. Finally, the rectangular waveguide to microstrip transition at the interested working frequency is presented and its transmission performance is explained.

5.2 Rectangular waveguide

Rectangular waveguides were one of the earliest transmission line topologies that served the purpose of propagating microwave signals. In recent applications, planar technology are widely

used. Waveguides, however, are still necessary in numerous applications due to the advantages that they present. Apart from the low loss advantage that we have mentioned before, they are also good at handling high power signals, which is often the case of those Local Oscillator excitations. Millimeter wave systems and precision test applications are some of other uses of waveguide topologies.

As a rectangular waveguide consists on an hollow structure with metallic walls, TM and TE modes can propagate whereas TEM modes are not compatible. In Figure 5.1 we can see a generic view of a rectangular waveguide, where the length of the longer side of the waveguide is denoted as a and the one for the shorter side b . The material filling the waveguide has permittivity ϵ and permeability μ .

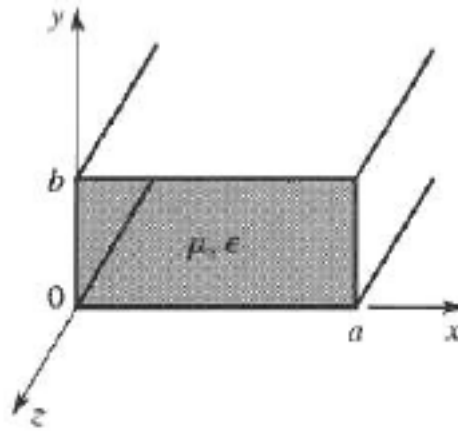


Figure 5.1: Cross section of a standard CPS line [5]

We will not go through all the field equations for rectangular waveguides here, as they can be found in [5]. However, as we will assume the propagation of the fundamental mode, which is in fact the TE_{10} mode, we will go through some of the formulas that are relevant for the selection of the rectangular waveguide as well as for the design of the proposed decision.

The cut off frequency of the fundamental mode TE_{10} is given by:

$$f_{c10} = \frac{1}{2a\sqrt{\mu\epsilon}} \quad (5.1)$$

The propagation constant is

$$\beta_{10} = \sqrt{k^2 - \left(\frac{\pi}{a}\right)^2} \quad (5.2)$$

And the guided wavelength, which is the actual wavelength of the waves inside the waveguide, can be obtained from:

$$\lambda_{guide} = \frac{\lambda_{freespace}}{\sqrt{1 - \left(\frac{c}{2af}\right)^2}} \quad (5.3)$$

A general feature of transmission lines that we will make use of consists on the fact that, if a short circuit is placed at one end of the structure, a maximum can be found $\lambda_{guide}/4$ away from the short circuit. More maxima of the propagated fields can be found each $\lambda_{guide}/2$.

The rectangular waveguide will be excited by the $LO/2$ signal, as stated in Chapter 2. The frequency of that excitation will be 46 GHz. Actually, there are two commercial rectangular waveguide standards available for the transmission of signals of such frequency. Their characteristics are listed in Table 5.1.

Waveguide name	Frequency range (GHz)	Inner dimensions (mm)	Wall thickness (mm)
WR22	33 - 50	5.6896×2.8848	1.016
WR19	40 - 60	4.7752×2.3876	1.016

Table 5.1: Usable rectangular waveguides for 46 GHz

Both of them are suitable for excitations at 46 GHz. WR22 is selected as it has bigger dimensions and would allow more freedom for the design of Yagi Uda antennas to achieve a correct transition behavior. We will see that in fact the probe of the designed Yagi antenna is almost as wide as the inner dimensions of the rectangular waveguide WR22, and WR 19 would be just too small.

Using the Equation in 5.3, we will obtain a guided wavelength of 7.9585mm. This value will be relevant for the design of the transition.

5.3 Yagi Uda antenna

To be able to successfully convert microwave signals from a rectangular waveguide to a planar technology, we will use Yagi Uda antennas. Yagi Uda antennas, basically, consists on a parasitic linear array of parallel dipoles. A parasitic array differs from a conventional array in the way each element is fed; if only few elements of the array are directly fed, it can be considered as a parasitic array. In fact, only one element is fed in a Yagi antenna, that is, the driver.

In Figure 5.2 we can see an example of a Yagi Uda antenna. It is constructed by mainly three different types of elements. The leftmost is a reflector and it is usually slightly longer than the driver element, next to the reflector at its right. The rest of the elements are called directors, being slightly shorter than the driver. The amount of them is variable, where usually a great number of directors leads to a higher directivity.

The advantages of Yagi Uda antennas is that the design process is not much more complex than a single dipole antenna, while offering flexible directivity varying the number of elements. In comparison with some array antennas, Yagi Uda antennas present a much easier feeding way. In [20] we can find tables regarding the parameters of a Yagi Uda antenna, as can be seen in Figure 5.2. Nevertheless, it is always necessary to perform simulations before constructing

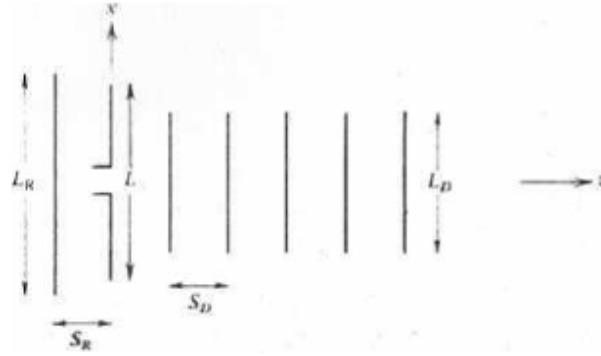


Figure 5.2: Generic configuration of Yagi Uda antenna [20]

antennas directly to avoid undesired situations.

For the purpose of the transition, a two element Yagi Uda antenna is chosen, consisting on a driving element and a director. The driver is connected to a CPS line, which will be converted later to microstrip topology using the transition developed in the previous chapter.

5.4 Rectangular waveguide to CPS transition

After reviewing key points of both rectangular waveguides now it is time to move on to the design of the transition. The principles of the transition that we are going to built is based on [15] and have already been covered in Section 3.4.1. In this section, we will only go through the design steps.

First of all, the rectangular waveguide is short circuited at one of its ends. In this way we can calculate approximately the position of the maximums of the propagated wave inside the waveguide. The Yagi Uda antenna will be placed at one of the field maximum points inside the rectangular waveguide. There is a slot in the short circuit, so as to allow planar circuitry to go outside of the waveguide.

However, there are still concerns about the allocation of the Yagi Uda antenna. The substrate used, onto which we will deploy the Yagi antenna, the CPS lines and microstrip lines, as well as the mixer, is extremely thin. This means that it might happen that the structure is twisted, if it is not well supported or too much weight is applied upon it. For this reason, it is of great interest to keep most part of the circuitry inside the rectangular waveguide. The only elements that would be out of the waveguide are a section of CPS line and a radiating element, that is, an antenna, for the radiofrequency port of the mixer.

Thus, we have to consider both the lengths of CPS to microstrip transitions, and the space that the mixer circuit would occupy. This implies that the Yagi Uda antenna used for transition will not be placed $\lambda_{guide}/4$ away from the short circuit end of the rectangular waveguide, but it will be placed at field maximum locations that can be expressed as $\lambda_{guide}/4 + n \times \lambda_{guide}/2$, being n a positive integer number. Although we have to take into account that the further we

are from the waveguide short circuit, the weaker the field maximums might be. For this reason, we are interested in the minimum distance expressed as $\lambda_{guide}/4 + n \times \lambda_{guide}/2$, that fulfills the condition for which it is long enough to fit the CPS to microstrip transitions and the mixer circuit.

Now, regarding the Yagi Uda antenna, we have mentioned that in [20] there are tables containing the dimensions of the elements. Still, the obtained behavior from that table are not ideal, and simulations should be carried out to optimize the performance of the antenna. In any case, [20] gives a first idea regarding the range of the size of the elements.

The dimensions of the elements of the antenna are usually expressed in terms of wavelength. In [15] we can find an expression for the wavelength of CPS lines:

$$\lambda_{cps} = \frac{\lambda_0}{\sqrt{\epsilon_r + 1}} \quad (5.4)$$

At the frequency of 46 GHz, it results in a λ_{cps} of 2.6263 mm. This will be useful for the last section of this chapter.

5.4.1 Early prototype

In an early stage of the development of the current project, a complete receiver was designed and simulated. Nonetheless, at that point, the main goals of the project, as well as the exact research lines, was still poorly defined. The original idea was pretty similar, aiming at a receiver working around 90 - 100 GHz. The most basic radiating element, a half wavelength dipole was used, connected to a section of CPS, followed by the rectangular waveguide to CPS transition covered before. However, the mixer were not included, and the sub harmonic topology for the mixer were not considered either. For this reason, the entire system would work only at one frequency, which is maintained from the dipole to the rectangular waveguide. This implies that some aspects of the transition will differ from what we have explained.

To begin with, the dimensions of the rectangular waveguide will be another one:

Waveguide name	Frequency range (GHz)	Inner dimensions (mm)	Wall thickness (mm)
WR10	75 - 100	2.54×1.27	2.032

Table 5.2: Rectangular waveguides used in an early prototype

Which is indeed much smaller than the options in Table 5.1. This involves in a narrower dielectric substrate, alongside with wavelengths that are much shorter, leading to an overall dimension reduction of the transition. We can see in Figure 5.3 the overall view of the complete structure.

It is clear that the planar circuit consists only on a Yagi antenna, a CPS line and a dipole. In Figure 5.4 we can find the return loss for the transition presented above, where a waveguide port is placed in the rectangular waveguide end of the structure.

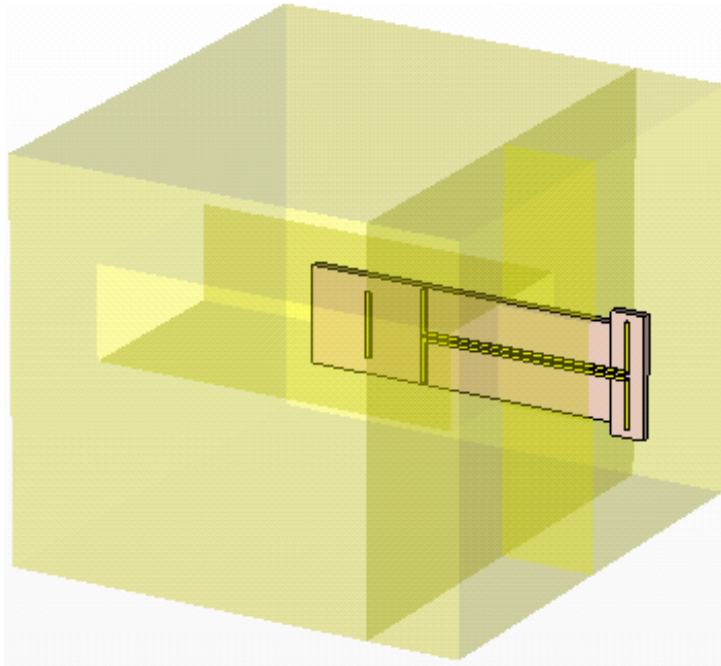


Figure 5.3: Early prototype

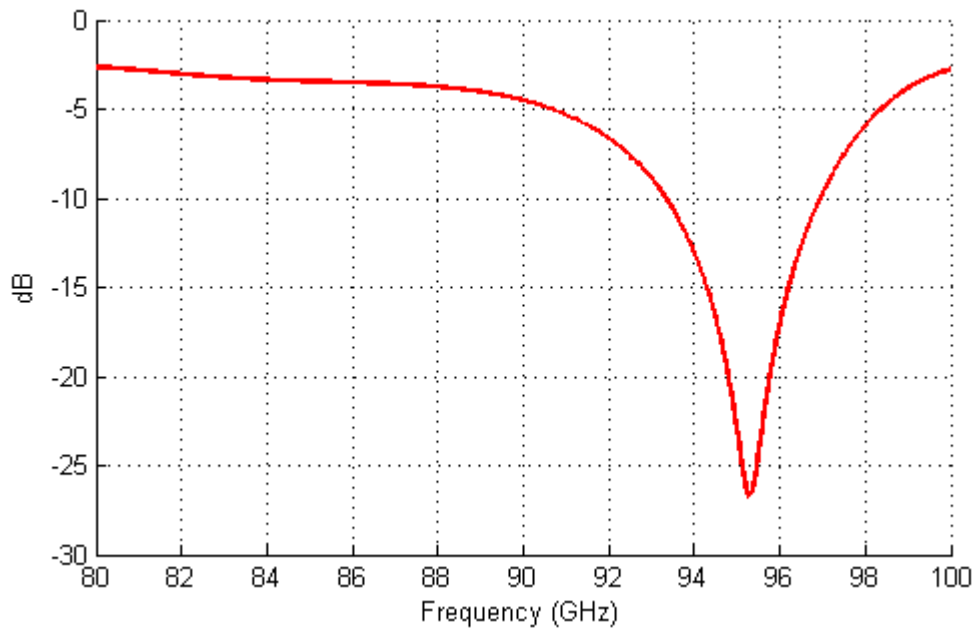


Figure 5.4: Simulated S_{11} of the early prototype

As it can be seen, the structure works for a narrow bandwidth. The return loss is better than -10 dB from 93 GHz to 97 GHz. The main reason for the narrow frequency band is that a dipole antenna does not work in a wide range of frequencies. Still, the simulation of this

prototype indicates that the general idea of the current project seems to work. In Figure 5.5 we can see the radiation pattern of the dipole at 94 GHz, where a directivity greater than 8.5 dB was obtained.

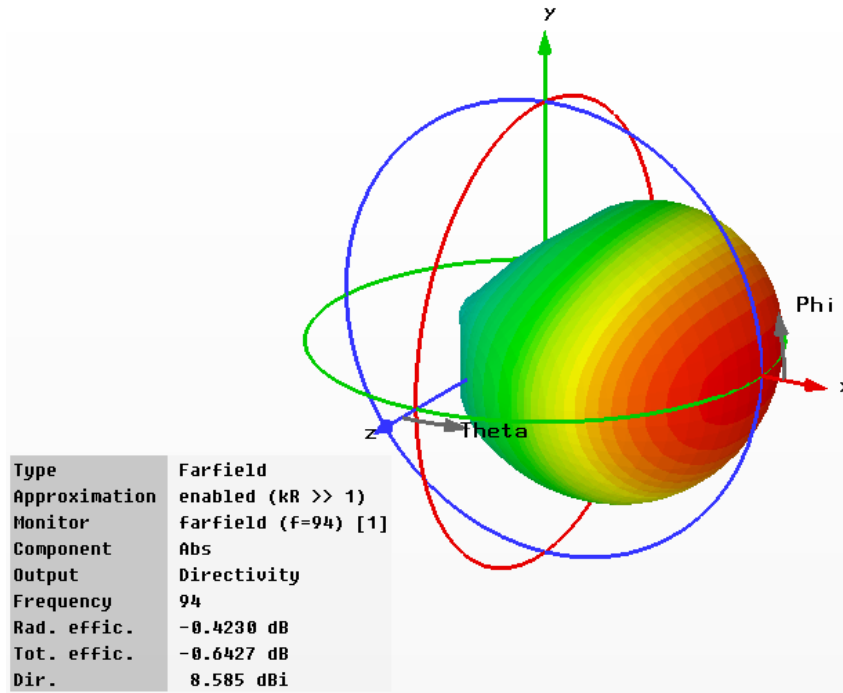


Figure 5.5: Radiation pattern of the early prototype

5.5 Rectangular waveguide to microstrip transition

Finally, it is time to combine all the elements that we have discussed in Chapters 4 and 5 to design and simulate the rectangular waveguide to CPS transition. To begin with, the length of the mixer circuitry is below 24 mm and the total length of the microstrip to CPS transition is below 50mm. Thus, the distance between the Yagi Uda antenna and the short circuited end of the rectangular waveguide will be $5 \times \lambda_{guide}/2$, which is a theoretical distance of 9.95 mm. The parameters of the Yagi Uda antenna are taken from [20]. However, all these values are theoretical and initially they did not lead to desired simulation results. To overcome this situation, many parametric simulations were launched to obtain the best fit amongst all the variables. It was found that the most relevant factor were the length of the driver element of the Yagi antenna, as a slight size change lead to an important frequency shift. Other elements, such as the length of the director or the distance between the director and the driver element, contributes to a better or worse matching of the transition.

In table 5.3 we can find the values of the most relevant measures of the rectangular waveguide to microstrip transition. Note that the part of the CPS to microstrip transition is exactly the

same one discussed in the previous chapter.

Element	Value (mm)
Director	1.4
Driver element	2.83
Distance between director and driver	1.2
Distance between Yagi and waveguide short circuit	9.5
Thickness of the short circuit	1.016

Table 5.3: Parameters of the rectangular waveguide to microstrip transition

It is interesting to point out that the length of the driver element is almost as long as the width of the rectangular waveguide. Also, a short circuit that is too thin leads to unsatisfactory behaviors. In Figure 5.6 we can see the overall view of the transition.

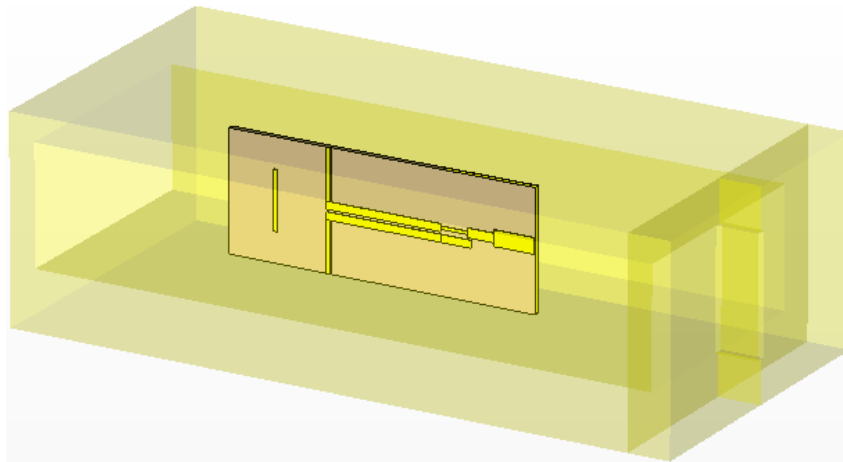


Figure 5.6: Layout of the rectangular waveguide to microstrip transition

The simulated S parameters is presented in Figure 5.7.

It is easy to realize that the bandwidth of the complete transition is very narrow. The reason is that there are several elements that imposes different working frequencies: the location of the Yagi Uda antenna, the Yagi Uda antenna itself, and the CPS to microstrip transition. The ideal matching among all the element is not straight forward, meaning that the transition could be improved at high costs. Nevertheless, the bandwidth is not crucial here as the structure is supposed to provide a pure 46 GHz Local Oscillator excitation to the mixer. An insertion loss of 2 dB is obtained at the interested frequency. Both return losses are better than -6 dB.

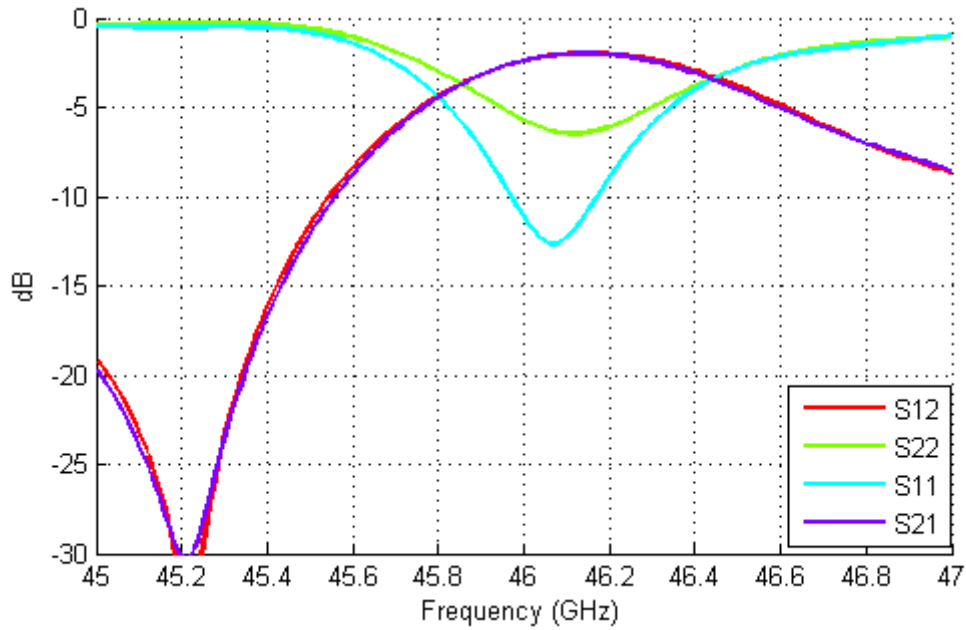


Figure 5.7: Simulated S parameters of the rectangular waveguide to microstrip transition

5.6 Conclusion

In this chapter we have finally developed the rectangular waveguide to microstrip transition, which actually has an intermediate CPS stage. Parametric simulations were performed to adjust the working frequency of the transition. Although the bandwidth is very narrow, mainly due to a non optimal coupling between different stages, an insertion loss of 2dB is obtained. The return losses at both ends of the structure is better than -6 dB.

Conclusions and future research lines

6.1 Conclusions

As we have seen during the past chapters, a set of designs and simulations were carried out. Due to time constraints and resource constraints, the work proposed in Section 1 was not fully covered. Nevertheless, the most important parts of the system have been studied.

First, the subharmonic mixer was properly designed, obtaining positive simulation results. Matching for all the 3 ports were better than -20 dB. The conversion efficiency was not optimal, mainly due to the usage of a diode that works only up to 80 GHz. The isolation of the system was also good, obtaining more than -50 dB of isolation at the IF port from both OL and RF inputs. The working bandwidth is not great, but considering that the signal has to be downscaled to 8 GHz, it seems to be acceptable.

Before jumping into CST simulation, a set of trials were done to verify the correctness of simulation results when defining structures in the program. A microstrip to CPS transition is analyzed and implemented, obtaining an insertion loss at the frequency of interest of 1.25 dB, with return losses around -20 dB. The transition also presents a very wide bandwidth. A back to back transition were simulated obtaining also coherent results. However, when coaxial ports were added to the simulation, the results had worsen fairly. The back to back topology were also constructed to be measured, obtaining results similar to the simulated ones, with insertion loss around 8 dB. The main suspect for this bad behavior were the coaxial ports and the additional supports.

A dipole prototype, meaning a dipole connected to the CPS end of the transition were also modeled. It was discovered that the radiation pattern is very susceptible to the distance from the dipole to the ground plane of the microstrip end. Parametric simulations were carried out to find out the optimal distance, achieving a directivity of 4dB and a return loss better than -20 dB.

Next, the Yagi Uda antenna was briefly analyzed and the rectangular waveguide to CPS transition was modeled. Connecting it with the CPS to microstrip transition, the rectangular

waveguide to microstrip transition is simulated, obtaining an insertion losses around 2 dB, which is quite acceptable considering that there have been 2 technology jumps. An early prototype was also presented, that verified the viability of the system in an initial stage.

6.2 Future research lines

There are some aspects of the proposed system that have not been covered and possible research lines in the future are listed below:

- Construct and measure the mixer circuit
- Design a CPS to microstrip transition for the RF end of the mixer circuit
- Design an radiating element for the reception of the RF signal
- Verify whether a hole in the wall of the rectangular waveguide affects the functionality of the whole system and check the quality of the signal at the IF output
- Test the performance of the complete system combining all the elements

This project, along with the points listed above, lays the foundation for future researches where real applications can be added to this microwave system. For instance, as it was mentioned in the introduction section, a junction of several receiver systems can form an millimeter wave imaging array with a decent pixel resolution thanks to the reduced size. Also, it is possible to make use of the elements that have been developed during this project to design construct other microwave systems serving other kind of purposes.

Appendices

Appendix A

Layout

Several block diagrams are listed in this appendix.

A.1 Mixer circuit

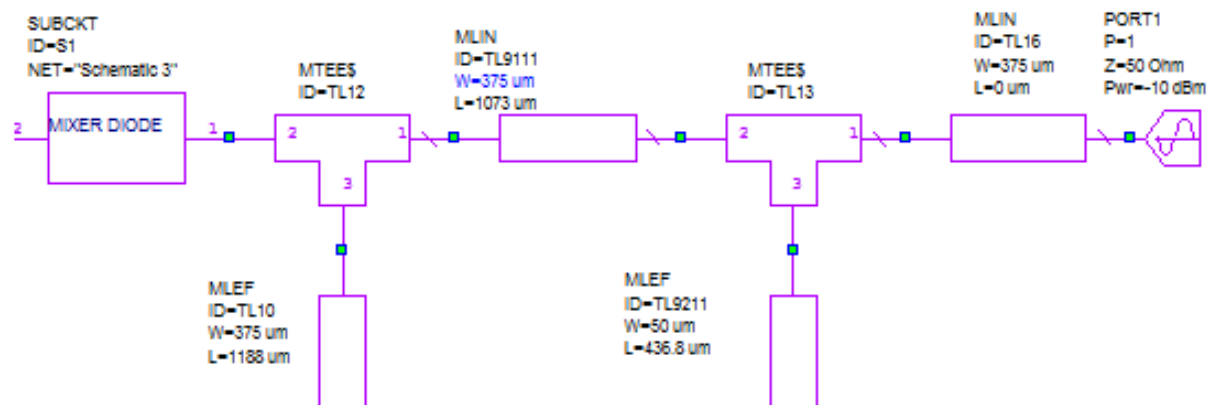


Figure A.1: RF matching circuit and mixer diode

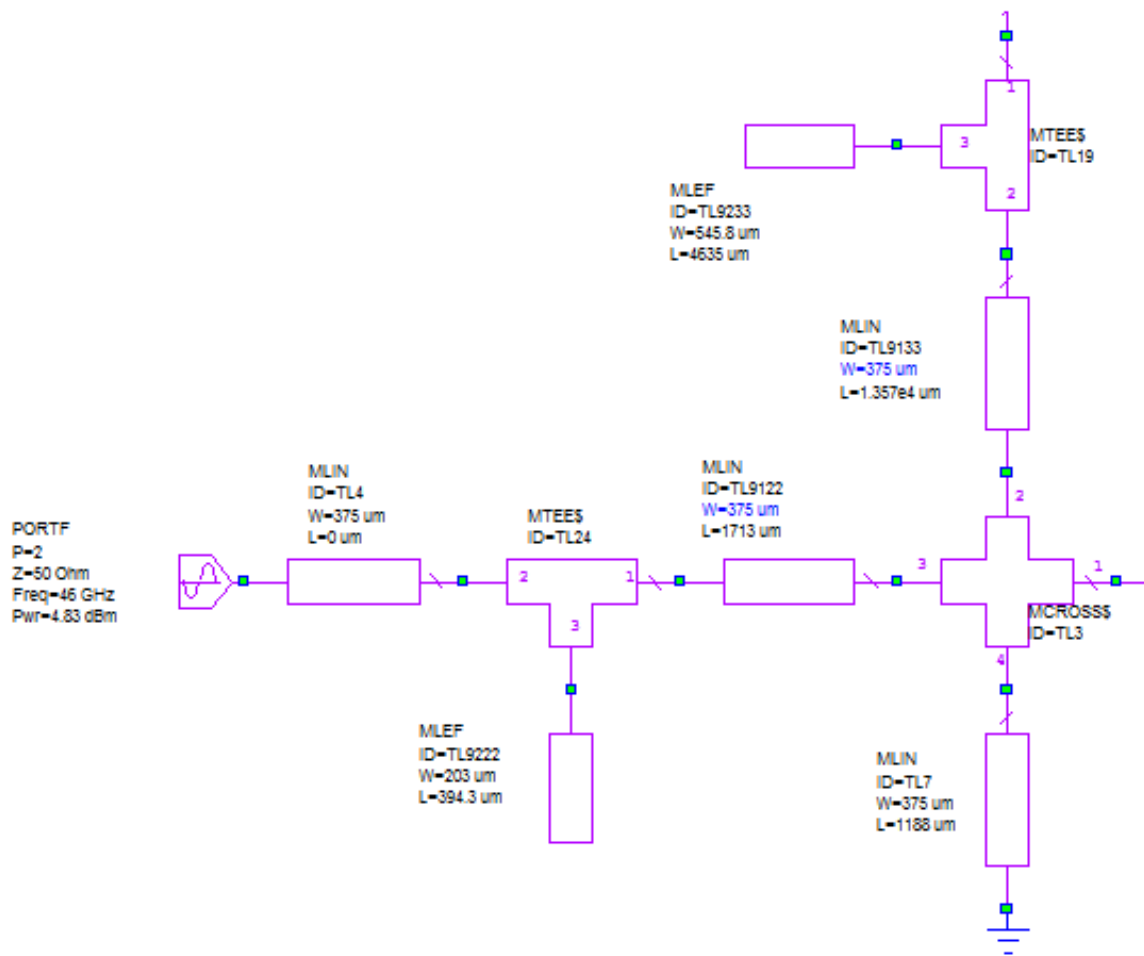


Figure A.2: OL matching network with IF matching network on top

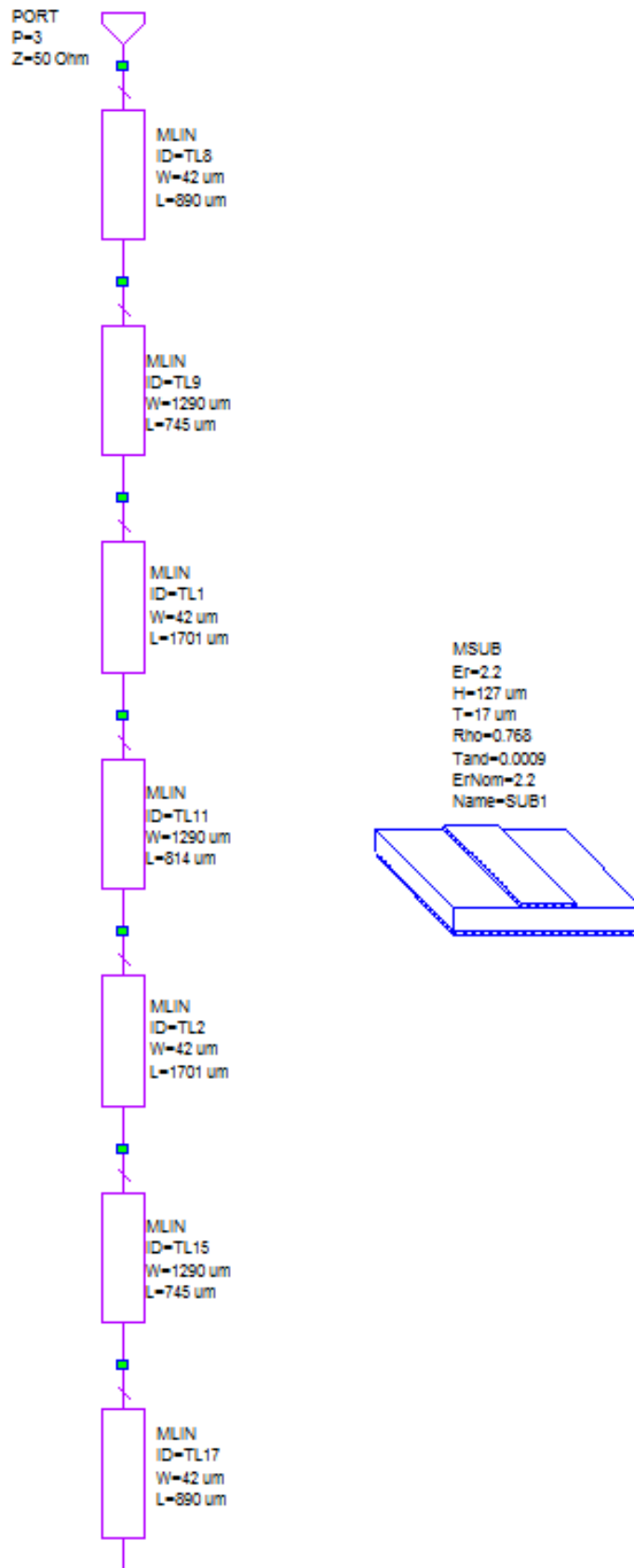


Figure A.3: IF filtering stage with microstrip definition

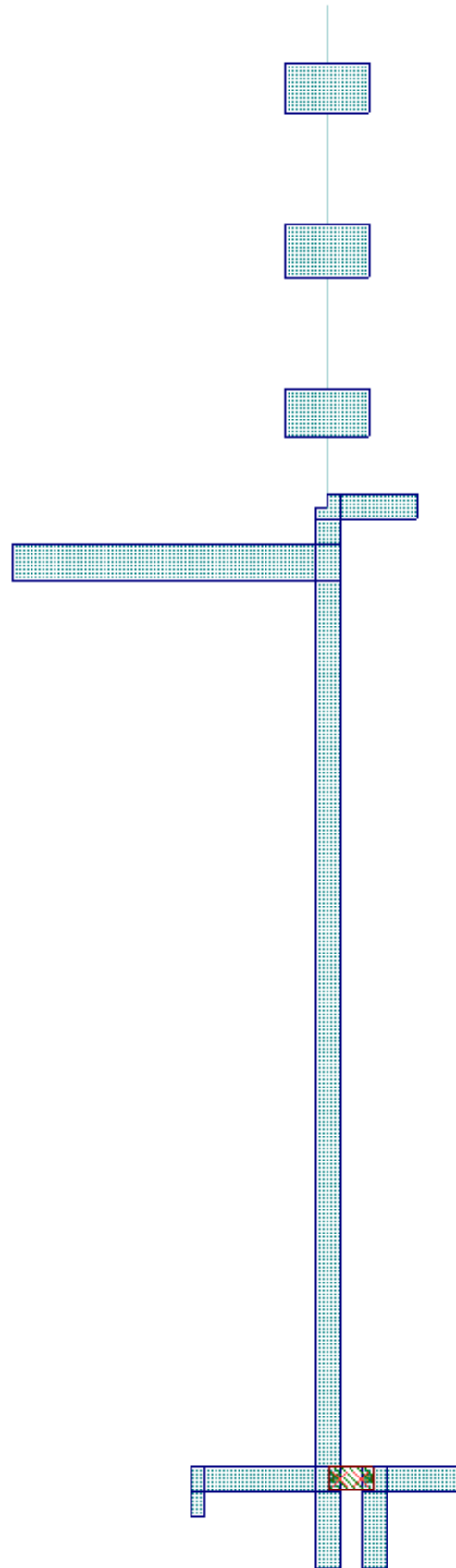


Figure A.4: Complete layout of the mixer circuit

A.2 Back to back microstrip to CPS transition

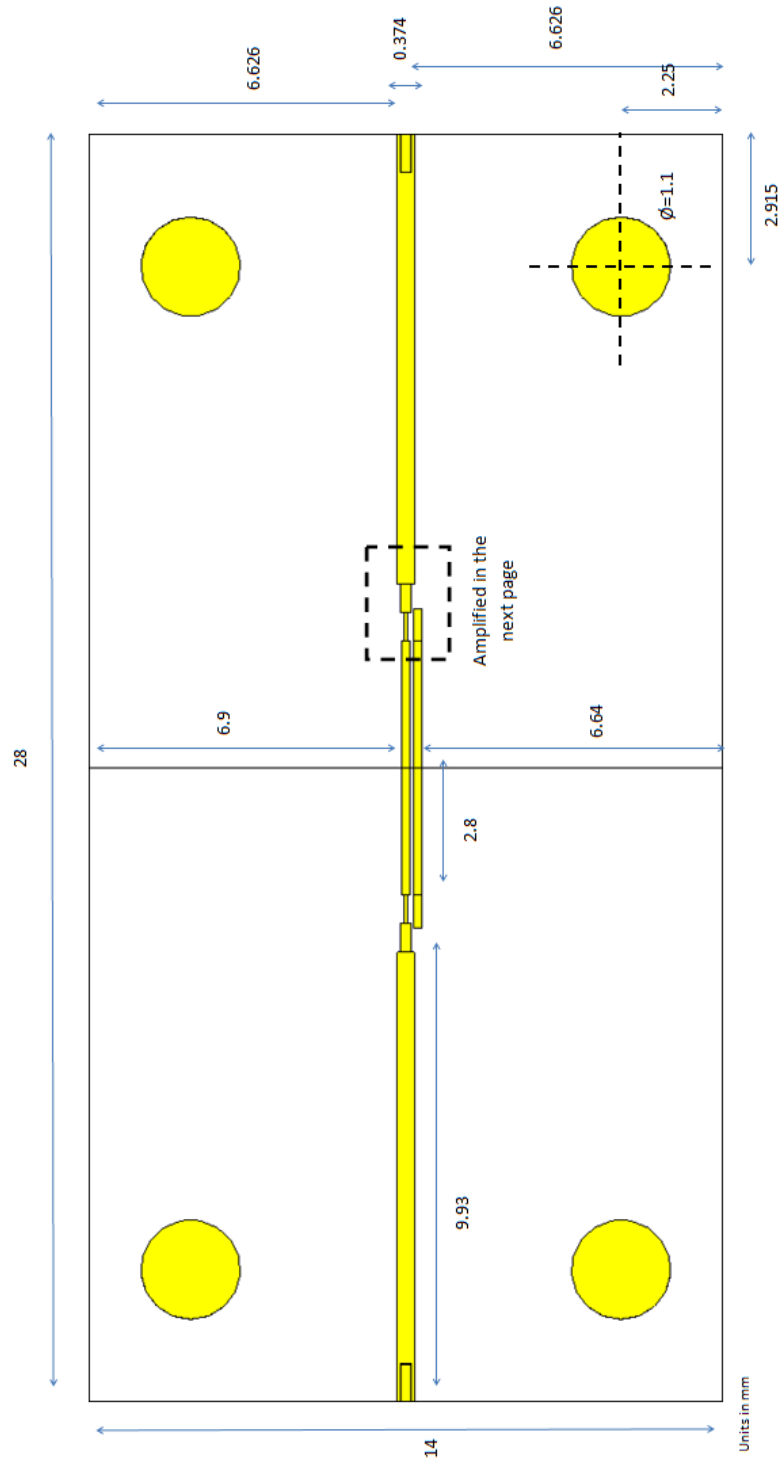


Figure A.5: Top view

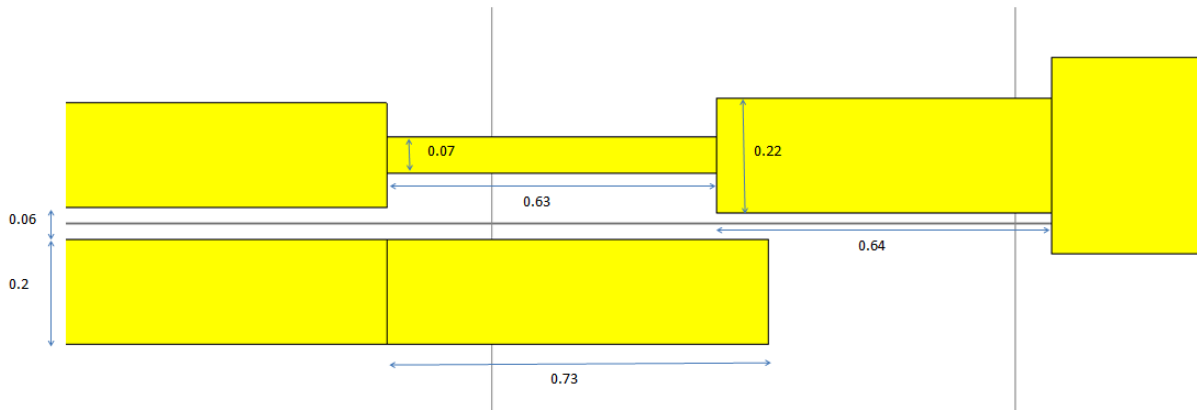


Figure A.6: Detailed top view

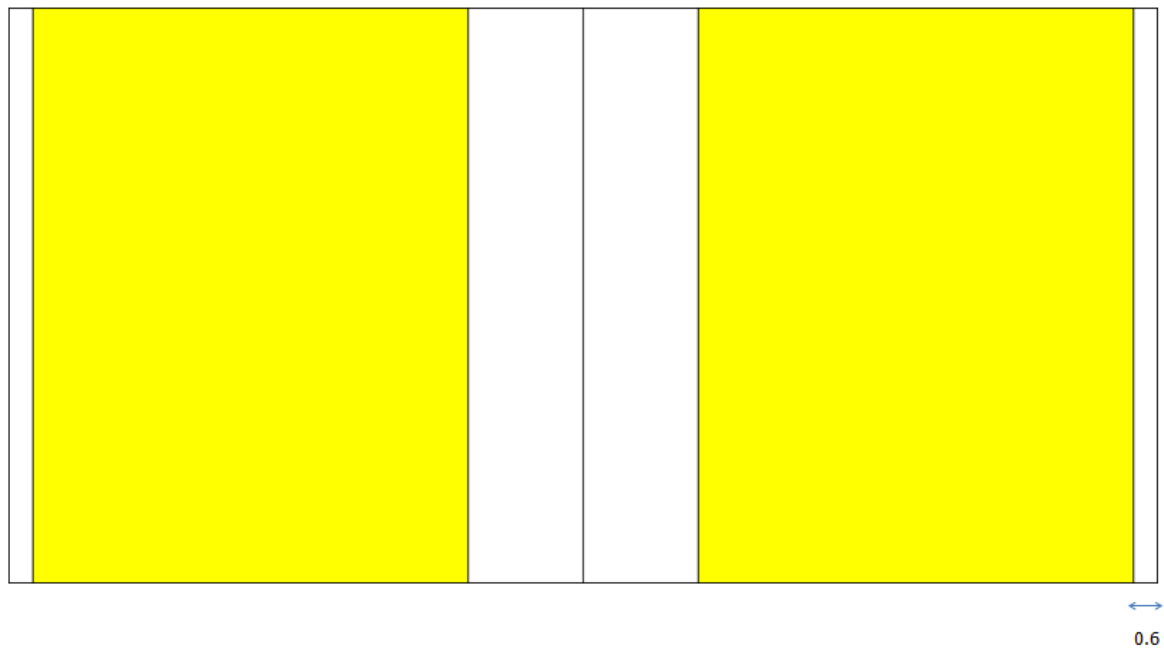


Figure A.7: Bottom view

Appendix B

Budget

The required budget to carry out the present project is discussed here, which spans from September 2011 to August 2012. A man month of dedication represents 131.25 hours of work. All the cost units are expressed in euros. All the costs can be classified into personnel budget, equipment cost and other costs.

Name	Category	Dedication (man - month)	Cost man - month	Cost
Yuchen Du	Engineer	7.54	2,694.39	20,315.70
Javier Montero de Paz	Engineer	1.51	2,694.39	4,068.53
Daniel Segovia Vargas	Senior engineer	0.75	4,289.54	3,217.16

Table B.1: Personnel budget

Description	Total cost	Percentage dedicated to project	Dedication (months)	Depreciation period (months)	Attributable cost
Network analyzer	100,000.00	100	0.07	60	116.67
Computer	1,000.00	100	11	60	183.33
Simulation software	2,000.00	100	11	60	366.67

Table B.2: Equipment cost

The attributable cost are calculated by using the following formula:

$$\text{Attributable cost} = \frac{\text{Total cost} \times \text{Percentage dedicated to project} \times \text{Dedication}}{\text{Depreciation period}} \quad (\text{B.1})$$

Description	Company	Cost
Construction of back to back transition	UC3M	100.00

Table B.3: Other cost

For all the above items, 20 % of indirect costs should be added. The complete budget is summarized in the following table.

Item	Cost
Personnel costs	27,601
Equipment costs	667
Other costs	100
Indirect costs	5,674
Total	34,042

Table B.4: Summary of costs

Bibliography

- [1] I. Ederra, L. Azcona, B. Alderman, A. Laisne, R. Gonzalo, C. Mann, D. Matheson, and P. de Maagt, "A 250 ghz subharmonic mixer design using ebg technology," *Antennas and Propagation, IEEE Transactions on*, vol. 55, pp. 2974 –2982, nov. 2007.
- [2] N. R. Canada, *The Electromagnetic Spectrum*.
- [3] U. L. R. George D. Vendelin, Anthony M. Pavio, *Microwave Circuit Design using linear and nonlinear techniques, Second Edition*. Wiley, 2005.
- [4] *MA4E1318 Datasheet*. MACOM Technology Solutions.
- [5] D. M. Pozar, *Microwave Engineering, Third Edition*. Wiley-Interscience, 2005.
- [6] K. B. J. J. Thaysen and J. Appel-Hansen, "A wideband balun - how does it work?," -, 2000.
- [7] S.-G. Mao, C.-T. Hwang, R.-B. Wu, and C. H. Chen, "Analysis of coplanar waveguide-to-coplanar stripline transitions," *Microwave Theory and Techniques, IEEE Transactions on*, vol. 48, pp. 23 –29, jan 2000.
- [8] Y.-S. Lin and C. H. Chen, "Lumped-element marchand-balun type coplanar waveguide-to-coplanar stripline transitions," in *Microwave Conference, 2001. APMC 2001. 2001 Asia-Pacific*, vol. 2, pp. 539 –542 vol.2, dec. 2001.
- [9] A. Vasylychenko, L. Wang, Z. Ma, W. De Raedt, and G. Vandenbosch, "A very compact cpw-to-cps balun for uwb antenna feeding," in *Electrical and Electronics Engineers in Israel, 2008. IEEEI 2008. IEEE 25th Convention of*, pp. 446 –449, dec. 2008.
- [10] R. Simons, N. Dib, and L. Katehi, "Coplanar stripline to microstrip transition," *Electronics Letters*, vol. 31, pp. 1725 –1726, sep 1995.
- [11] Y.-H. Suh and K. Chang, "A wideband coplanar stripline to microstrip transition," *Microwave and Wireless Components Letters, IEEE*, vol. 11, pp. 28 –29, jan. 2001.

-
- [12] T. Chiu and Y.-S. Shen, "A broadband transition between microstrip and coplanar stripline," *Microwave and Wireless Components Letters, IEEE*, vol. 13, pp. 66 – 68, feb 2003.
- [13] W.-H. Tu and K. Chang, "Wide-band microstrip-to-coplanar stripline/slotline transitions," *Microwave Theory and Techniques, IEEE Transactions on*, vol. 54, pp. 1084 – 1089, march 2006.
- [14] T. B. Lim and L. Zhu, "Compact microstrip-to-cps transition for uwb application," in *Art of Miniaturizing RF and Microwave Passive Components, 2008. IMWS 2008. IEEE MTT-S International Microwave Workshop Series on*, pp. 153 –156, dec. 2008.
- [15] N. Kaneda, Y. Qian, and T. Itoh, "A broadband microstrip-to-waveguide transition using quasi-yagi antenna," in *Microwave Symposium Digest, 1999 IEEE MTT-S International*, vol. 4, pp. 1431 –1434 vol.4, 1999.
- [16] V. Mottonen, "Wideband coplanar waveguide-to-rectangular waveguide transition using fin-line taper," *Microwave and Wireless Components Letters, IEEE*, vol. 15, pp. 119 – 121, feb. 2005.
- [17] V. Mottonen and A. Raisanen, "Novel wide-band coplanar waveguide-to-rectangular waveguide transition," *Microwave Theory and Techniques, IEEE Transactions on*, vol. 52, pp. 1836 – 1842, aug. 2004.
- [18] R. N. Simons, *Coplanar Waveguide Circuits, Components, and Systems*. John Wiley & Sons, Inc, 2001.
- [19] S. J. Orfanidis, *Electromagnetic Waves and Antennas*. Rutgers University, 2008.
- [20] W. L. Stutzman, *Antenna theory and design*. John Wiley & Sons, Inc, 1981.
- [21] A. Corporation, *AWR Microwave Office*.
- [22] *Rogers duroid 5880 datasheet Datasheet*. Rogers Corporation.